AMPLITUDE DEPENDENT GROUND RESONANCE STABILITY OF COUPLED ROTOR/FUSELAGE MODEL HAVING A NONLINEAR ELASTOMER

by
MADHUP SRIVASTAVA

DEPARTMENT OF MECHANICAL ENGINEERING
INDIAN INSTITUTE OF TECHNOLOGY KANPUR
May, 2000

AMPLITUDE DEPENDENT GROUND RESONANCE STABILITY OF COUPLED ROTOR/FUSELAGE MODEL HAVING A NONLINEAR ELASTOMER.

A Thesis Submitted
in Partial Fulfillment of the Requirements
for the Degree of

MASTER OF TECHNOLOGY

By

MADHUP SRIVASTAVA

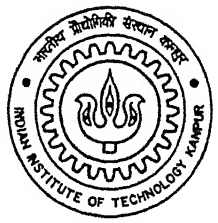

to the

DEPARTMENT OF MECHANICAL ENGINEERING
INDIAN INSTITUTE OF TECHNOLOGY KANPUR
MAY, 2000

I would like to
dedicate this thesis to
amma and nana saheb

Certificate

It is to certify that the work contained in the thesis entitled "*Amplitude dependent ground resonance stability of coupled rotor/fuselage model having a nonlinear elastomer*" by Madhup Srivastava has been carried out under our supervision and that this work has not been submitted elsewhere for a degree.

(Dr. C.Venketesan)

Professor
Department of Aerospace Engineering
Indian Institute of Technology
Kanpur – 208016
India.

(Dr. A.K. Mallik)

Professor
Department of Mechanical Engineering
Indian Institute of Technology
Kanpur – 208016
India.

Acknowledgment

I like to express my sense of gratitude to my supervisor *Prof. A.K. Mallik and Prof. C.Venketesan* to whom I owe more than I can possibly express, for there warm guidance that led to the completion of this work.

I take this opportunity to express my deepest gratitude to *my parents, my mausi mausaji,nikki and shubham* for their invaluable support and affection.

I would like to thanks *salil mishra,* especially, for having long technical discussions and moral support during the thesis work.

I would like to thank my friends, *Shobhit, Sunit,, Amit Kumar Masih , Amit Singh,Saurabh, Ashish, Pahun, DT, PK baba, Punit baba, Sam, Jaine ,mama and Anuj* for their warm affections and help to make my stay at IITK a pleasant one.

Madhup Srivastava

I.I.T,

Kanpur.

May, 2000

Abstract

The dynamic characteristics of rotor blades play a significant role in the overall performance and stability of helicopter. A time domain integration, approach is used to solve the set of non-linear differential equation defining behavior of rotor blade / fuselage with non-dimensional time.

Using Multiblade Coordinate Transformation an attempt to transforms the rotating coordinates into a non-rotating frame is made in order to study the time response of rotor degrees of freedom.

An attempt is made to develop a parameter, which measures the rate of divergence (instability) or convergence (stable response) and its level of dependence on the operating and/or initial condition.

Two sets of table are also drawn in order to study the effect of support damping and with zero support damping on the stability (or instability) of the system.

Contents

List of Figures

List of Tables

LIST OF SYMBOLS

C_x, C_y	non-dimensional linear damping coefficients of the support structure in roll and pitch mode, respectively.
EI	flexural rigidity of the blade.
F	Coulomb damping coefficient.
$\{F_{NL}(y, \dot{y}, \ddot{y})\}$	Vector representing nonlinear terms.
h	hysteretic damping coefficient of elastomer.
$\bar{h}$	height of the rotor above fuselage C.G.
I_x, I_y	non-dimensional mass moment of inertia of the support structures about the C.G. in roll and pitch mode, respectively.
K_1, K_3,K_5,K_7	Stiffness parameters of the nonlinear spring.
L	Blade length
m	mass per unit length of the blade
$\bar{M}, \bar{C}$ and $\bar{K}$	mass, damping and stiffness matrices for the ground resonance problem.
N	numbers of blade.
ND	number of data points.
n1	number of rotating modes.
S_v	in-plane force at the root of blade.
S_r	radial force at the root of blade.
t	time.
T	kinetic energy.
$\bar{u}$	axial displacement of the blade.
U_1	strain energy of the blade due to bending.
U_l	strain energy associated with the elastomer.
$\bar{v}$	in plane displacement of the blade.

v	non-dimensional in plane displacement of the blade, $\frac{\bar{v}}{L}$
W_d	work done by the dissipative elements of the elastomeric damper in lag mode.
$\bar{x}$, $\bar{y}$	perturbational motion of the hub center.
y_{1k}	generalized coordinate in lag motion.
{Y}	vector representing the degrees of freedom.

GREEK SYMBOLS

$\theta_x\ \theta_y$	body modes in roll and pitch, respectively.
ξ	non-dimensional length, $\frac{x}{L}$
ξ_1, ξ_2	non-dimensional blade segments, elastomer and torque tube locations, respectively, $\frac{L_1}{L}, \frac{L_2}{L}$
τ	non-dimensional time, Ωt
$\bar{\phi}_1$	first rotating mode shape in lag motion.
ω	experimentally data fitted frequency.
$\zeta_{\theta_x}, \zeta_{\theta_y}$	damping ratio of the support in roll and pitch mode, respectively.
ω_x, ω_y	support structure frequency in roll and pitch mode, respectively.
Ω	angular velocity of the rotor.
ψ_k	azimuth angle of the k–th blade.
Δ_i	deformation of spring in lag mode.
$\hat{\Psi}_1^I$	normalised deformation of spring in lag mode.

SPECIAL SYMBOLS

$\delta(\ )$	Variation of ( )
$(\dot{\ }), (\ddot{\ })$	derivative with respect to non dimensional time, τ
$\text{sgn}\,\lvert\dot{x}\rvert$	signum function, absolute value of $\dot{x}$

CHAPTER 1

INTRODUCTION

1.1 Bearingless Helicopter Rotor Blade:

The main rotor system of a helicopter is the most important component of the vehicle. The rotor system has to fulfill multiple roles of generating lift, propulsive and control forces. Therefore, the dynamic characteristics of rotor blades play a significant role in the overall performance and stability of the vehicle. There has been a continued effort to develop a rotor blade and hub configuration which is mechanically simple yet efficient.

The development of a bearingless rotor system aims to eliminate the conventional pitch bearing as well as the external damper by incorporating a specialised elastomer with high loss factor. In this rotor system, the blade is attached to the hub through a flexible structural element called flexbeam. The flexbeam is designed to provide the required stiffness in the flap and lag bending deformations of the blade, but it is highly flexible in torsion. Surrounding the flexbeam, there is a stiff cuff denoted as torque tube which is attached to the blade-flexbeam junction at the outboard end and to a pitch link at the inboard end as shown in figure [1.1(a)]. The pitch control of the blade is achieved by rotating the torque tube through up/down movement of the point P, which in turn twists the flexbeam. An elastomer is placed between the torque tube and the flexbeam to provide adequate lag damping. It also serves the purpose of a spacer between the torque tube and the flexbeam. Though a bearingless rotor is mechanically simple , see figure [1.1(b)], its dynamic analysis becomes very complicated due to the presence of multiple load paths and non-linear elastomeric damper. It is important to point out that in a practical bearingless rotor blade configuration, the flexbeam and blade properties will be different. In this thesis, it is assumed that the blade and the flexbeam have same uniform properties. The reason for this assumption is (i) practical blade data is not available (ii) by considering

uniform property for bearingless rotor, one can obtain good physical insight of the effects of non-linear elastomer.

1.2 Background Information:

Over the years, considerable effort has been put in by the helicopter industries in developing soft-in-plane bearingless main rotors with acceptable performance and stability characteristics. Huber[1] presented a comprehensive review of the bearingless main rotor programme pursued at different helicopter industries in the world. A brief history on the development of bearingless rotors is provided in Refs. [2,3]. Lockheed developed the first prototype of a bearingless rotor in mid 1960's having "matched stiffness" (equal stiffness in both in-plane and out of plane bending). During test flight, the prototype encountered an air-resonance instability which was eliminated by increasing the fuselage inertia. During late 1970's intense activity continued in developing the prototype of Bearingless Main Rotor (BMR). The Boeing Helicopter company developed a BMR with a high fundamental flap frequency and tested it on and MBB B0-105 Helicopter. It was observed that the landing gear of B0-105 had to be stiffned in order to improve the ground resonance stability. Another design was proposed by the Bell Helicopter with a four bladed M680 rotor. An elastomeric damper was provided to augment edgewise damping. In 1990 the Boeing-Sikorsky company developed a five bladed BMR (for the new helicopter known as RAH-66 Comanchi) with elastomeric dampers. This vehicle is currently under going tests, [2]. In Europe, Eurocopter recently built and flight tested EC135 helicopter with a BMR,[4]. For the analysis and design of bearingless rotor blades, most of the rotorcraft manufacturers have developed their own in-house methodologies and computer codes. Hence, very little information is available about them in the open literature. Recently Pohit,G. *et.al* [5] have analyzed the influence of non-linear elastomer on isolated lag dynamics and rotor/fuselage aeromechanical stability and studied the non-linear free vibrations of the rotating blade under lag bending. Numerical perturbation technique is used to determine the frequency-amplitude relationship. A conclusion has been drawn that up to a fairly high value of amplitude, a seventh order expansion for the resorting force is sufficient to correctly predict the frequency-amplitude relationship. They have also carried out amplitude dependent stability analysis for a coupled rotor/fuselage system under ground resonance

resonance condition. The non linearities of elastomer were treated by an equivalent linearisation approach. They observed that the elastomer amplitude does not alter the stability of the system in the region of maximum instabilities, but the stability of the progressive lag mode increases appreciably with increasing amplitude. Also, the location of the elastomer and torque tube have significant influence on the stability of the system, there is an optimum location for the torque tube providing least instability in the system.

1.3 Elastomeric Damper:

Elastomeric materials are becoming increasingly popular for vibration attenuation applications due to the tremendous advantage they offer over mechanical dampers. In the case of bearingless rotors, conventional hydraulic dampers are being replaced by specialised elastomeric material with high loss factor. Under dynamic conditions, elastomeric materials exhibit visco-elastic behaviour dissipating energy through hysteresis. The characteristics of an elastomeric material are also non-linear with respect to the amplitude of motion. Consequently it has been a challenging task to develop an analytical model that can accurately represent the behaviour of the elastomeric dampers.

The non-linear characteristics of elastomers have been analysed in detail in several recent publications. In Ref. [5], the non-linear characteristics of the elastomeric material have been idealised by a combination of linear and non-linear restoring and dissipative elements. Figure (1.2) represents an idealized model consisting of a non-linear spring, coulomb damper and hysteric damper, which differs from the model proposed by Gandhi et. al. [7] in the sense that their model has a viscous damping element. Figure (1.3) shows the variation of in-phase (k′) and quadrature (k′′) stiffnesses, which correlate well with the experimental data.

The model developed in Ref. [5] has been used in the present study.

1.4 Aeromechanical Stability Analysis of Helicopter:

The aeromechanical stability of a helicopter is a complex phenomenon, involving coupling between the rotor and body degrees of freedom. The rotor lead-lag

regressing mode usually couples with the body pitch and roll modes to cause instability. This phenomenon is denoted as ground resonance when the helicopter is on ground. The aeromechanical stability is severe in nature. In case of bearingless rotors, a specialised elastomer with high loss factor is used as a damper.

The analysis of aeromechanical stability characteristics of a coupled rotor/fuselage system requires the development of a mathematical model representing the dynamics of the coupled system. Over the years, considerable progress has been made in modelling the system dynamics. Friedmenn and Venkatesan [7,8] developed analytical models for the aeromechanical stability of a coupled rotor/fuselage system and compared their theoretical results with the experimental data presented Venkatesan [10] analysed the effects of pitch-lag, pitch-flap and structural flap-lag couplings individually and in combination, on the stability of lag mode under ground resonance condition. In Ref. [6], ground resonance stability, using an idealised model of the coupled rotor/fuselage system has been analysed and is shown in figure [1.4]. In this model, the blade is assumed to undergo only lag motion and the elastomer is represented by non-linear spring and damping elements. The torque tube is assumed to be rigid and massless. The fuselage is allowed to undergo rigid body pitch and roll motions. Emphasis is placed on the effect of non-linearity of the elastomer on the ground resonance problem. The nonlinearities were linearised for a given amplitude using equivalent linearisation approach performing a linearised stability analysis. He observed that effect of amplitude on ground resonance analysis is that the progressive lag mode becomes more stable with increasing amplitude for the baseline configuration (ξ_1=0.1 and ξ_2=0.25) and C_x=0, C_y=0.

The present study is an extension of the study carried out in Ref. [6].

1.5 Objective of the Present Study:

The major objectives of the present study are to:

(i) Obtain equation of motion for coupled rotor/fuselage system including elastomer nonlinearities, under ground resonance condition.

(ii) Analyse the amplitude dependent aeromechanical stability by directly integrating the governing differential equations in time domain, for various sets of operating and initial conditions.

(iii) Identify the region of instability.

(iv) Formulate a measure of instability of the system and study its variation with both operating and initial conditions.

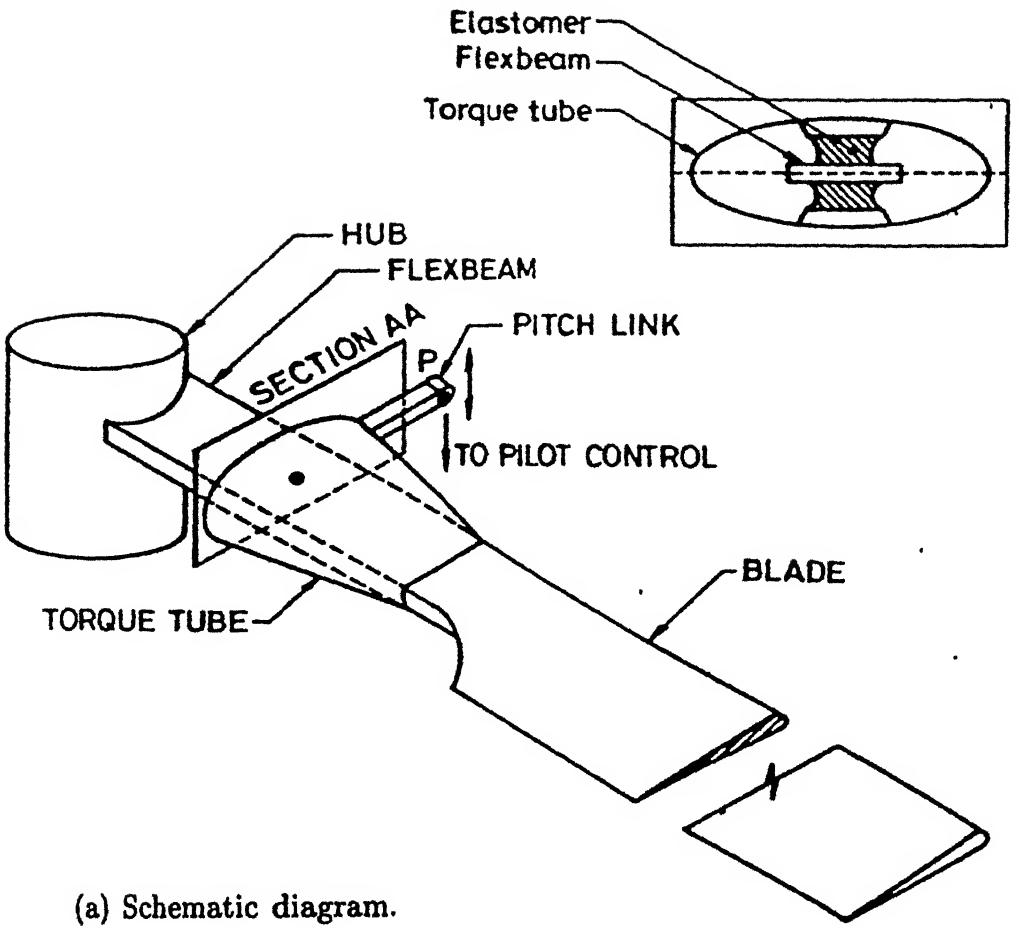

(a) Schematic diagram.

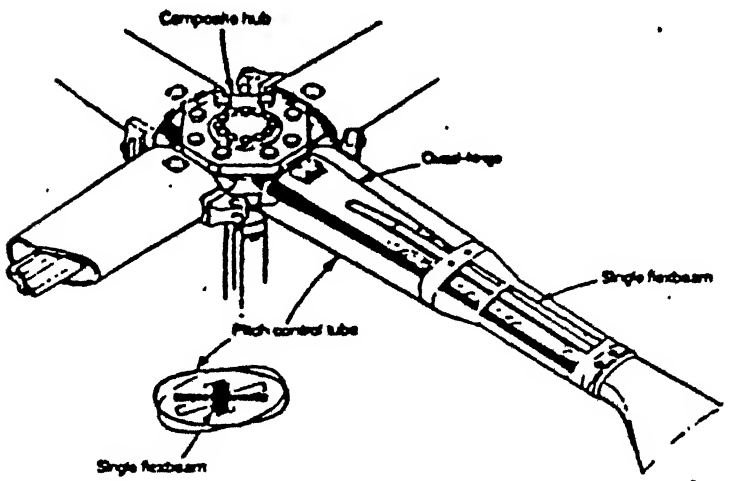

(b) Actual rotor hub (taken from Ref. [4]).

Fig 1.1 Bearingless rotor hub and Blade configuration

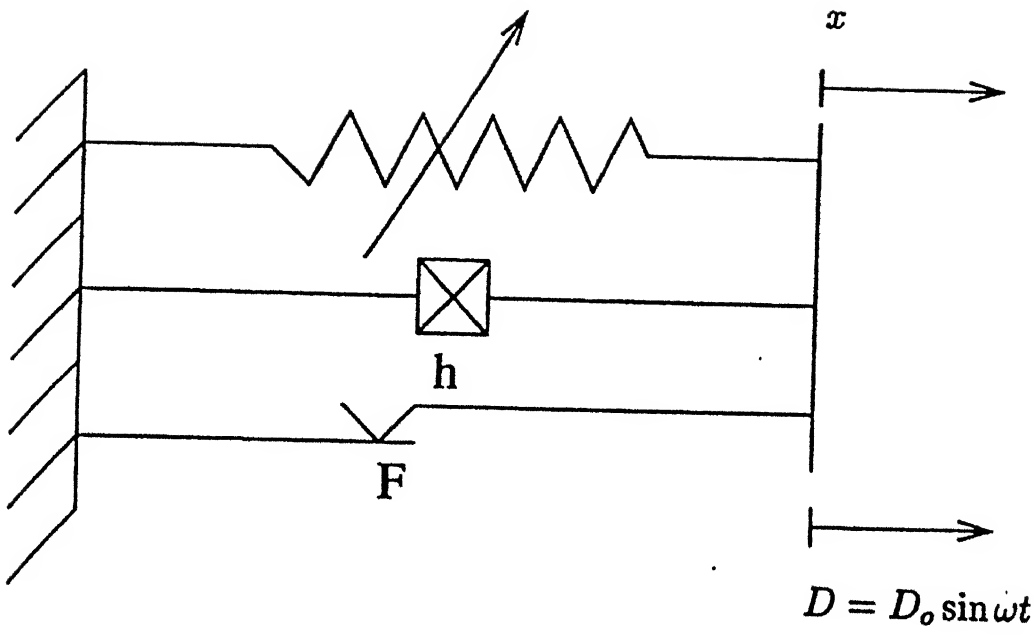

Fig. 1.2 Idealised elastomer model

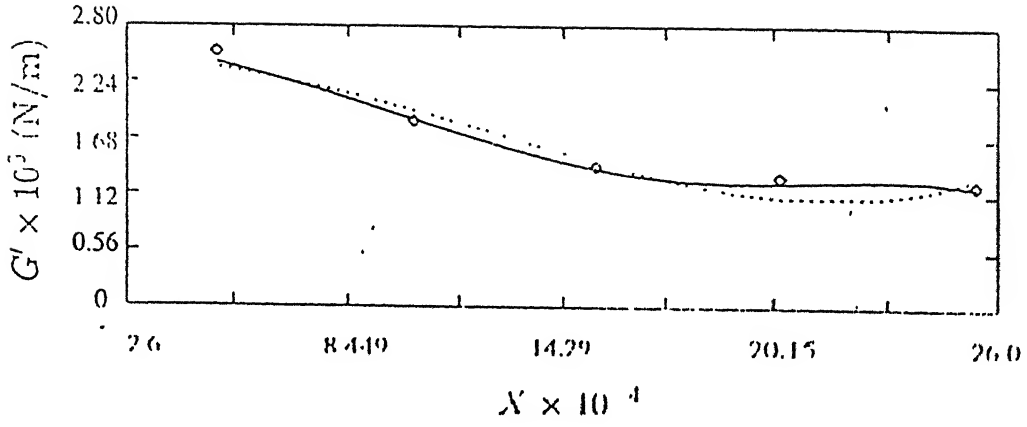

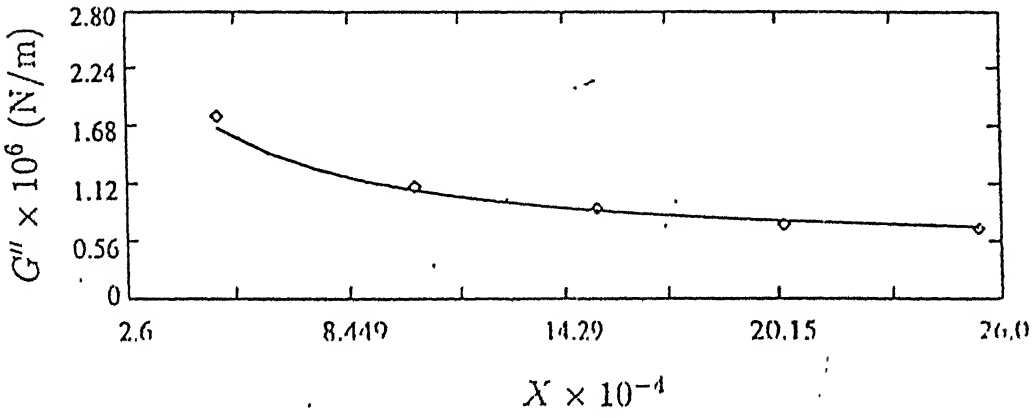

Fig 1.3 Variation of in-phase and quadrature stiffness, Ref. [5]

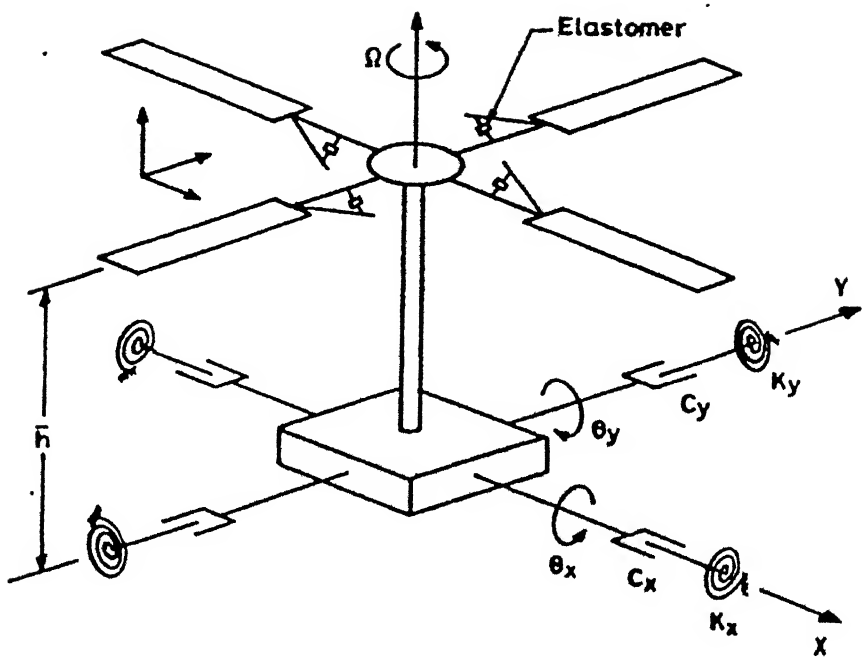

Fig. 1.4 Coupled rotor / fuselage model

CHAPTER 2

EQUATION OF MOTION

2.1 Ground Resonance Analysis

The aeromechanical stability of a helicopter is a complex phenomenon, involving coupling between the rotor and the body degrees of freedom. The rotor lead-lag regressive mode usually couples with the body pitch and/or body roll to cause the instability. When the helicopter is on the ground, such instability is referred to as ground resonance. In the case of bearingless rotor, the ground resonance is usually avoided by providing elastomeric damper to the rotor blade and damping in the landing gear.

The formulation of equation of motion presented in this chapter is for coupled rotor/fuselage system under ground resonance condition.

2.2 Bearingless Rotor Model:

An idealised model of the coupled rotor/fuselage system is shown in figure [1.4]. The blade is assumed to undergo only the lag motion. The elastomer is represented by non-linear spring and damping elements. The torque tube is assumed to be rigid and massless. The effect of pitch link in the lag mode is neglected. The hub is located at a height ($\bar{h}$) above the C.G. of the fuselage. The fuselage is allowed to undergo rigid body pitch and roll motions. The characteristics of the fuselage support (landing gear) are represented by a linear spring and a linear damper.

2.3 Formulation of the Elastomeric Damper Model:

The non-linear characteristic of an elastomeric material can be idealised by a combination of linear restoring and dissipative elements, since the static stress-strain

curve of an elastomeric material is non-linear. Figure [1.2] represents an idealized model consisting of a non-linear spring, a coulomb damper and hysteric damper. The reason for choosing a coulomb damper is that the damping force is very high at low amplitude. In addition, coulomb and hysteric dampers provide damping forces which are independent of frequency. This type of idealization differs form the model proposed by Gandhi *et. al* [30], in the sense that their model has viscous damping element.

The non-linear force-deformation relation of the spring is assumed to be of the form

$$F_S = K_1 x - K_3 x^3 + K_5 x^5 - K_7 x^7 \tag{2.1}$$

Where F_s is the force exerted by the restoring element under deformation x with K_1, K_3, K_5, and K_7 as positive constants. The constitutive differential equation of the elastomer model under external loading can be written as

$$K_1 x - K_3 x^3 + K_5 x^5 - K_7 x^7 + F \operatorname{sgn}|x| + \frac{h}{\omega}\dot{x} = \text{Externally applied force}$$

Numerical values of the system parameters of the elastomeric damper model are taken directly form Ref. [5] and is presented in table (2.1)

2.4 Formulation of Equation of Motion

Several assumptions have been made while formulating the equation of motion. These are:

i. The rotor blade is an Euler-Bernuolli beam made of homogenous isotropic material, and undergoing lag deformation.
ii. The torque tube and pitch link are rigid and massless elements (usually, the torque tube has a very high stiffness relative to that of the flexbeam or rotor blade section).
iii. Aerodynamic effects are not considered since emphasis is placed on the effect of non linearity of the elastomer on the ground resonance phenomenon.
iv. Effect of pitch link is neglected.

The dynamical equations of motion of the coupled rotor/ fuselage model consist of two sets of equations : one corresponding to the blade motion and the other

representing the motion of the fuselage. The equations of motion are derived using Hamilton" principle.

2.4.1 Blade Equation

The important ingredients required for the formulation of blade equations are:

(a) The kinetic energy of the blade.

(b) The strain energy of the blade.

(c) The strain energy associated with the elastomer.

(d) Dissipative energy associated with the elastomer.

2.4.1.1 Kinetic Energy of the Blade:

The kinetic energy of the k^{th} blade in an N-bladed rotor system can be written as

$$T(t)=\frac{1}{2}\int_0^L m\left[\left\{\frac{\partial \bar{u}}{\partial t}-\Omega\bar{v}+\frac{d\bar{x}}{dt}\cos\psi_k+\frac{d\bar{y}}{dt}\sin\psi_k\right\}^2 + \left\{\frac{\partial \bar{v}}{\partial t}+\Omega x+\Omega\bar{u}-\frac{d\bar{x}}{dt}\sin\psi_k+\frac{d\bar{y}}{dt}\cos\psi_k\right\}^2\right]dx \tag{2.2}$$

Where $\bar{x}(=\theta_y\bar{h})$ and $\bar{y}(=-\theta_x\bar{h})$ are the perturbational displacements of the hub centre due to fuselage motion in pitch and roll models, respectively. ψ_k is the azimuth angle of the K^{th} blade. $\bar{u}$ and $\bar{v}$ are the axial and in-plane displacements of the blade.

2.4.1.2 Strain Energy of the Blade due to Bending:

The Expression for strain energy due to bending is

$$U_1=\frac{1}{2}\int_0^L EI\left[\frac{\partial^2\bar{v}(x,t)}{\partial x^2}\right]^2 dx \tag{2.3}$$

2.4.1.3 Strain Energy Associated with the Elastomer:

The expression for the strain energy of the spring due to deformation Δ_l is

$$U_l=\frac{1}{2}k_1\Delta_l^2-\frac{1}{4}k_3\Delta_l^4+\frac{1}{6}k_s\Delta_l^6-\frac{1}{8}k_7\Delta_l^8 \tag{2.4}$$

where $\Delta_l=\left[v(L_2,t)-(L_2-L_1)\frac{\partial v((L_2,t)}{\partial x}-v(L_1,t)\right]$

2.4.1.4 Dissipative Energy Associated with the Elastomer:

The expression for the virtual work done by the dissipative (coulomb and hysteretic) elements of the elastomeric damper in the lag mode is given by

$$\delta W_d = F_d \delta \Delta_l \tag{2.5}$$

where Δ_l is the deformation of spring in lag mode

$$= \left[v(L_2,t) - (L_2 - L_1)\frac{\partial v(L_2,t)}{\partial x} - v(L_1,t) \right] \tag{2.6}$$

and

$$F_d = \frac{h}{\omega}\dot{\Delta}_l + F\,\mathrm{sgn}\left|\dot{\Delta}_l\right| \tag{2.7}$$

where h is the hysteretic damping coefficient

F is the coulomb damping coefficient

ω is the frequency, experimentally data fitted value, value taken is 3.3Hz.

2.4.2 Fuselage Equations

The in-plane (S_v) and the radial (S_r) forces at the root of the kth blade are given by

$$S_v = \int_0^L (-m\ddot{\bar{v}} + m\Omega^2 \bar{v})dx - (\ddot{\bar{x}}\sin\Psi_k + \ddot{\bar{y}}\cos\Psi_k)\int_0^L m dx \tag{2.8}$$

and

$$S_r = \int_0^L m\Omega^2 x dx - \int_0^L 2\Omega\dot{\bar{v}} m dx - (\ddot{\bar{x}}\cos\psi_k + \ddot{\bar{y}}\sin\psi_k)\int_0^L m dx \tag{2.9}$$

In-plane (S_v) and radial forces (S_r) can be re-written in non-dimensional form as given below;

<u>In-plane force:</u>

$$S_v = -m\Omega^2 L^2 [\int_0^1 \bar{\phi}_1(\xi)d\xi]\ddot{y}_{1k}(\tau) - (\ddot{\bar{x}}\sin\Psi_k - \ddot{\bar{y}}\cos\Psi_k)\cdot(mL)$$

Since

$$\bar{x} = \bar{h}\theta_y \text{ and } \bar{y} = -\bar{h}\theta_x$$

$$S_v = -m\Omega^2 L^2 [\int_0^1 \bar{\phi}_1(\xi)d\xi]\ddot{y}_{1k}(\tau) - \bar{h}\cdot(mL)\cdot\{\ddot{\theta}_y \sin\Psi_k + \ddot{\theta}_x \cos\Psi_k\} \qquad (2.8.a)$$

Radial force:

$$S_r = \frac{1}{2}(m\Omega^2 L^2) - 2(m\Omega^2 L^2)[\int_0^1 \bar{\phi}_1(\xi)d\xi]\dot{y}_{1k}(\tau) - \bar{h}\cdot(mL)\cdot\{\ddot{\theta}_y \cos\Psi_k - \ddot{\theta}_x \sin\Psi_k\}$$

(2.9.a)

The forces acting on the hub can be obtained by resolving the blade- root shear forces in the non-rotating frame and summing over all the N-blades, in our case N=4.

In X-direction:

$$PH_x = \sum_{K=1}^{4}(\cos\Psi_k S_r - \sin\Psi_k S_v)$$

On substituting the values from eq 2.8 (a) and 2.9(a) we get

$$PH_x = (-2m\Omega^2 L^2)\cdot[\int_0^1 \bar{\phi}_1(\xi)d\xi]\cdot[\cos\Psi_1 \dot{y}_{11} + \cos\Psi_2 \dot{y}_{12} + \cos\Psi_3 \dot{y}_{13} + \cos\Psi_4 \dot{y}_{14}$$
$$+ (m\Omega^2 L^2)\cdot[\int_0^1 \bar{\phi}_1(\xi)d\xi]\cdot[\sin\Psi_1 \ddot{y}_{11} + \sin\Psi_2 \ddot{y}_{12} + \sin\Psi_3 \ddot{y}_{13} + \sin\Psi_4 \ddot{y}_{14}]$$

In Y-direction:

$$PH_y = \sum_{K=1}^{4}(\sin\Psi_k S_r - \cos\Psi_k S_v)$$

On substituting the values from eq 2.8(a) and 2.9(a) we get

$$PH_y = (-2m\Omega^2 L^2)\cdot[\int_0^1 \bar{\phi}_1(\xi)d\xi]\cdot[\sin\Psi_1 \dot{y}_{11} + \sin\Psi_2 \dot{y}_{12} + \sin\Psi_3 \dot{y}_{13} + \sin\Psi_4 \dot{y}_{14}]$$
$$- (m\Omega^2 L^2)\cdot[\int_0^1 \bar{\phi}_1(\xi)d\xi]\cdot[\cos\Psi_1 \ddot{y}_{11} + \cos\Psi_2 \ddot{y}_{12} + \cos\Psi_3 \ddot{y}_{13} + \cos\Psi_4 \ddot{y}_{14}]$$

Considering the support structure as a combination of mass-spring-damper system having pitch and roll motions, equations of motion of the support can be written on balancing the moments in pitch and roll direction as

$$I\ddot{\theta}_x + C\dot{\theta}_x + K\theta_x = -PH_y \cdot \bar{h}$$

and

$$I\ddot{\theta}_y + C\dot{\theta}_y + K\theta_y = PH_x \cdot \bar{h}$$

On substituting the expressions for PH_x and PH_y the fuselage equation of motion can be written as

$$I_x\ddot{\theta}_x + C_x\dot{\theta}_x + K_x\theta_x = 2(\frac{\bar{h}J}{L})\{\sin\Psi_1\dot{y}_{11} + \sin\Psi_2\dot{y}_{12} + \sin\Psi_3\dot{y}_{13} + \sin\Psi_4\dot{y}_{14}\} + (\frac{\bar{h}J}{L})\{\cos\Psi_1\ddot{y}_{11} + \cos\Psi_2\ddot{y}_{12} + \cos\Psi_3\ddot{y}_{13} + \cos\Psi_4\ddot{y}_{14}\} \quad (2.10)$$

and

$$I_y\ddot{\theta}_y + C_y\dot{\theta}_y + K_y\theta_y = -2(\frac{\bar{h}J}{L})\{\cos\Psi_1\dot{y}_{11} + \cos\Psi_2\dot{y}_{12} + \cos\Psi_3\dot{y}_{13} + \cos\Psi_4\dot{y}_{14}\} + (\frac{\bar{h}J}{L})\{\sin\Psi_1\ddot{y}_{11} + \sin\Psi_2\ddot{y}_{12} + \sin\Psi_3\ddot{y}_{13} + \sin\Psi_4\ddot{y}_{14}\} \quad (2.11)$$

where,

I_x, I_y are non-dimensional mass moments of inertia of the support structure about the C.G. in roll and pitch modes, respectively.

$$I_x, I_y = \frac{I}{mL^2\bar{h}}$$

C_x, C_y are non-dimensional linear damping coefficients of the support structure in roll and pitch mode, respectively.

$$C_x, C_y = \frac{C}{m\Omega L^2\bar{h}}$$

K_x, K_y are non-dimensional stiffnesses of the support structure in roll and pitch modes, respectively.

$$K_x, K_y = \frac{K}{m\Omega^2 L^2\bar{h}}$$

and

$$\alpha_4 = J = \int_0^1 \bar{\phi}_1(\xi)d\xi$$

Ψ_k is the azimuth location of the K-th blade. Locations of all the four blades, for rotor/fuselage model, are given by

$$\Psi_k = \Psi + \frac{2\Pi(k-1)}{N} \qquad \text{K=1,2,3,4} \qquad (2.12)$$

first blade : $\Psi_1 = \Psi$

second blade : $\Psi_2 = \Psi + \frac{\Pi}{2}$

third blade : $\Psi_3 = \Psi + \Pi$

fourth blade : $\Psi_4 = \Psi + \frac{3\Pi}{2}$

The azimuth angle of each blade changes at every instant i.e., it is a function of time and is given by, in non-dimensional form, as

$$\Psi = \Omega t = \tau$$

2.4.3 Equations in Non-Dimensional Form:

The blade equations (2.2) to (2.7) and fuselage equations (2.10) and (2.11) are written in terms of the real time variable. These equations can be put into non-dimensional forms using the non-dimensional time (τ).

Introducing the following dimensionless quantities

$$\xi = \frac{x}{L}, \quad T = \Omega t, \quad \xi_i = \frac{L_j}{L} (j = 1,2)$$

$$v(x,t) = \frac{\bar{v}(x,t)}{L}$$

the non-dimensional lag deformation of the blade is assumed to be of the from :

$$v(\xi,\tau) = \sum_{i=1}^{n1} \bar{\phi}_i(\xi) y_{ik}(\tau) \qquad (2.13)$$

where $\bar{\phi}_i$ is the rotating mode shape of the kth blade, explained in section 2.5. n1 is the number of rotating modes. For the present study the value of n1 is taken as 1.The blade equations can be re-written as explained below.

2.4.3.1 Kinetic energy of the blade:

The kinetic energy of the blade is given in sec. 2.4.1.1. Assuming that the blade is very stiff in the axial direction, the following inextensionality condition is imposed :

$$\bar{u} = -\frac{1}{2}\int_0^x (\frac{\partial \bar{v}}{\partial x})^2 dx \tag{2.14}$$

On substituting the given inextensionality condition and stated dimenssionless quantities, kinetic energy of the blade in non-dimensional from can be written as

$$T(\tau) = \frac{1}{2}(mL)\int_0^1 \{-\Omega\int_0^x \{\bar{\phi}'_1(\xi)\}^2 y_{1k}(\tau)\dot{y}_{1k}(\tau)dx - \Omega L\bar{\phi}_1(\xi)y_{1k}(\tau) + \Omega\bar{h}\dot{\theta}_y\cos\Psi_k - \Omega\bar{h}\dot{\theta}_x\sin\Psi_k\}^2 + \{L\Omega\bar{\phi}_1(\xi)\dot{y}_{1k}(\tau) + \Omega x - \frac{\Omega}{2}\int_0^x \{\bar{\phi}'_1(\xi)y_{1k}(\tau)\}^2 dx - \Omega\bar{h}\dot{\theta}_y\sin\Psi_k - \Omega\bar{h}\dot{\theta}_x\cos\Psi_k\}^2 d\xi \tag{2.15}$$

2.4.3.2 Strain energy of the blade due to bending:

The strain energy of the blade is given in sec. 2.4.1.2. On using eq.(2.3), it can be re-written as

$$U_1 = \frac{1}{2}\int_0^1 (\frac{EI}{L})\{\bar{\phi}''_1(\xi)y_{1k}(\tau)\}^2 d\xi \tag{2.16}$$

where EI is the flexural rigidity of the blade.

2.4.3.3. Strain energy associated with elastomer:

The expression for the strain energy of the spring due to deformation Δ_l is given in sec 2.4.1.3. Using assumed lag mode deformation of the blade it can be written in non-dimensional form as

$$U_1 = \frac{1}{2}k_1\{L\hat{\Psi}_1^l Y_{1k}(\tau)\}^2 - \frac{1}{4}k_3\{L\hat{\Psi}_1^l Y_{1k}(\tau)\}^4 + \frac{1}{6}k_5\{L\hat{\Psi}_1^l Y_{1k}(\tau)\}^6 - \frac{1}{8}k_7\{L\hat{\Psi}_1^l Y_{1k}(\tau)\}^8 \tag{2.17}$$

Therefore, the spring deformation in lag mode (Δ_l) is written, using assumed lag deformation of the blade, as

$$\Delta_l = L[\{\bar{\phi}_1(\xi_2)Y_{1k}(\tau)\} - (\xi_2 - \xi_1)\{\bar{\phi}'_1(\xi_2)Y_{1k}(\tau)\} - \{\bar{\phi}_1(\xi_1)Y_{1k}(\tau)\}] \tag{2.18}$$

or,

$$\Delta_l = L\hat{\Psi}_1^{l} Y_{1k}(\tau)$$

where,

$$\hat{\Psi}_1^{l} = \hat{\phi}_1(\xi_2) - (\xi_2 - \xi_1)\hat{\phi}'_1(\xi_2) - \hat{\phi}_1(\xi_1) \tag{2.19}$$

The quantity $\hat{\Psi}_1^{l}$ can be interpreted as normalized deformation of the spring in the first lag mode.

2.4.3.4. Dissipated energy associated with elastomer:

In non-dimensional from it can be written as

$$W_d = \{\frac{h}{\omega}\dot{\Delta}_l + F\,\mathrm{sgn}\,|\,\dot{\Delta}_l\,|\}.\Delta_l$$

or

$$W_d = \{\frac{h}{\omega}(\Omega L\hat{\Psi}_1^{l} Y_{1k}(\tau)) + F\,\mathrm{sgn}\,|\,\Omega L\hat{\Psi}_1^{l}\dot{Y}_{1k}(\tau)\,|\}.\{L\hat{\Psi}_1^{l} Y_{1k}(\tau)\} \tag{2.20}$$

Introducing equations (2.15) to (2.20) into variational principle

$$\delta\int_{t1}^{t2}(T - U_L - U_1 + W_d)dt = 0 \tag{2.21}$$

and collecting all the terms, we obtain.

$$\{-y_{1k}^2(\tau)\ddot{y}_{1k}(\tau) - y_{1k}(\tau)\dot{y}_{1k}^2(\tau)\}(\alpha_1) + \{y_{1k}(\tau) - \dot{y}_{1k}(\tau)\}(\alpha_2) +$$

$$(\frac{\bar{h}}{L})\{\ddot{\theta}_Y\cos\Psi_k y_{1k}(\tau) - \ddot{\theta}_x\sin\Psi_k y_{1k}(\tau)\}(\alpha_3) - \{y_{1k}(\tau)\}(\alpha_5) +$$

$$\{y_{1k}^3(\tau)\}(\frac{\alpha_1}{2}) + (\frac{\bar{h}}{L})\{\ddot{\theta}_x\cos\Psi_k + \ddot{\theta}_Y\sin\Psi_k\}(\alpha_4)$$

$$-\frac{K_1(\hat{\Psi}_1^{l})^2}{m\Omega^2 L}\{y_{1k}(\tau)\} + \frac{K_3 L}{m\Omega^2}(\hat{\Psi}_1^{l})^4\{y_{1k}^3(\tau)\}$$

$$-\frac{K_5 L^3}{m\Omega^2}(\hat{\Psi}_1^{l})^6\{y_{1k}^5(\tau)\} + \frac{K_7 L^5}{m\Omega^2}(\hat{\Psi}_1^{l})^8\{y_{1k}^7(\tau)\}$$

$$+\frac{h}{m\Omega\omega L}(\hat{\Psi}_1^{l})^2\{\dot{y}_{1k}(\tau)\} + \frac{F\hat{\Psi}_1^{L}}{m\Omega^2 L^2}\{\mathrm{sgn}\,|\,\Omega L\hat{\Psi}_1^{l}\dot{y}_{1k}(\tau)\,|\}$$

$$-\frac{EI}{m\Omega^2 L^4}\{y_{1k}(\tau)\}(\alpha_6) = 0$$

where

$$\alpha_1 = \int_0^1 [\int_0^x \{\bar{\phi'}_1(\xi)\}^2 dx].[\int_0^x \{\bar{\phi'}_1(\xi)\}^2] d\xi$$

$$\alpha_2 = \int_0^1 \{\bar{\phi}_1(\xi)\}^2 d\xi$$

$$\alpha_3 = \int_0^x \{\bar{\phi}_1'(\xi)\}^2 dx] d\xi$$

$$\alpha_4 = \int_0^1 \bar{\phi}_1(\xi) d\xi$$

$$\alpha_5 = \int_0^1 [x].[\int_0^x \{\bar{\phi}_1'(\xi)\}^2 dx] d\xi$$

$$\alpha_6 = \int_0^1 \{\bar{\phi}_1'(\xi)\}^2 dx] d\xi$$

On rearranging the terms, we get four second order coupled non-linear differential equations which govern the behavior of the corresponding blade as follows:

$$\ddot{y}_{1k} = \frac{1}{(\alpha_2 + \alpha_1 y_{1k}^2)} [(a_1)\{\text{sgn} \mid \Omega L \hat{\Psi}_1^l \dot{y}_{1k} \mid\} + (b_1)\{\dot{y}_{1k}\} - (i_1)\{y_{1k} \dot{y}_{1k}^2\}$$

$$+ (h_1)\{\dot{y}_{1k}^3\} + (\alpha_2 - \alpha_5 - l_1 - d_1)\{\dot{y}_{1k}\} + (e_1)\{y_{1k}^3\} - (f_1)\{y_{1k}^5\} + (g_1)\{y_{1k}^7\} +$$

$$(m_1)\{\ddot{\theta}_x \cos\Psi_k + \ddot{\theta}_y \sin\Psi_k\} + (j_1)\{\ddot{\theta}_y \cos\Psi_k y_{1k} - \ddot{\theta}_x \sin\Psi_k y_{1k}\}]$$

for k=1 to 4 (2.22)

Thus, for the coupled rotor / fuselage model we have a set of six second order non-linear differential equations, which have to be integrated in time domain in order to analyze the time development of various degrees-of-freedom.

The non-dimensional coefficients used in eq (2.22) are

$$a_1 = \frac{F \hat{\Psi}_1^l}{m\Omega^2 L^2}$$

$$b_1 = \frac{h(\hat{\Psi}_1^l)^2}{m\Omega\omega L}$$

$$i_1 = \alpha_1$$

$$h_1 = \frac{\alpha_1}{2}$$

$$l_1 = \frac{EI(\alpha_6)}{m\Omega^2 L^4}$$

$$d_1 = \frac{k_1(\hat{\Psi}_1^{\,l})^2}{m\Omega^2 L}$$

$$e_1 = \frac{K_1(\hat{\Psi}_1^{\,l})^4}{m\Omega^2}$$

$$f_1 = \frac{K_5 L^3(\hat{\Psi}_1^{\,l})^6}{m\Omega^2}$$

$$g_1 = \frac{K_7 L^3(\hat{\Psi}_1^{\,l})^8}{m\Omega^2}$$

$$m_1 = (\frac{\bar{h}}{L})(\alpha_4) = \beta$$

$$j_1 = (\frac{\bar{h}}{L})(\alpha_3)$$

Equations are arranged in the from

$$[\bar{M}]\{\ddot{y}\} + [\bar{C}]\{\dot{y}\} + [\bar{K}]\{y\} + \{F_{NL}(y, \dot{y}, \ddot{y})\} = 0 \qquad (2.23)$$

where $[\bar{M}]$, $[\bar{C}]$ and $[\bar{K}]$ denote the mass, spring and stiffness matrices, respectively.

The vector {y} represents the degrees of freedom, i.e.,

$$\{y\} = \{y_{11} \quad y_{12} \quad y_{13} \quad y_{14} \quad \theta_x \quad \theta_y\}^T$$

Vector $\{F_{NL}(y, \dot{y}, \ddot{y})\}$ includes the non-linear term.

$[\bar{M}]$ is given by

$$[\bar{M}] = \begin{bmatrix} -\alpha_2 & 0 & 0 & 0 & \beta\cos\Psi_1 & \beta\sin\Psi_1 \\ 0 & -\alpha_2 & 0 & 0 & \beta\cos\Psi_2 & \beta\sin\Psi_2 \\ 0 & 0 & -\alpha_2 & 0 & \beta\cos\Psi_3 & \beta\sin\Psi_3 \\ 0 & 0 & 0 & -\alpha_2 & \beta\cos\Psi_4 & \beta\sin\Psi_4 \\ \beta\cos\Psi_1 & \beta\cos\Psi_2 & \beta\cos\Psi_3 & \beta\cos\Psi_4 & -I_x & 0 \\ \beta\sin\Psi_1 & \beta\sin\Psi_2 & \beta\sin\Psi_3 & \beta\sin\Psi_4 & 0 & -I_y \end{bmatrix}$$

Where $\beta = (\frac{\bar{h}}{L}) \int_0^i \bar{\phi}(\xi) d\xi$ (2.24)

Damping matrix is given by

$$[\bar{C}] = \begin{bmatrix} \frac{h}{m\Omega wL}(\hat{\Psi}_1^{\,l})^2 + \frac{F\hat{\Psi}_1^{\,L}}{m\Omega^2 L^2}\text{sgn}\,|\Omega L\hat{\Psi}_1^{\,L}\dot{y}_{11}| & 0 & 0 & 0 & 0 & 0 \\ 0 & \frac{h}{m\Omega wL}(\hat{\Psi}_1^{\,l})^2 + \frac{F\hat{\Psi}_1^{\,L}}{m\Omega^2 L^2}\text{sgn}\,|\Omega L\hat{\Psi}_1^{\,L}\dot{y}_{12}| & 0 & 0 & 0 & 0 \\ 0 & 0 & \frac{h}{m\Omega wL}(\hat{\Psi}_1^{\,l})^2 + \frac{F\hat{\Psi}_1^{\,L}}{m\Omega^2 L^2}\{\text{sgn}\,|\Omega L\hat{\Psi}_1^{\,L}\dot{y}_{13}| & 0 & 0 & 0 \\ 0 & 0 & 0 & b_1 + a_1\,\text{sgn}\,|\Omega L\hat{\Psi}_1^{\,L}\dot{y}_{14}| & 0 & 0 \\ 2\beta\sin\psi_1 & 2\beta\sin\psi_2 & 2\beta\sin\psi_3 & 2\beta\sin\psi_4 & -C_x & 0 \\ -2\beta\cos\psi_1 & -2\beta\cos\psi_2 & -2\beta\cos\psi_3 & -2\beta\cos\psi_4 & 0 & -C_y \end{bmatrix}$$

(2.25)

Stiffness matrix is given by

$$[\bar{k}] = \begin{bmatrix} \alpha_2 - \alpha_5 - d_1 - l_1 & 0 & 0 & 0 & 0 & 0 \\ 0 & \alpha_2 - \alpha_5 - d_1 - l_1 & 0 & 0 & 0 & 0 \\ 0 & 0 & \alpha_2 - \alpha_5 - d_1 - l_1 & 0 & 0 & 0 \\ 0 & 0 & 0 & \alpha_2 - \alpha_5 - d_1 - l_1 & 0 & 0 \\ 0 & 0 & 0 & 0 & -K_x & 0 \\ 0 & 0 & 0 & 0 & 0 & -K_y \end{bmatrix}$$

(2.26)

$$\alpha_2 - \alpha_5 - d_1 - l_1 =$$

$$\int_0^1 \{\bar{\phi}_1(\xi)\}^2 d\xi - \int_0^1 \{x\} \cdot [\int_0^x \{\bar{\phi}'_1(\xi)\}^2 dx] d\xi - \frac{K_1(\hat{\psi}_1^l)^2}{m\Omega^2 L} - \left(\frac{EI}{m\Omega^2 L^4}\right) \int_0^1 \{\bar{\phi}''_1(\xi)\}^2 d\xi$$

The vector representing the non-linear term is given by

$$\{F_{NL}(y, \dot{y}, \ddot{y})\} =$$

$$\begin{bmatrix}
(\alpha_1)\{-y_{11}^2 \ddot{y}_{11} - y_{11} \dot{y}_{11}^2\} + (\eta)\{\ddot{\theta}_y \cos\psi_1 y_{11} - \ddot{\theta}_x \sin\psi_1 y_{11}\} + (\frac{a_1}{2})\{y_{11}^3\} + (e_1)\{y_{11}^3\} - (f_1)\{y_{11}^5\} + (g_1)\{y_{11}^7\} \\
(\alpha_1)\{-y_{12}^2 \ddot{y}_{12} - y_{12} \dot{y}_{12}^2\} + (\eta)\{\ddot{\theta}_y \cos\psi_2 y_{12} - \ddot{\theta}_x \sin\psi_2 y_{12}\} + (\frac{a_1}{2})\{y_{12}^3\} + (e_1)\{y_{12}^3\} - (f_1)\{y_{12}^5\} + (g_1)\{y_{12}^7\} \\
(\alpha_1)\{-y_{13}^2 \ddot{y}_{13} - y_{13} \dot{y}_{13}^2\} + (\eta)\{\ddot{\theta}_y \cos\psi_3 y_{13} - \ddot{\theta}_x \sin\psi_3 y_{13}\} + (\frac{a_1}{2})\{y_{13}^3\} + (e_1)\{y_{13}^3\} - (f_1)\{y_{13}^5\} + (g_1)\{y_{13}^7\} \\
(\alpha_1)\{-y_{14}^2 \ddot{y}_{14} - y_{14} \dot{y}_{14}^2\} + (\eta)\{\ddot{\theta}_y \cos\psi_4 y_{14} - \ddot{\theta}_x \sin\psi_4 y_{14}\} + (\frac{a_1}{2})\{y_{14}^3\} + (e_1)\{y_{14}^3\} - (f_1)\{y_{14}^5\} + (g_1)\{y_{14}^7\} \\
0 \\
0
\end{bmatrix} \tag{2.27}$$

where $\eta = (\frac{\bar{h}}{L}) \int_0^1 [\int_0^x \{\phi_1'(\xi)\}^2 dx] d\xi$

2.5 Rotating Mode Shape ($\bar{\phi}_i$):

Using Ref. [5], the comparison function used for the solution is

$$\hat{\phi}_i(\xi) = \xi^i [\frac{(i+2)(i+3)}{6}\xi - \frac{i(i+3)}{3}\xi^2 + \frac{i(i+1)}{6}\xi^3] \tag{2.28}$$

Using data given in table (2.2) the rotating mode shape is obtained as

$$\bar{\phi}_i(\xi) = \sum_{i=1}^{ND} a_i \hat{\phi}_i(\xi) \tag{2.29}$$

where ND is the number of data points. On normalizing, the rotating mode shape in lag motion for the first log mode is given by

$$\begin{aligned}
\bar{\phi}_i(\xi) = {} & 2.779429\xi^2 + 2.486567\xi^3 - 51.667119\xi^4 + 173.865540\xi^5 \\
& - 248.239771\xi^6 + 119.209239\xi^7 + 36.689602\xi^8 + 57.729132\xi^9 \\
& - 275.708214\xi^{10} + 376.62177\xi^{11} - 430.849056\xi^{12} + 528.113695\xi^{13} \\
& - 472.708624\xi^{14} + 370.175502\xi^{15} - 670.940371\xi^{16} + 978.500923\xi^{17} \\
& - 658.407224\xi^{18} + 163.348979\xi^{19}
\end{aligned} \tag{2.30}$$

This can be used in the blade equations to evaluate the integrals.

System Parameters	Seventh Order Approximation
K_1 (N/m)	2.673989×10^6
K_3 (N/m^3)	1.315287×10^{12}
K_5 (N/m^5)	3.519586×10^{17}
K_7 (N/m^7)	3.176266×10^{22}
F (N)	4.797347×10^2
h (N/m)	4.569120×10^5

Table 2.1 System Parameters of the elastomeric damper model.

a_1	- 0.054210
a_2	- 0.050783
a_3	0.372845
a_4	- 0.642042
a_5	0.315563
a_6	0.141461
a_7	- 0.030847
a_8	- 0.216103
a_9	0.213805
a_{10}	- 0.169271
a_{11}	0.206519
a_{12}	- 0.197030
a_{13}	0.051855
a_{14}	- 0.126215
a_{15}	0.286001
a_{16}	- 0.140557

Table 2.2 Coefficients a_i's for the rotating mode shape, in 1st lag mode with $\omega_n = 0.7773$, from Ref. [6]

CHAPTER 3

SOLUTION PROCEDURE AND TIME DOMAIN INTEGRATION

This chapter describes the methodology used for solving the non-linear ordinary coupled differential equations, representing coupled rotor-body dynamics, in time domain. The Time Domain Integration approach provides the transient response behavior of blades and fuselage with time.

This chapter is divided into three sections, which deals with, respectively

i) Solution procedure, for solving the coupled blade and fuselage equations using numerical integration technique at every time step.

ii) Multiblade coordinate transformation.

iii) Formulation of an index to measure the rate of convergence (stability) or divergence (instability) of the system for the prescribed operating and initial conditions.

3.1 Solution Procedure

The amplitude-dependent stability analysis of a coupled rotor/fuselage system is obtained by simultaneously solving the non-linear coupled equations by numerical integration technique in time domain at every time step.

It can be seen from equations written in the matrix form in section 2.4.3, that the mass matrix $[\overline{M}]$ is time-dependent. Thus, in order to find vector {Y} which represents the system degree of freedom the $[\overline{M}]$ has to be inverted at every time step.

The blade and fuselage equations are solved simultaneously by a numerical integration routine (NAG)- D02BBF based on Runge-Kutta-Marson algorithm for

prescribed initial conditions. Blades data are taken from Ref. [1] and are presented in table (3.1).

The response of the system has been evaluated for various combinations of rotor rpm and magnitude of initial condition (disturbance).

To check the validity of the time step, time integration was carried out with two time steps viz., $\Delta t = 0.0015$ sec. and $\Delta t = 0.003$ sec. (real time), both the results are found to converge to the same value. Hence, in all subsequent computations, a real time step of $\Delta t = 0.003$ sec. is used. The results are produced for $\xi_1 = 0.1$ and $\xi_2 = 0.25$. In order to study the effect of support damping, the same procedure is repeated one with support damping and the other without support damping.

3.2 Multiblade Coordinate Transformation

For an N-bladed rotor with blades evenly spaced around, the azimuth angle for the k^{th} blade, at any instant, can be written as

$$\psi_k = \psi + \frac{2\pi}{N}(k-1) \qquad k = 1,2,3 \ldots\ldots N \tag{3.1}$$

where $\psi = \Omega t$, the non-dimensional time variable.

Let Y_{1k} be a generalized coordinate associated with any degree of freedom of the k^{th} blade. Since this Y_{1k} is associated with the blade, which is rotating, it is called a rotating coordinate. If there are N blades then there will be N rotating coordinates. By suitably choosing a transformation these N rotating coordinates can be transformed into another set of N coordinates, each of which is associated with the motion of the rotor disk as viewed from a non-rotating frame. This type of transformation is denoted as Multiblade Coordinate Transformation. Basically, this transforms the rotating coordinates into a non-rotating frame, which is obtained by the following operations.

Collective operator : $$Y_C = \frac{1}{N}\sum_{k=1}^{N} Y_{1k} \tag{3.2}$$

Alternating operator : $$Y_A = \frac{1}{N}\sum_{k=1}^{N} (-1)^k Y_{1k} \tag{3.3}$$

1-Cosine operator : $$Y_{1C} = \frac{1}{N}\sum_{k=1}^{N} (\cos\psi_k) Y_{1k} \tag{3.4}$$

1-Sine operator : $$Y_{1S} = \frac{1}{N}\sum_{k=1}^{N}(\sin\psi_k)Y_{1k} \quad (3.5)$$

In our case, N = 4. Knowing the time response of each blade degree of freedom, one can easily obtain the time response of rotor degrees of freedom.

3.3 Measure Of Instability

The objective is to formulate an index, which measures the rate of divergence (instability) or convergence (stable response) and to correlate this index with the operating and/or initial condition

Following procedure is adopted, to obtain the index:

In the divergent case, the non-dimensional time at which the response of the blades and/or fuselage becomes double of the given initial disturbance, is taken as the index. This is explained in figure [3.1].

In the convergent case, the non-dimensional time at which the response of the blades and/or fuselage reaches $1/10^{th}$ of the given initial disturbance, is taken as the index. This is explained in figure [3.2].

A 3-D plot has been generated with rotor rpm and amplitude as the variables in order to study the correlation between the two on the system response.

Blade Data:	
mass per unit Length, m	9.7 Kg/m
Length, L	6.6 m
$\overline{a}\left(=\frac{EI}{m\Omega^2 L^4}\right)$	0.0301
Rotor angular velocity, Ω	32.8 rad/s
Non-dimensional fuselage data:	
mass moment of inertia (roll), Ix	1.0511
mass moment of inertia (pitch), Iy	3.1023
$\xi_h = \frac{\overline{h}}{L}$	0.2
$\omega_x = (\frac{K_x}{I_x})^{1/2}$ (roll)	$(\frac{4}{\Omega})2\pi$
$\omega_y = (\frac{K_y}{I_y})^{1/2}$ (pitch)	$(\frac{2}{\Omega})2\pi$
$C_x = 2\,\xi_{\theta x}\omega_x$, $C_y = 2\,\xi_{\theta y}\omega_y$	

Table 3.1 Blade and non-dimensional fuselage input data for ground resonance analysis

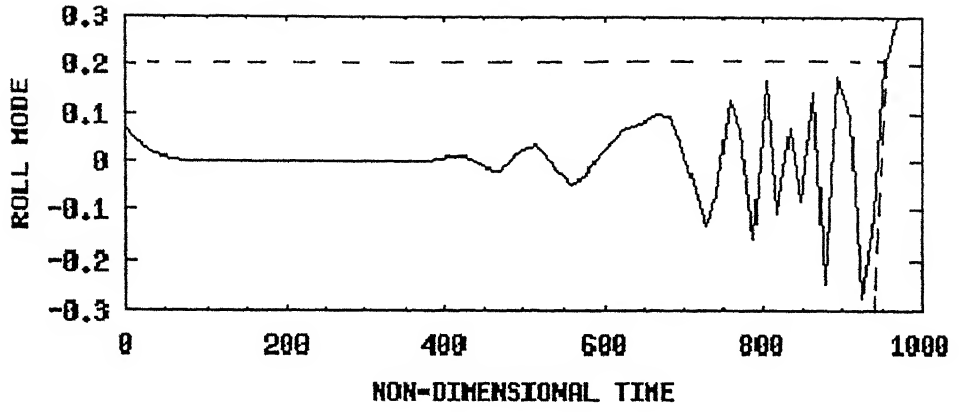

Fig 3.1 INDEX FOR MEASURE OF INSTABILITY

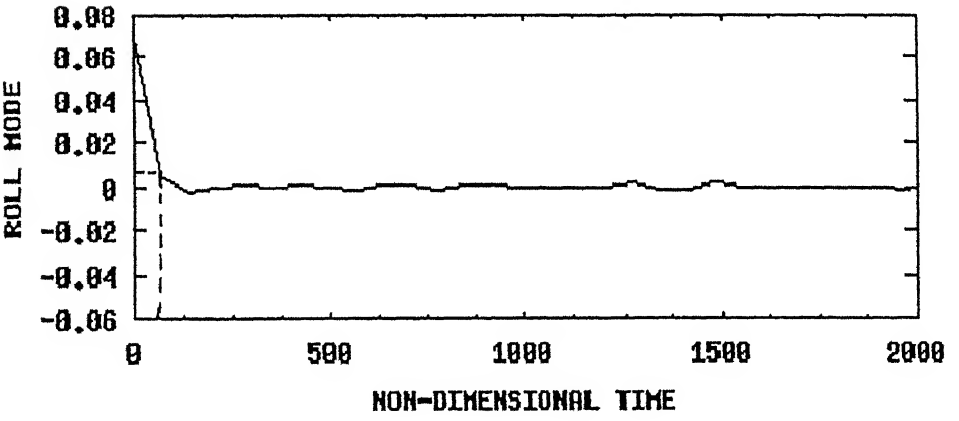

Fig 3.2 INDEX FOR MEASURE OF STABILITY

Chapter 4

RESULTS

The transient response analysis is carried out to examine the behavior of coupled rotor/fuselage system in time, for prescribed operating (rotor rpm) and initial conditions.

The response analysis has been carried for two cases, namely, system with support damping and without support damping. The results are presented in the following sections.

4.1 With support damping

For the baseline configuration the location of elastomer and torque tube are ξ_1= 0.1 and ξ_2= 0.25, respectively. The damping ratios in the pitch and roll modes are $\zeta_{\theta x}$= 0.082, $\zeta_{\theta y}$=0.0529.

The results are generated for a range of rotor r.p.m. and initial disturbance in roll mode. The r.p.m. range is 250 r.p.m. to 700 r.p.m. The roll input is in the range $\theta_x(0)$= 0.1 degree to 10 degree. The initial conditions corresponding to other degrees of freedom are taken as zero, for all the cases.

The qualitative nature of response of the system to initial disturbance is shown in Table 4.1. The table indicates the region of instability in both r.p.m. and initial disturbances in θ_x . The effect of non-linearity of the elastomer is to introduce an amplitude dependent instability, which can be clearly seen for the cases corresponding to rotor r.p.m., 450-640. At 450 r.p.m., the system is stable for initial disturbance $\theta_x(0) \leq$ 4 degrees and it is unstable for $\theta_x(0) \geq$ 6 degrees.

The time response of the individual blade and fuselage degrees of freedom are shown in fig. [4.1] to [4.12)] respectively for rotor r.p.m. 250,350,400,450,460,550,640 and 700.

Figures [4.1] and [4.2] show the response of all the degrees of freedom in the stable zone of operating condition (250,350 r.p.m.) and initial condition, $\theta_x(0)$= 4 degree,6 degree, respectively.

For 450 r.p.m., the results corresponding to four cases $\theta_x(0)$= (0.8deg.,4deg.,6deg. and 10deg.) are shown in figures [4.3] to [4.6].

Figures 4.7 to 4.8 shows the response of all the degrees of freedom for 460 rpm and it is observed that system is stable for initial disturbance $\theta_x(0) \leq$ 1 degree and it is unstable for $\theta_x(0) \geq$ 2 degree.

Maximum instability is seen for 550 rotor r.p.m., figure [4.9].

At 640 r.p.m., the system is stable for initial disturbance $\theta_x(0) \leq$ 4 degree and it is stable for $\theta_x(0) \geq$ 6 degree, shown in figure [4.10] and [4.11].

Figure [4.12] shows the response of all the degrees of freedom for operating condition 700 r.p.m., and initial condition $\theta_x(0)$= 4 degree and it is observed that the system gets stable at higher value of initial disturbance also.

4.2 Without support damping

For the system without support damping, nature of response of the system to initial disturbance is shown in Table 4.2. System response shows a similar behavior except for the short range of rotor r.p.m.,350r.p.m. At 350r.p.m., the system is stable for initial disturbance $\theta_x(0) \leq$ 4degree and it is unstable for $\theta_x(0) \geq$ 6 degree.

4.3 Multiblade Coordinate Transfomation

In order to study the behavior of rotors degree of freedom, blade degrees of freedom has been transformed and the response of blades in collective, alternating cosine-cyclic and sine-cyclic modes are presented for following three cases,

(a) 250 rpm, $\theta_x(0)$= 4 degrees (stable zone)

(b) 550 rpm, $\theta_x(0)$= 4 degrees (unstable zone)

(c) 700 rpm, $\theta_x(0)$= 4 degrees (stable zone)

Figure [4.23]- [4.25] explains the behavior of rotor blades in the transformed coordinates.

4.4 Measure of instability

Figures [4.1] and [4.2] show the response of all the degrees of freedom in the stable zone of operating condition (250,350 r.p.m.) and initial condition, $\theta_x(0)$= 4 degree,6 degree, respectively.

For 450 r.p.m., the results corresponding to four cases $\theta_x(0)$= (0.8deg.,4deg.,6deg. and 10deg.) are shown in figures [4.3] to [4.6].

Figures 4.7 to 4.8 shows the response of all the degrees of freedom for 460 rpm and it is observed that system is stable for initial disturbance $\theta_x(0) \leq$ 1 degree and it is unstable for $\theta_x(0) \geq$ 2 degree.

Maximum instability is seen for 550 rotor r.p.m., figure [4.9].

At 640 r.p.m., the system is stable for initial disturbance $\theta_x(0) \leq$ 4 degree and it is stable for $\theta_x(0) \geq$ 6 degree, shown in figure [4.10] and [4.11].

Figure [4.12] shows the response of all the degrees of freedom for operating condition 700 r.p.m., and initial condition $\theta_x(0)$= 4 degree and it is observed that the system gets stable at higher value of initial disturbance also.

4.2 Without support damping

For the system without support damping, nature of response of the system to initial disturbance is shown in Table 4.2. System response shows a similar behavior except for the short range of rotor r.p.m.,350r.p.m. At 350r.p.m., the system is stable for initial disturbance $\theta_x(0) \leq$ 4degree and it is unstable for $\theta_x(0) \geq$ 6 degree.

4.3 Multiblade Coordinate Transfomation

In order to study the behavior of rotors degree of freedom, blade degrees of freedom has been transformed and the response of blades in collective, alternating cosine-cyclic and sine-cyclic modes are presented for following three cases,

(a) 250 rpm, $\theta_x(0)$= 4 degrees (stable zone)

(b) 550 rpm, $\theta_x(0)$= 4 degrees (unstable zone)

(c) 700 rpm, $\theta_x(0)$= 4 degrees (stable zone)

Figure [4.23]- [4.25] explains the behavior of rotor blades in the transformed coordinates.

4.4 Measure of instability

A 3-D plot has been generated in order to study the correlation between the rate of convergence/divergence with the rotor rpm and initial disturbance in roll direction. From figure [4.26] it is seen that

(1) the rate of divergence is maximum around 550 rpm.

(2) slope of the surface first decreases upto 600 rpm and then starts increasing for higher degree.

A similar plot is shown for stable case also in figure [4.27].

4.5 Validation

The result obtained from time domain integration approach matches well with the range predicted by the linearized stability analysis. Maximum instability is also seen at 550 rpm . A short range of instability occurs at 350 rpm and $\theta_x(0) \geq 6$ degree for zero damping case . Results so obtained from the time integration approach for the non-linear system matches fairly well with the results produced in Ref. [5].

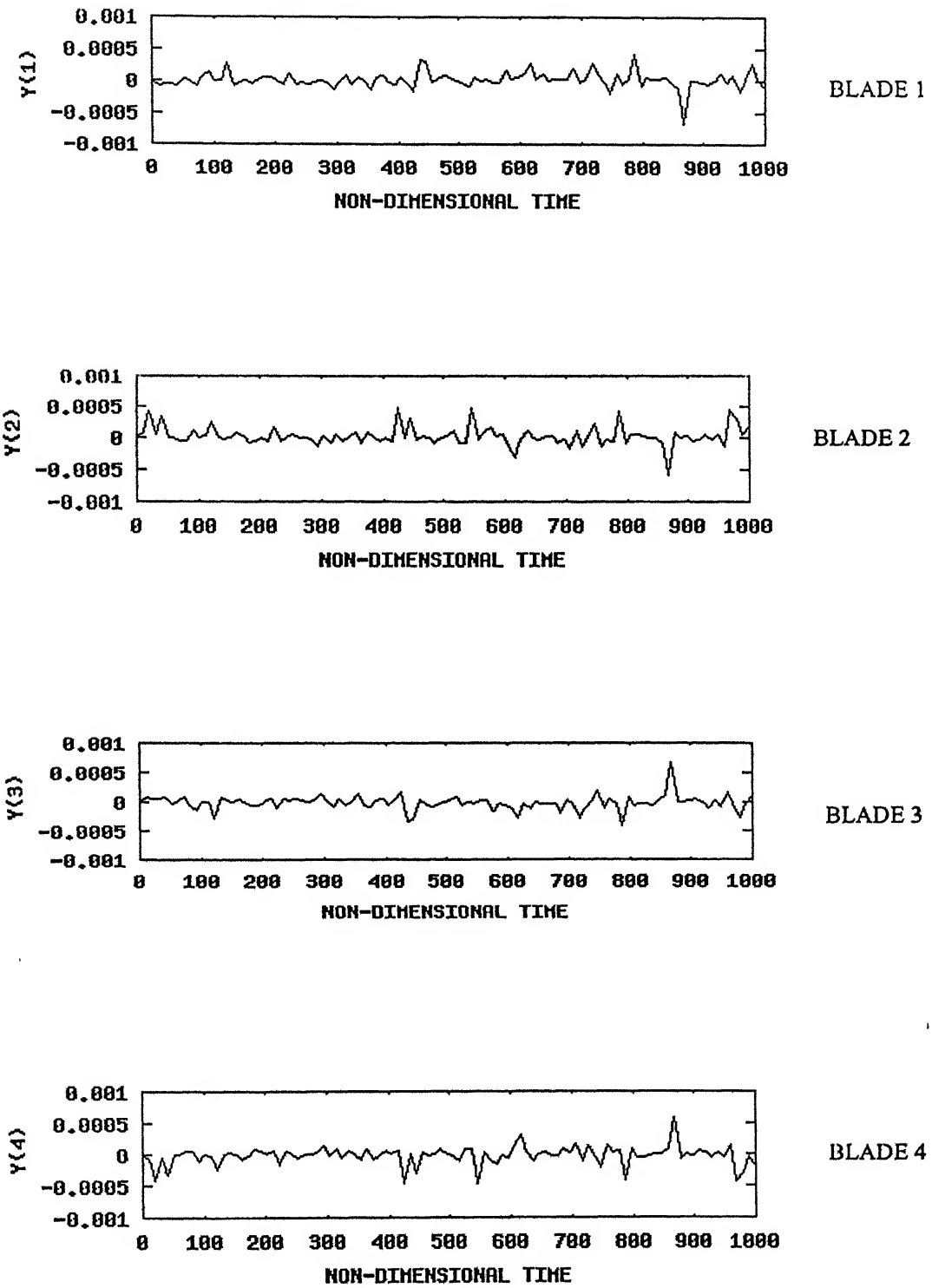

Fig. 4.1(a) Blade response in non-dimensional time domain

250 rpm, $\theta_X(0) = 4$ degree, ($\zeta_{0X} = 0.082$, $\zeta_{0Y} = 0.0529$)

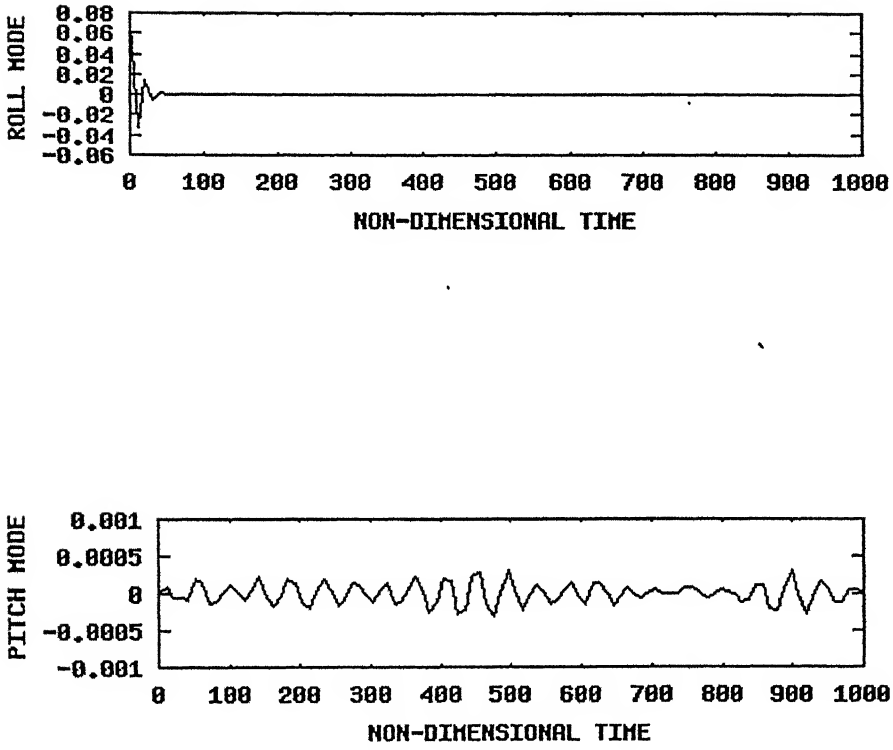

Fig. 4.1(b) Fuselage motion in non-dimensional time domain

250 rpm , $\theta_X(0) = 4$ degree, ($\zeta_{\theta X} = 0.082$, $\zeta_{\theta Y} = 0.0529$)

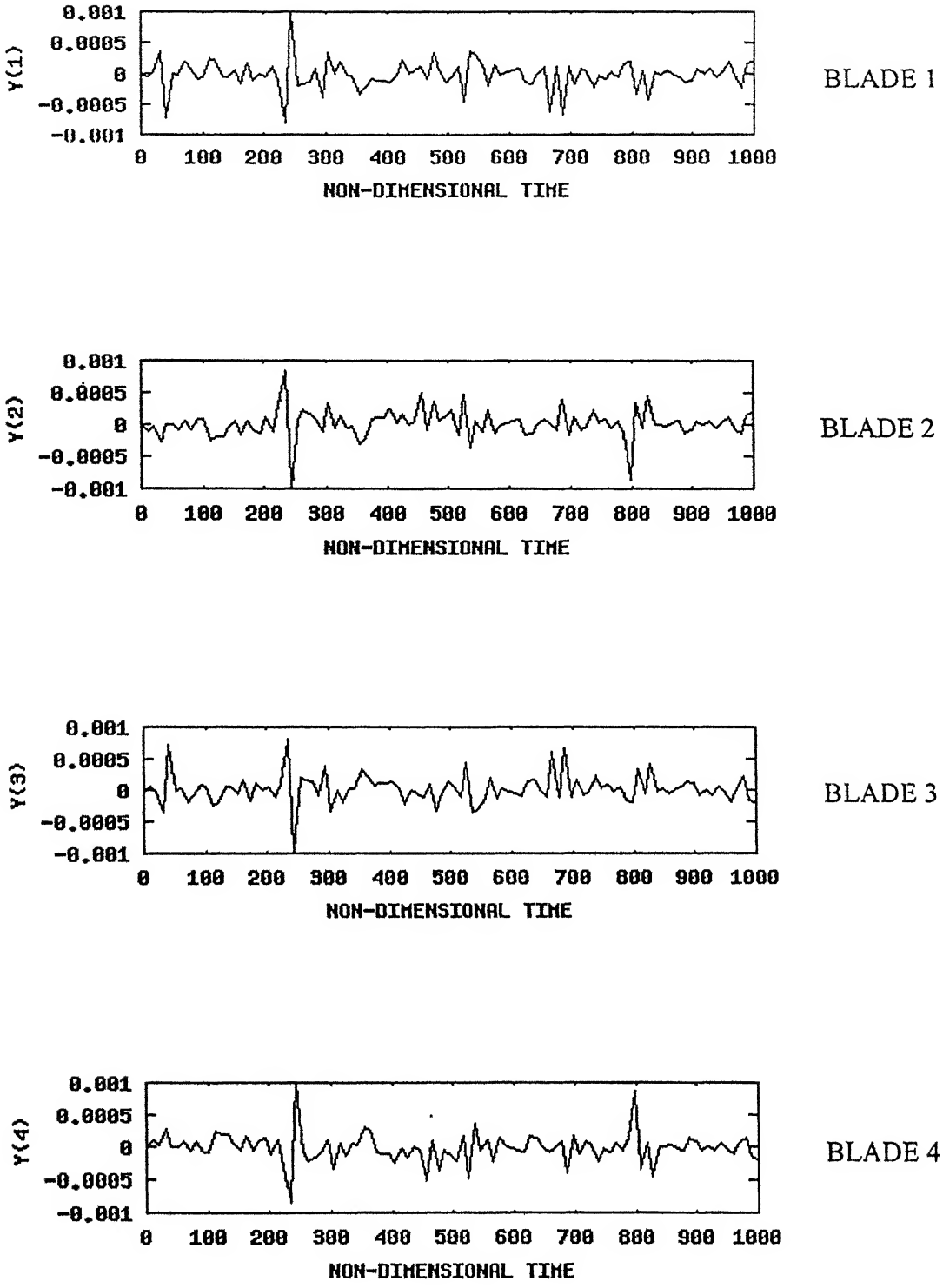

Fig. 4.2(a) Blade response in non-dimensional time domain

350 rpm, $\theta_X(0) = 6$ degree, ($\zeta_{0X} = 0.082$, $\zeta_{0Y} = 0.0529$)

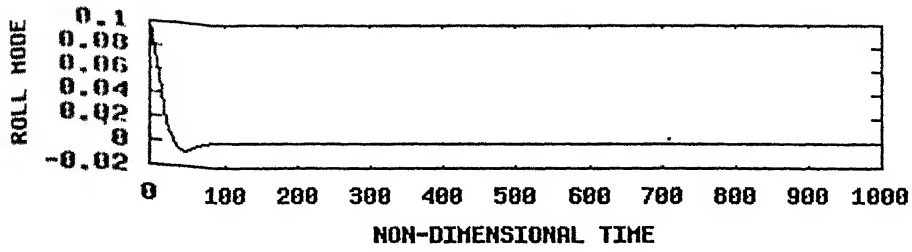

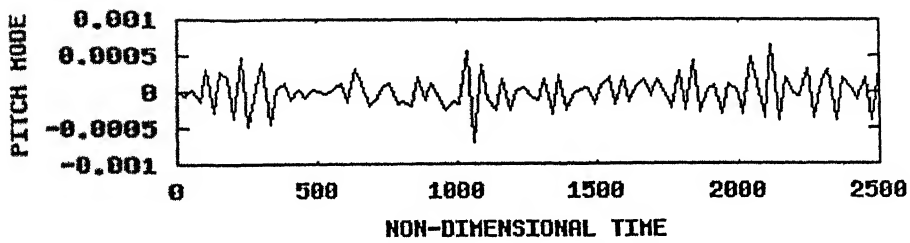

Fig. 4.2(b) Fuselage motion in non-dimensional time domain

350 rpm , $\theta_X(0) = 6$ degree, ($\zeta_{0X} = 0.082$, $\zeta_{0Y} = 0.0529$)

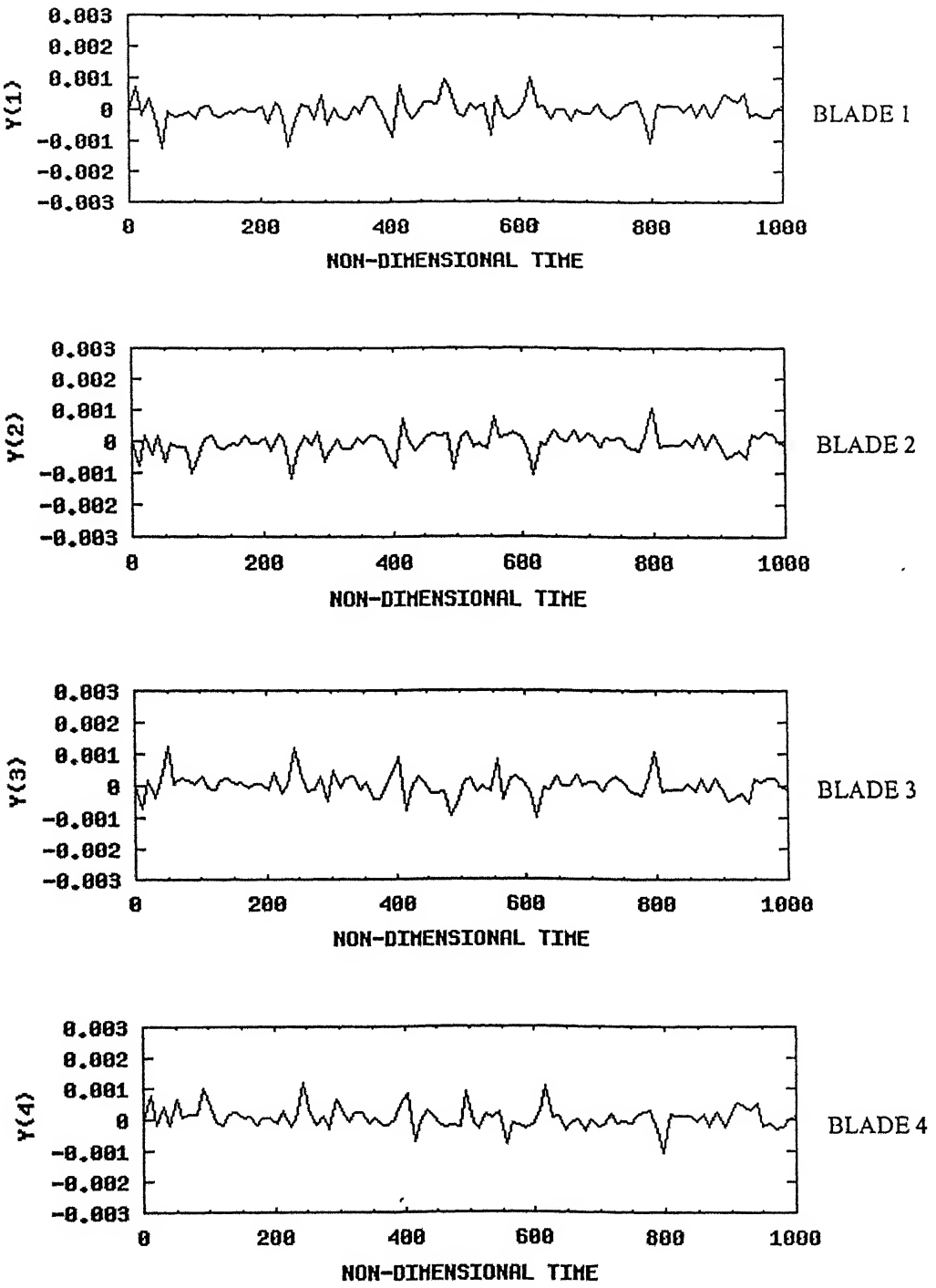

Fig. 4.3(a) Blade motion in non-dimensional time domain

450 rpm, $\theta_x(0)$= 0.8 degree, ($\zeta_{\theta x}$=0.082, ζ_{0y}= 0.059)

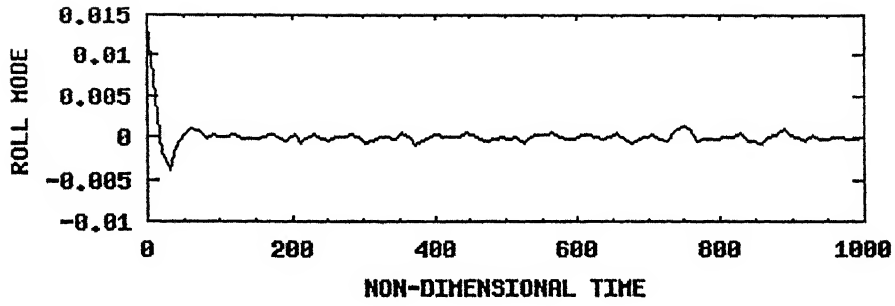

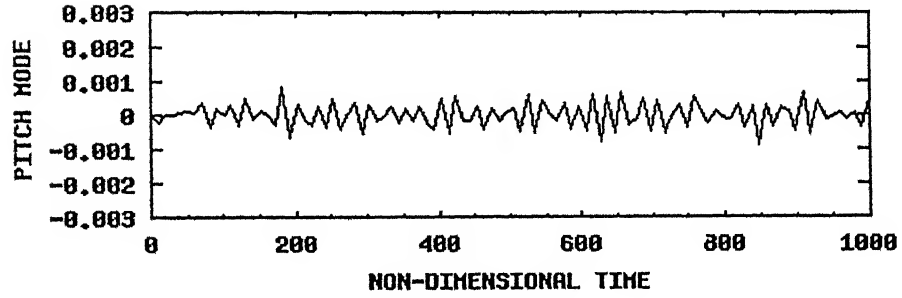

Fig. 4.3 (b) Fuselage motion in non-dimensional time domain

450 rpm, $\theta_x(0)$= 0.8 degree, ($\zeta_{\theta x}$=0.082, $\zeta_{\theta y}$=0.0529)

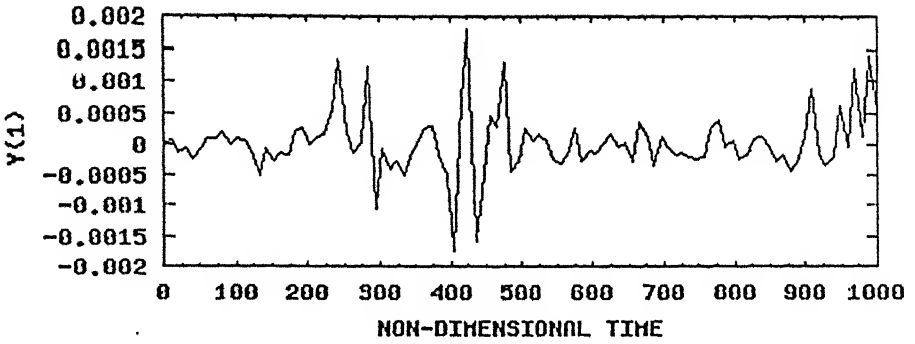

BLADE 1

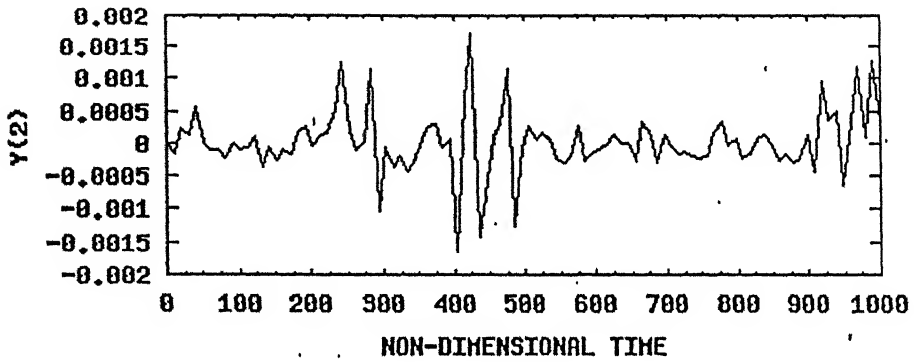

BLADE 2

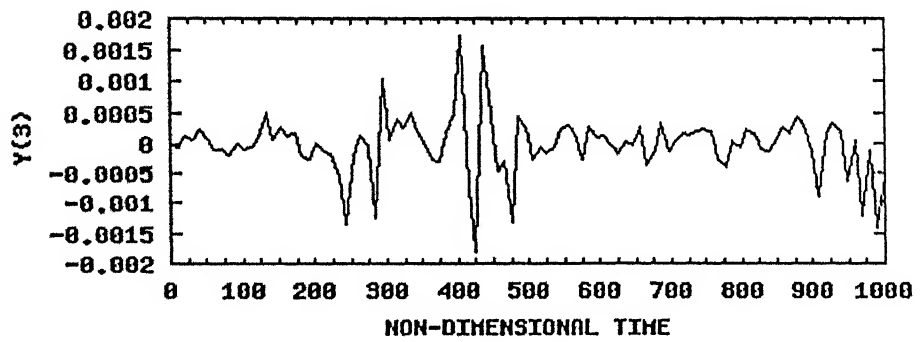

BLADE 3

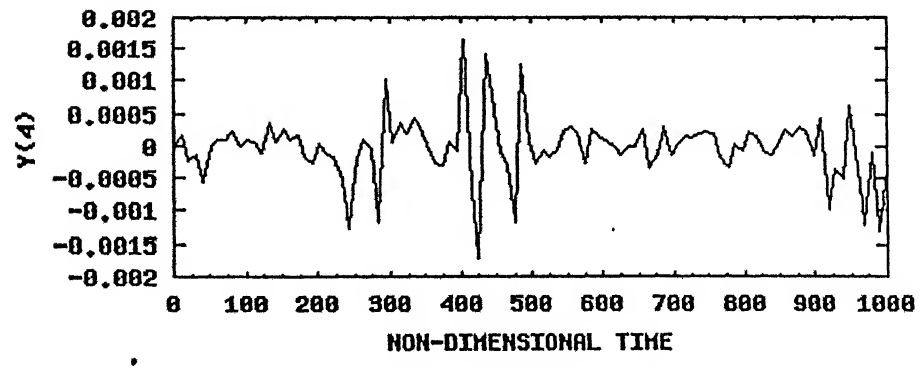

BLADE 4

Fig. 4.4(a) Blade response in non-dimensional time domain

450 rpm , $0_X(0) = 4$ degree, ($\zeta_{0X} = 0.082$, $\zeta_{0Y} = 0.0529$)

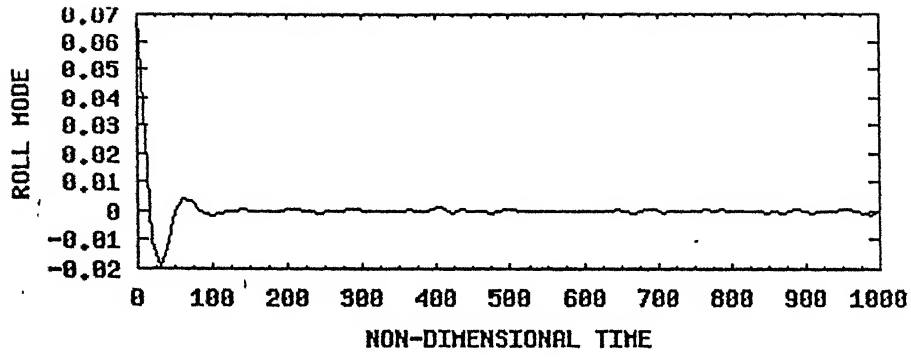

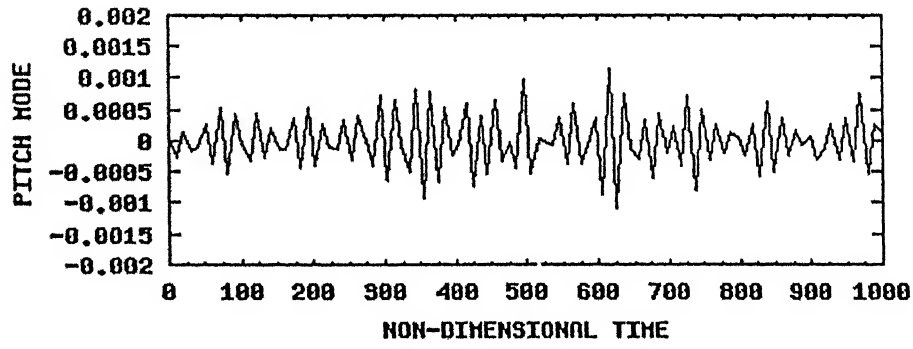

Fig. 4.4(b) Fuselage motion in non-dimensional time domain

450 rpm , $0_X(0) = 4$ degree, ($\zeta_{0X} = 0.082$, $\zeta_{0Y} = 0.0529$)

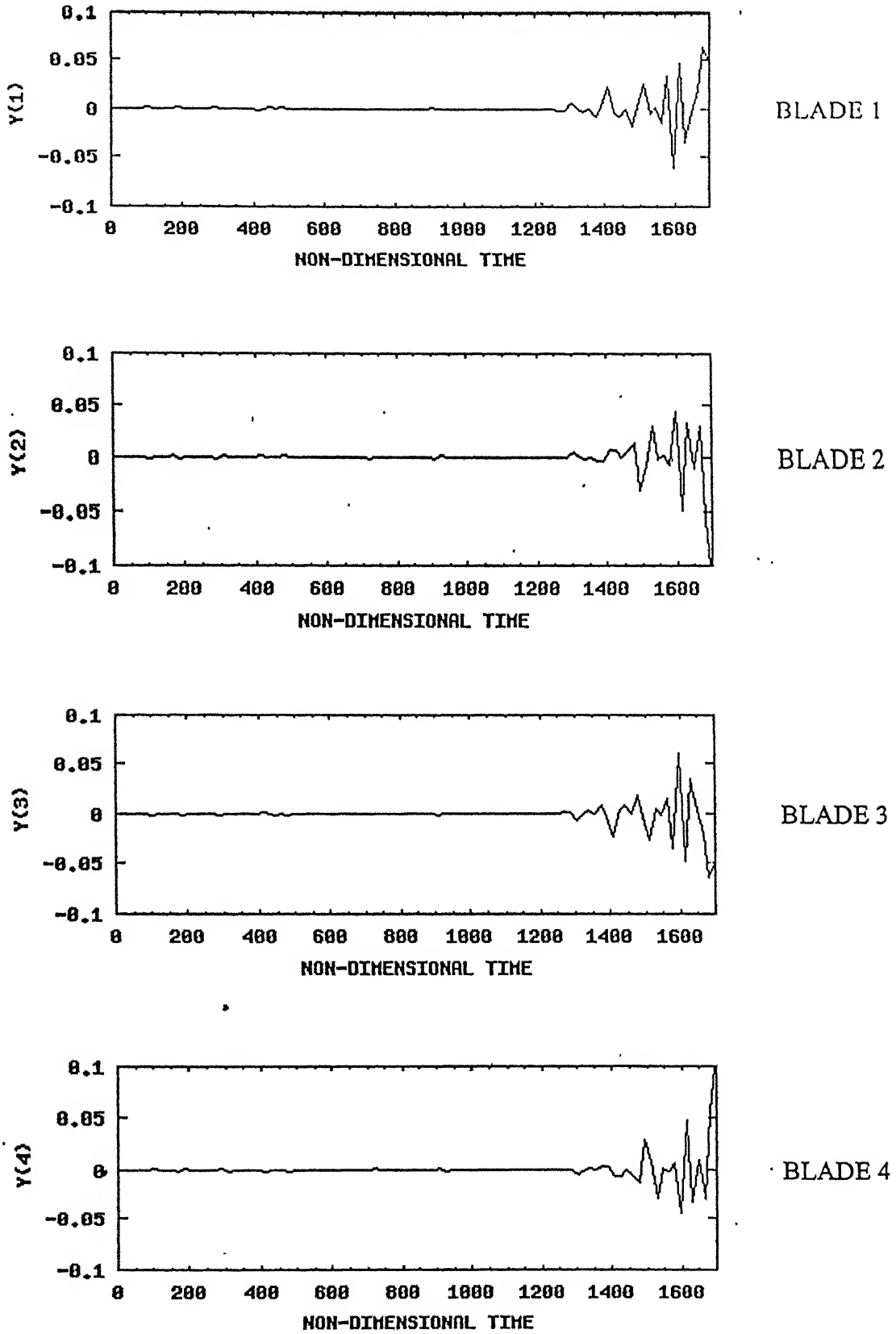

Fig. 4.5(a) Blade response in non-dimensional time domain

450 rpm , $\theta_X(0) = 6$ degree, ($\zeta_{0X} = 0.082$, $\zeta_{0Y} = 0.0529$)

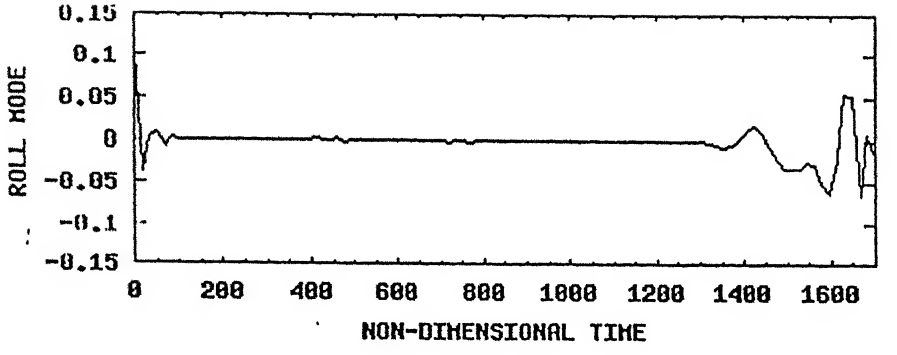

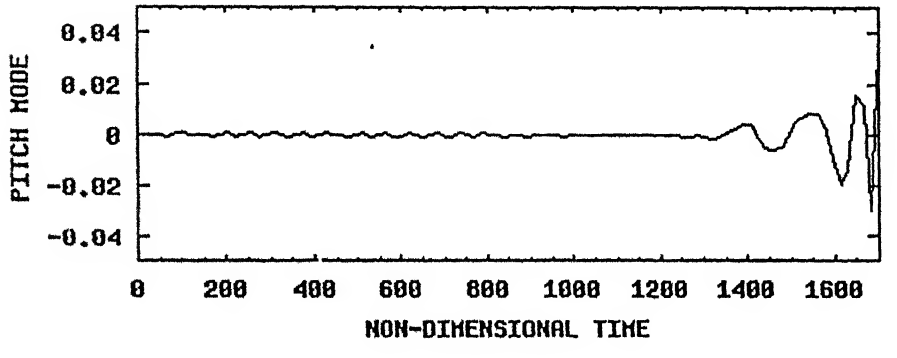

Fig. 4.5(b) Fuselage motion in non-dimensional time domain

450 rpm , $\theta_X(0) = 6$ degree, ($\zeta_{\theta X} = 0.082$, $\zeta_{\theta Y} = 0.0529$)

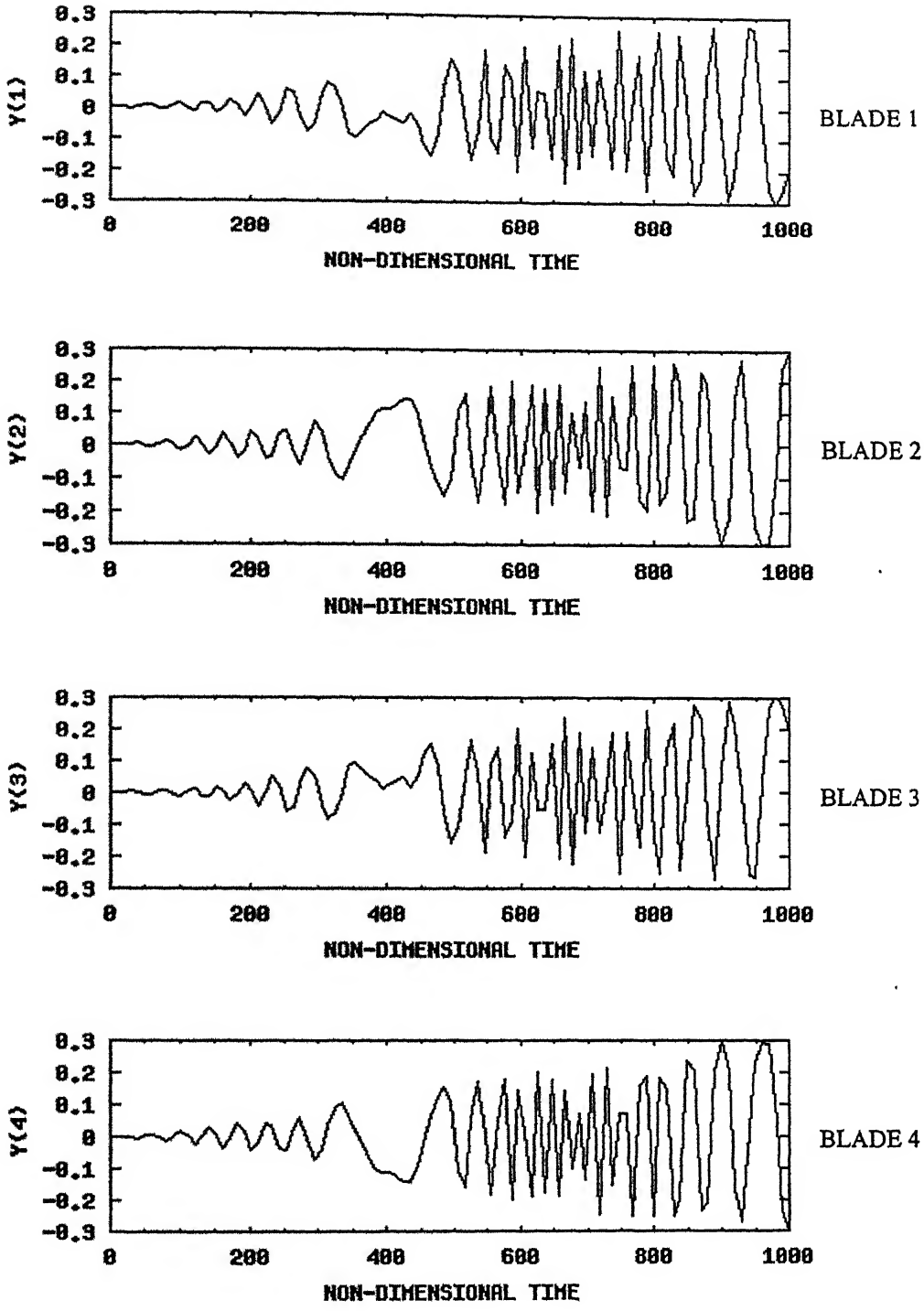

Fig. 4.6 (a) Blade motion in non-dimensional time domain

450 rpm , $\theta_X(0)$ = 10 degree, ($\zeta_{\theta X}$ = 0.082 , $\zeta_{\theta Y}$ = 0.0529)

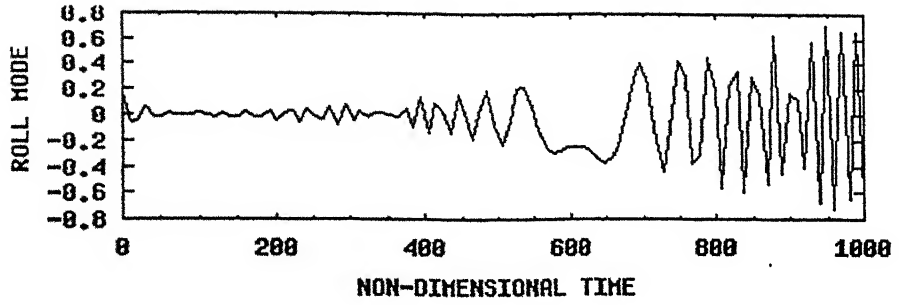

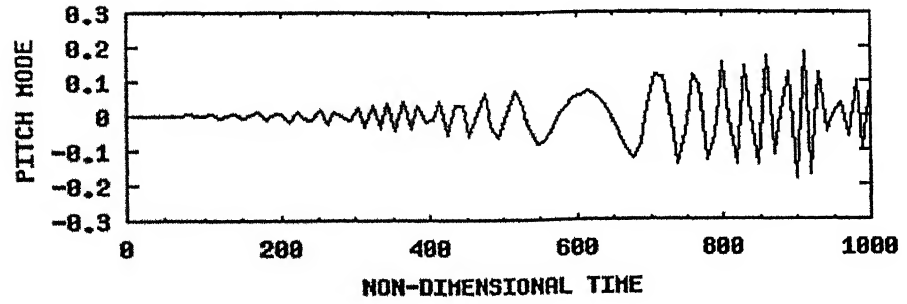

Fig. 4.6 (b) Fuselage motion in non-dimensional time domain

450 rpm , $\theta_X(0) = 10$ degree, ($\zeta_{\theta X} = 0.082$, $\zeta_{\theta Y} = 0.0529$)

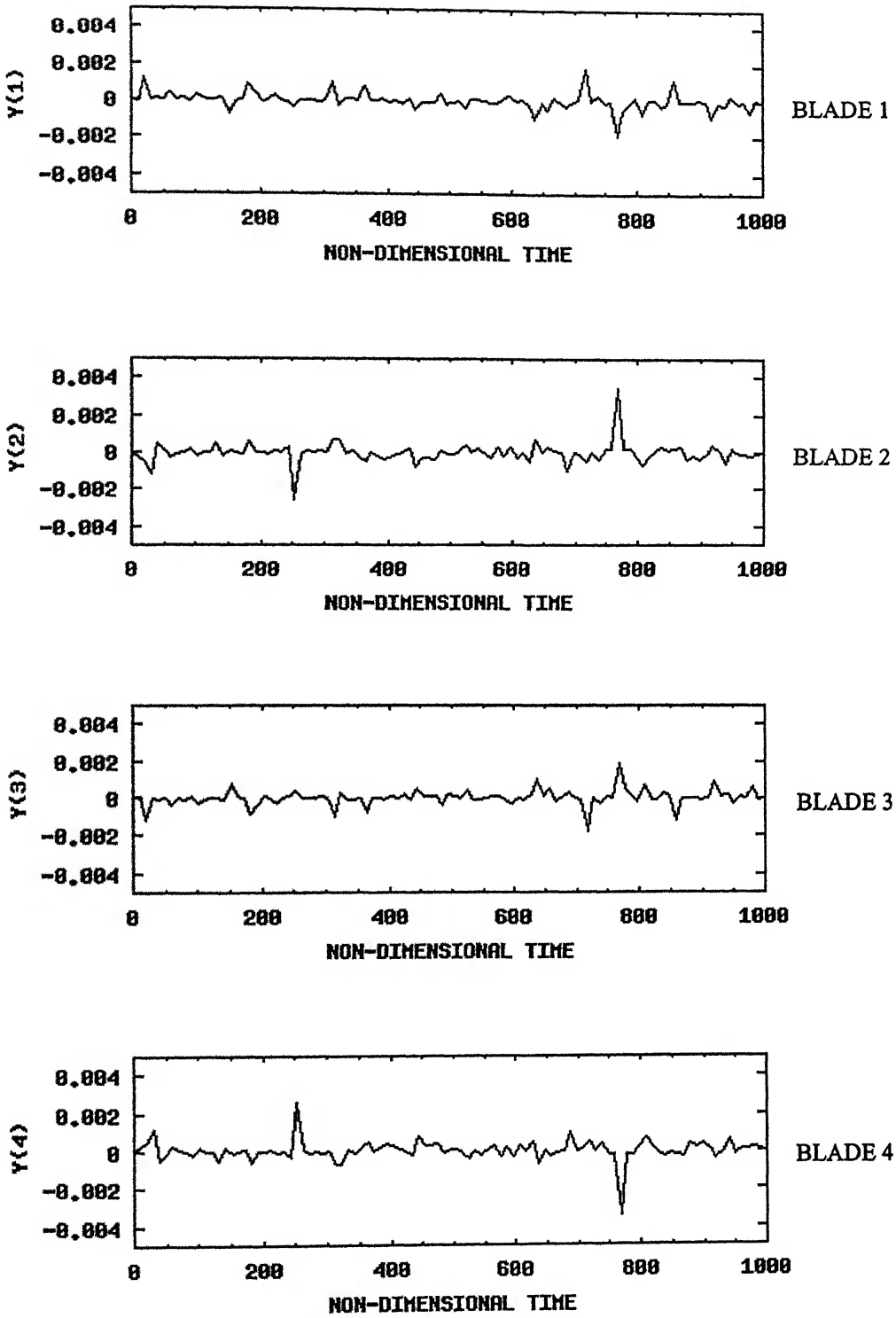

Fig.4.6 (c) Motion of blade in non-dimensional time domain
450 rpm, $\theta_x(0)$= 10 degree, linear elastomer, ($\zeta_{\theta x}$=0.082, $\zeta_{\theta y}$=0.0529)

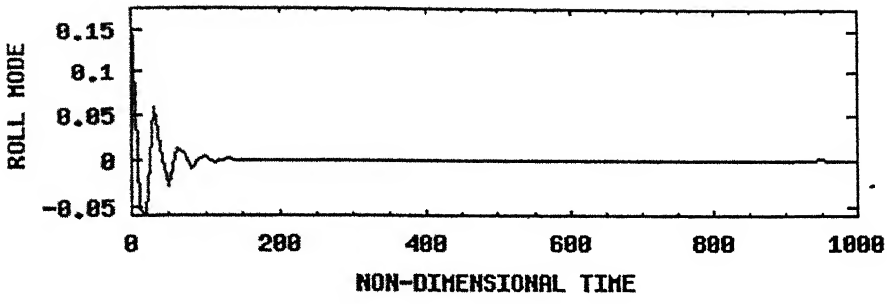

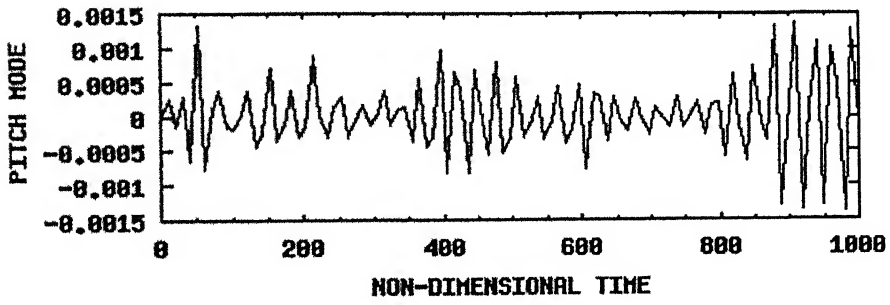

Fig.4.6 (d) Motion of the fuselage in non-dimensional time domain
450 rpm, $\theta_x(0)$= 10 degree, linear elastomer, ($\zeta_{\theta x}$=0.082, $\zeta_{\theta y}$=0.0529)

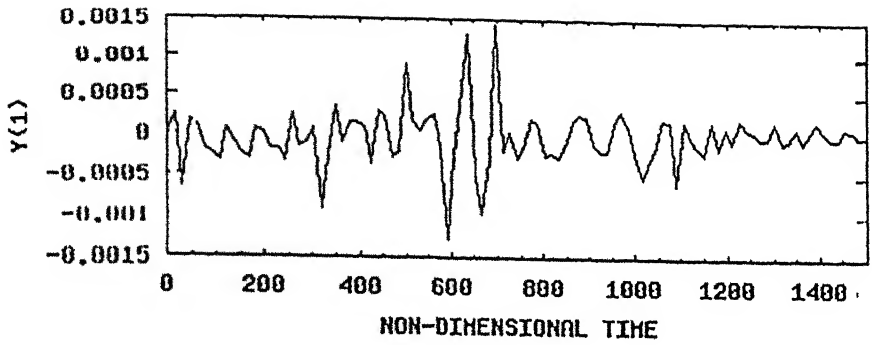

BLADE 1

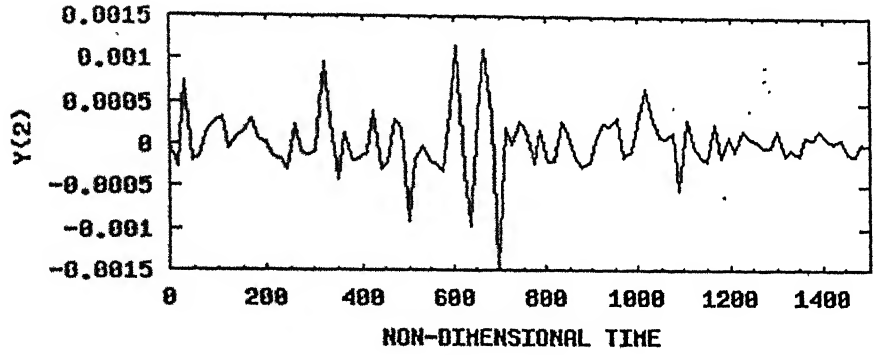

BLADE 2

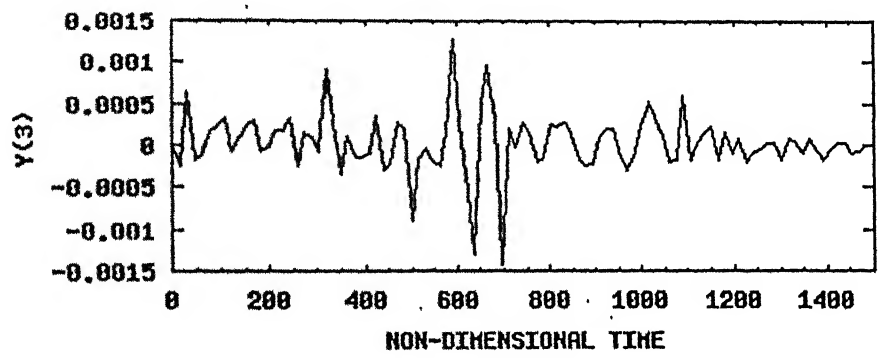

BLADE 3

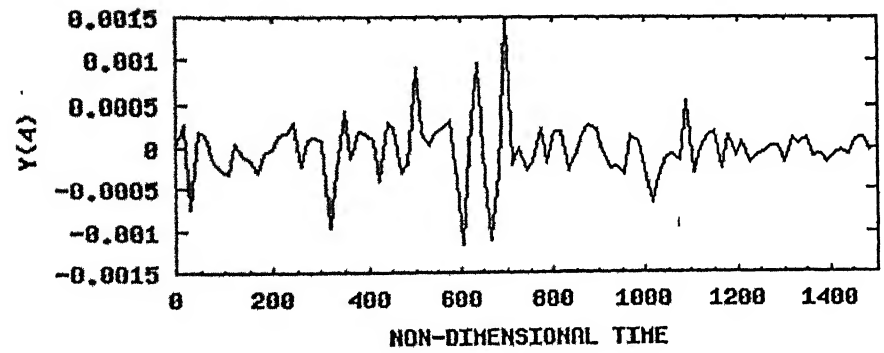

BLADE 4

Fig. 4.7(a) Blade response in non-dimensional time domain

460 rpm , $\theta_X(0) = 1$ degree, ($\zeta_{\theta X} = 0.082$, $\zeta_{\theta Y} = 0.0529$)

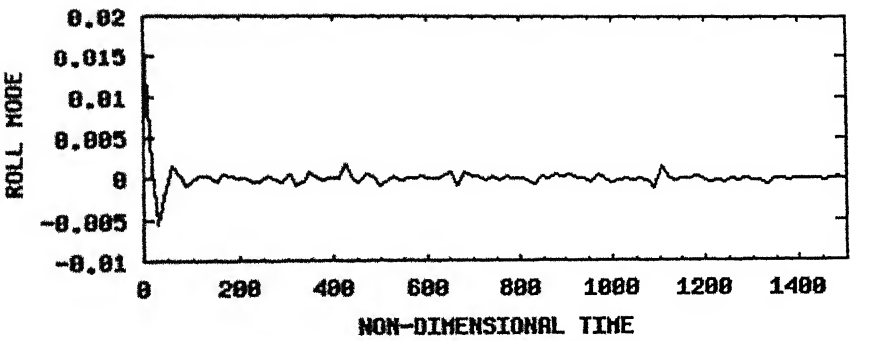

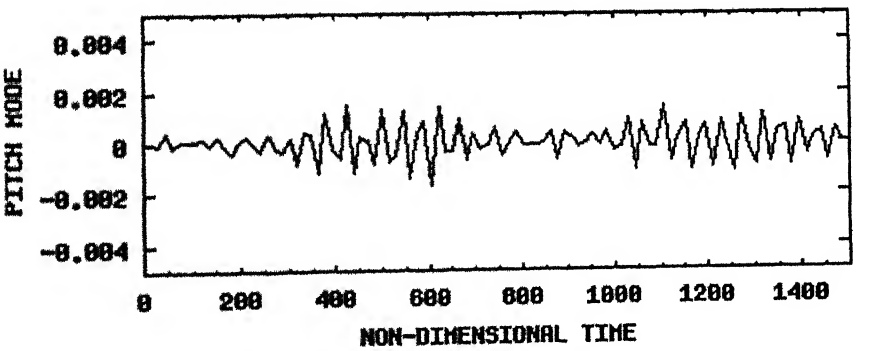

Fig. 4.7 (b) Fuselage motion in non-dimensional time domain

460 rpm , $\theta_X(0)$ = 1 degree, ($\zeta_{\theta X}$ = 0.082 , $\zeta_{\theta Y}$ = 0.0529)

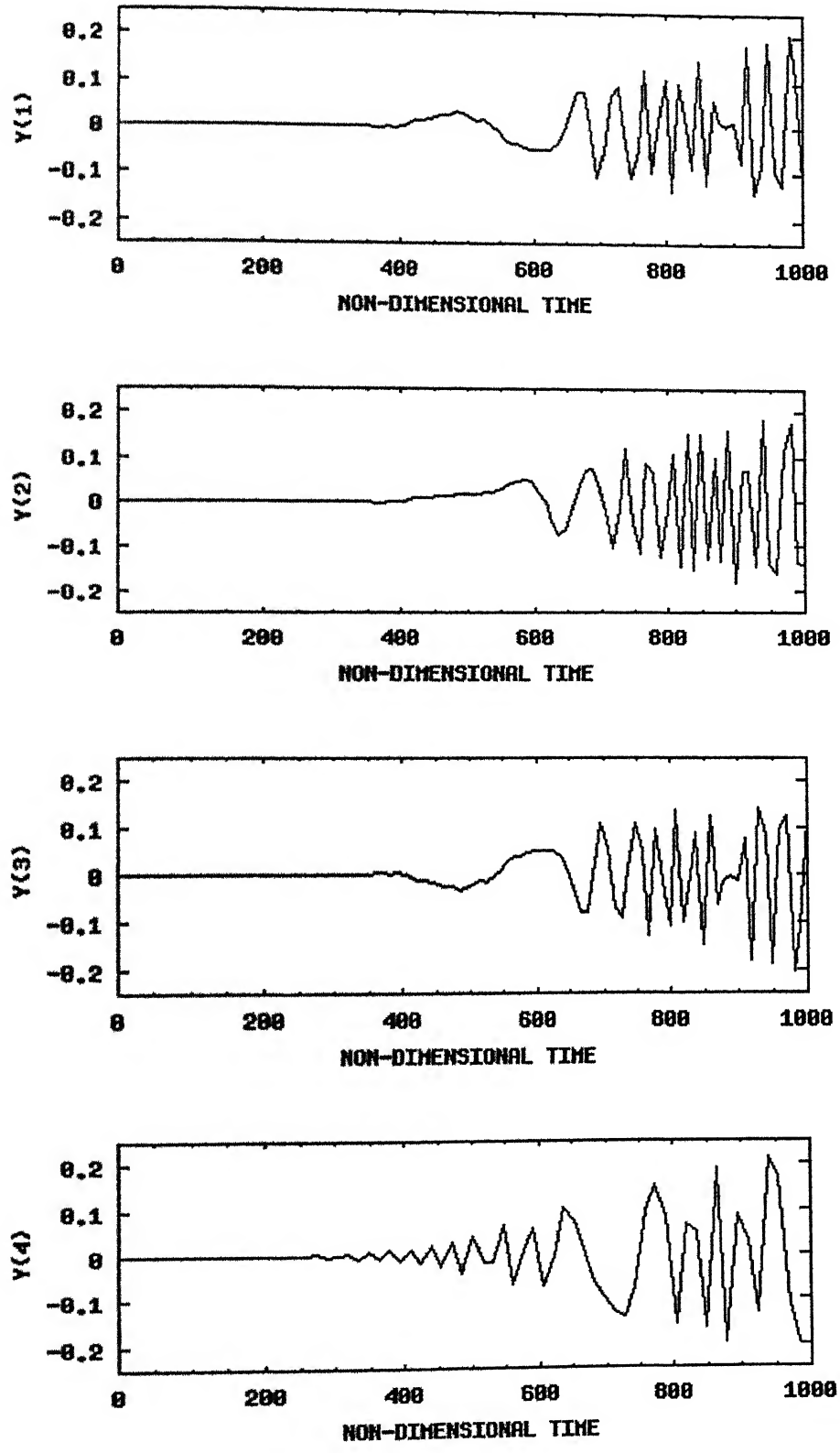

Fig. 4.8(a) Blade response in non-dimensional time domain

460 rpm , $\theta_X(0) = 2$ degree, ($\zeta_{\theta X} = 0.082$, $\zeta_{\theta Y} = 0.0529$)

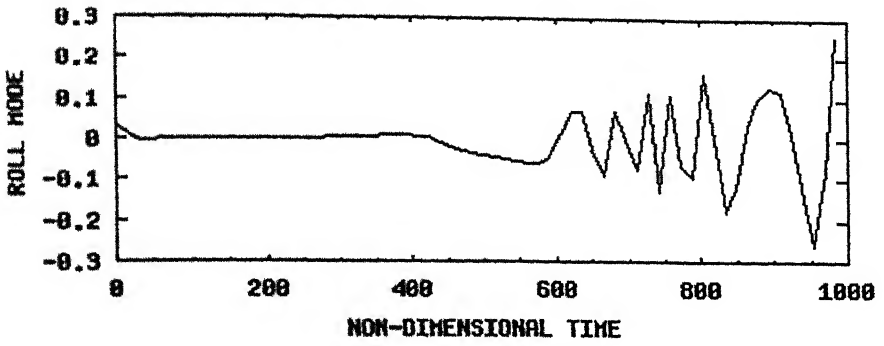

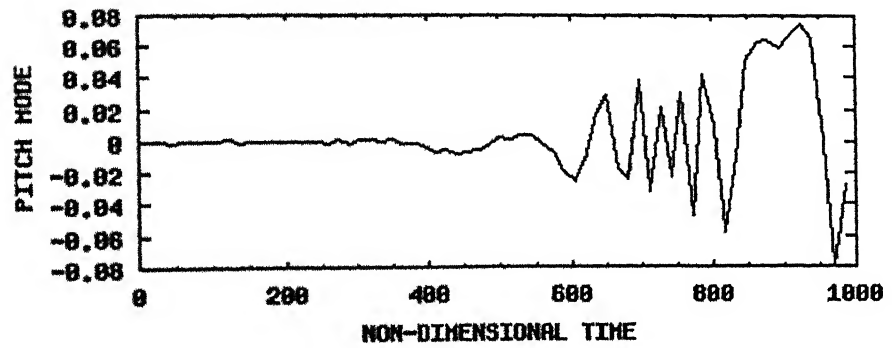

Fig. 4.8 (b) Fuselage motion in non-dimensional time domain

460 rpm , $\theta_X(0) = 2$ degree, ($\zeta_{\theta X} = 0.082$, $\zeta_{\theta Y} = 0.0529$)

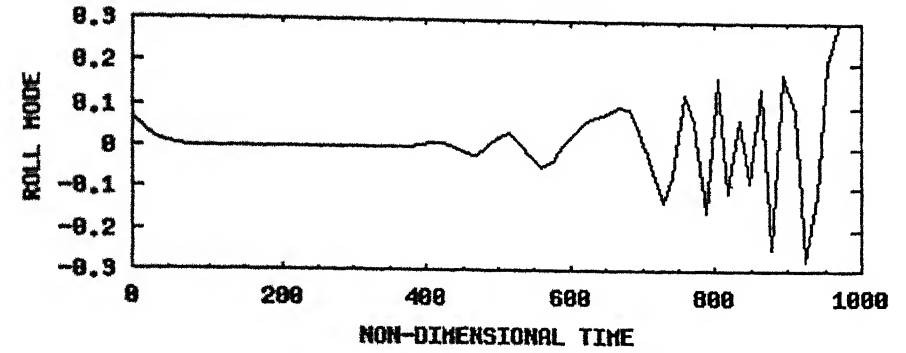

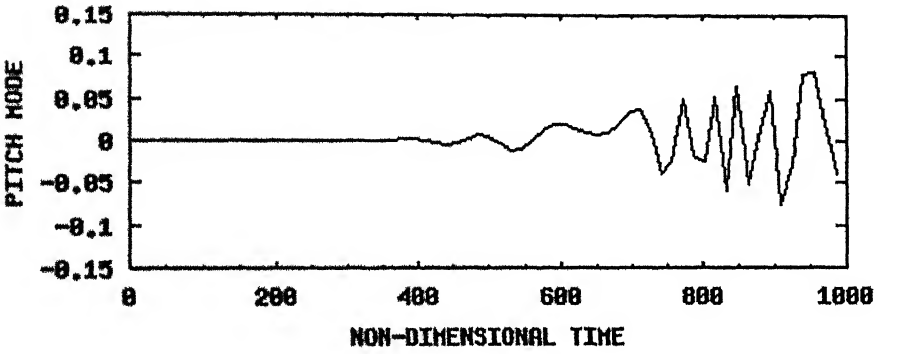

Fig. 4.9(b) Fuselage motion in non-dimensional time

550 rpm , $\theta_X(0) = 4$ degree, ($\zeta_{\theta X} = 0.082$, $\zeta_{\theta Y} = 0.0529$)

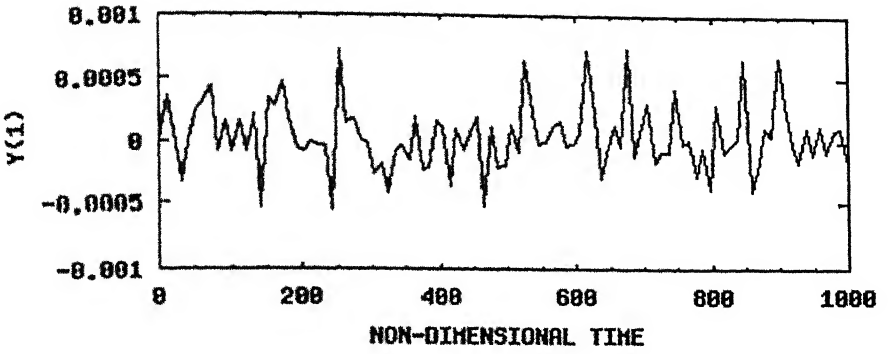

BLADE 1

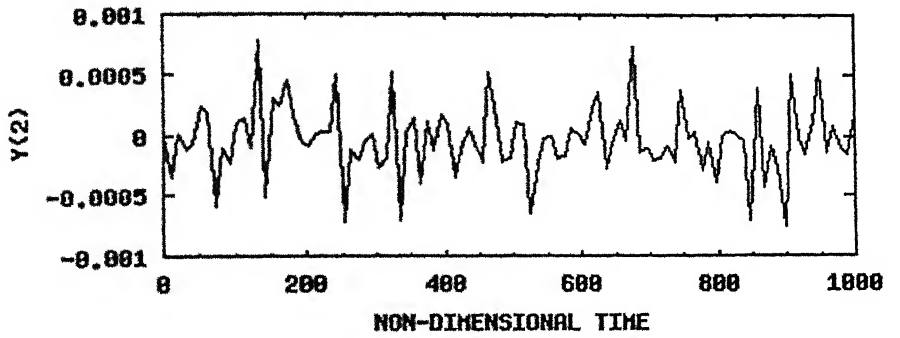

BLADE 2

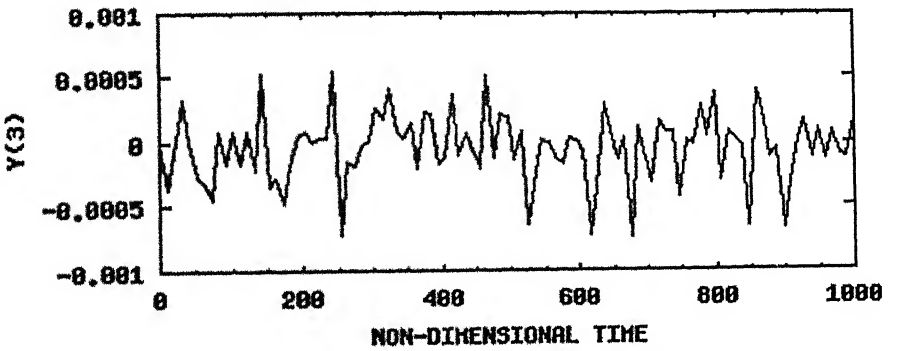

BLADE 3

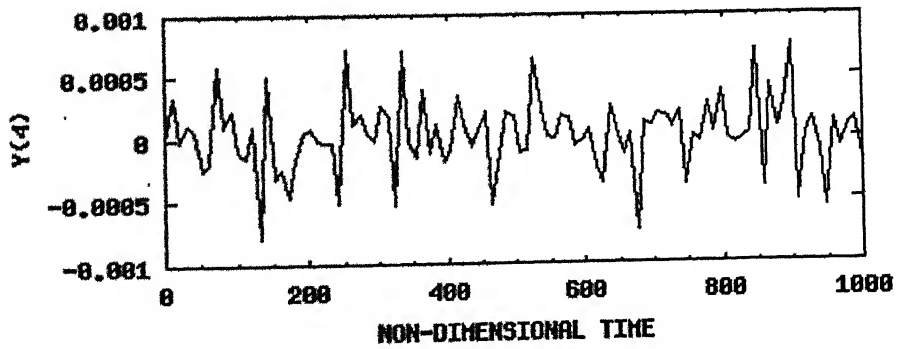

BLADE 4

Fig. 4.10(a) Blade response in non-dimensional time domain

640 rpm , $\theta_X(0) = 4$ degree, ($\zeta_{\theta X} = 0.082$, $\zeta_{\theta Y} = 0.0529$)

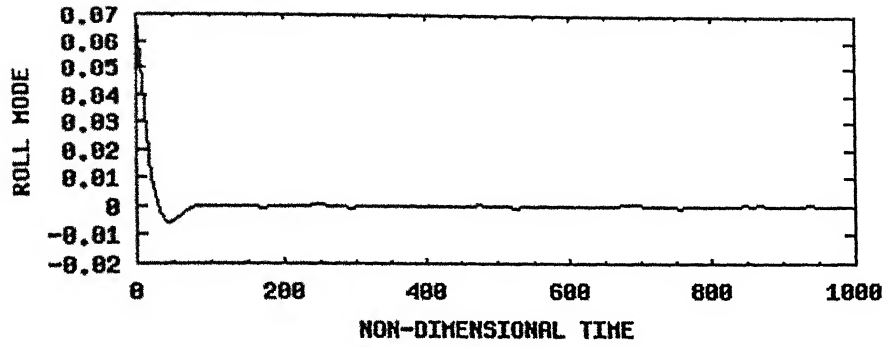

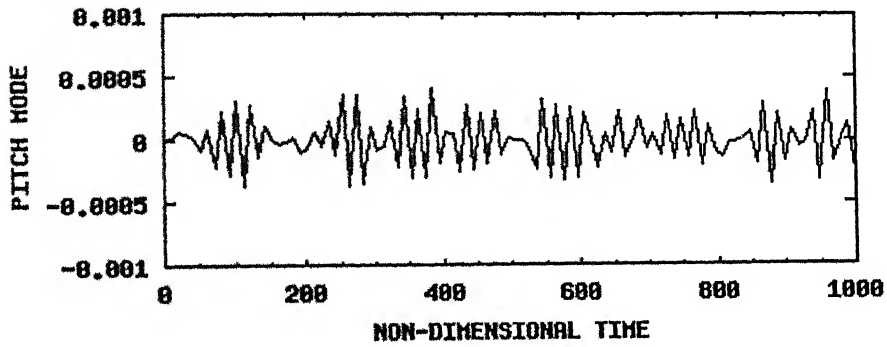

Fig. 4.10 (b) Fuselage motion in non-dimensional time domain

640 rpm , $\theta_X(0) = 4$ degree, ($\zeta_{\theta X} = 0.082$, $\zeta_{\theta Y} = 0.0529$)

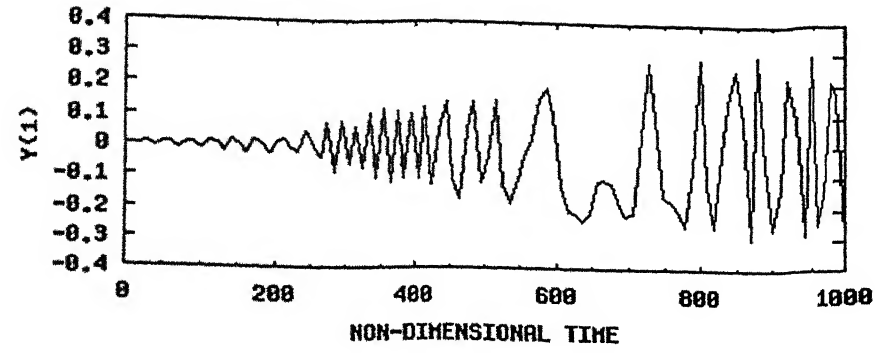

BLADE 1

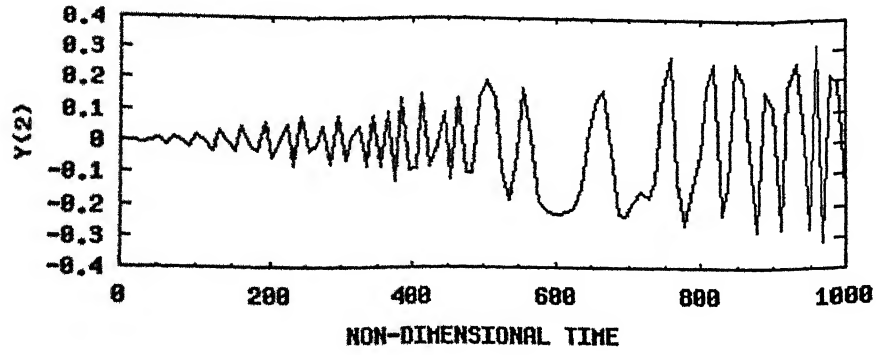

BLADE 2

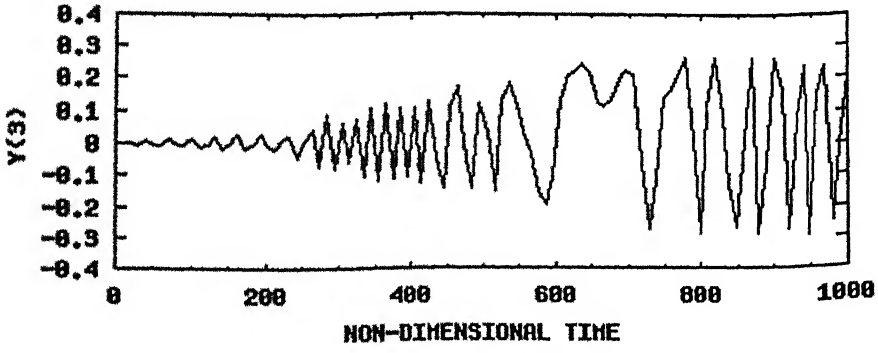

BLADE 3

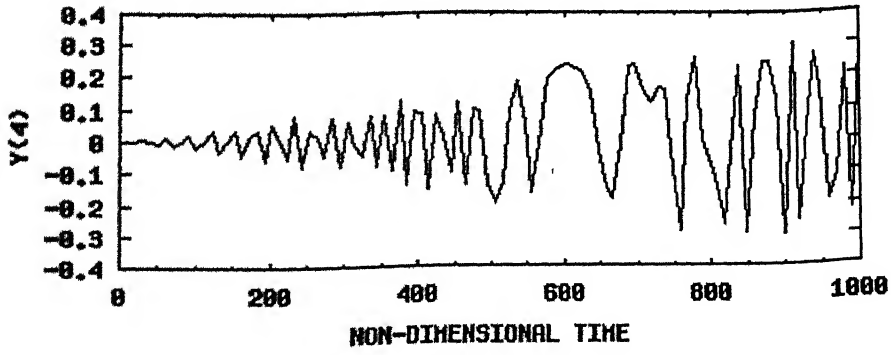

BLADE 4

Fig. 4.11(a) Blade response in non-dimensional time domain

640 rpm , $\theta_X(0) = 6$ degree, ($\zeta_{\theta X} = 0.082$, $\zeta_{\theta Y} = 0.0529$)

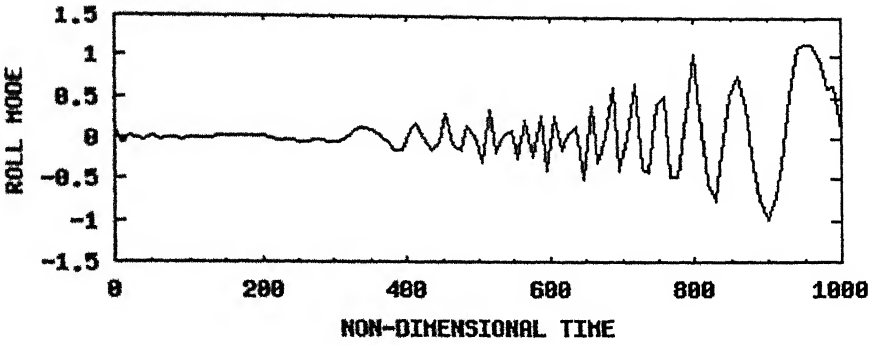

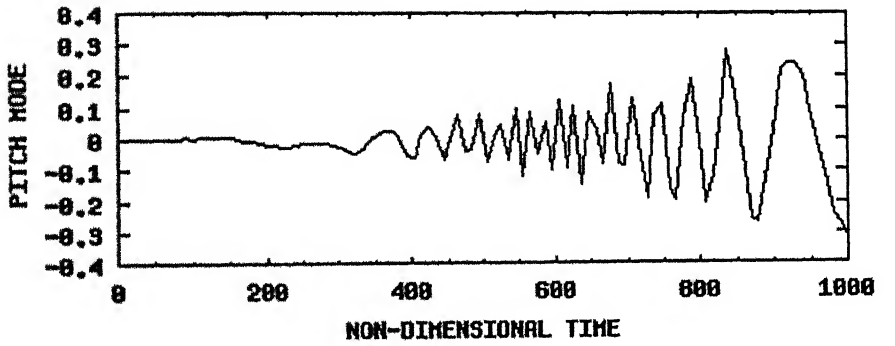

Fig. 4.11 (b) Fuselage motion in non-dimensional time domain

640 rpm , $\theta_X(0) = 6$ degree, ($\zeta_{\theta X} = 0.082$, $\zeta_{\theta Y} = 0.0529$)

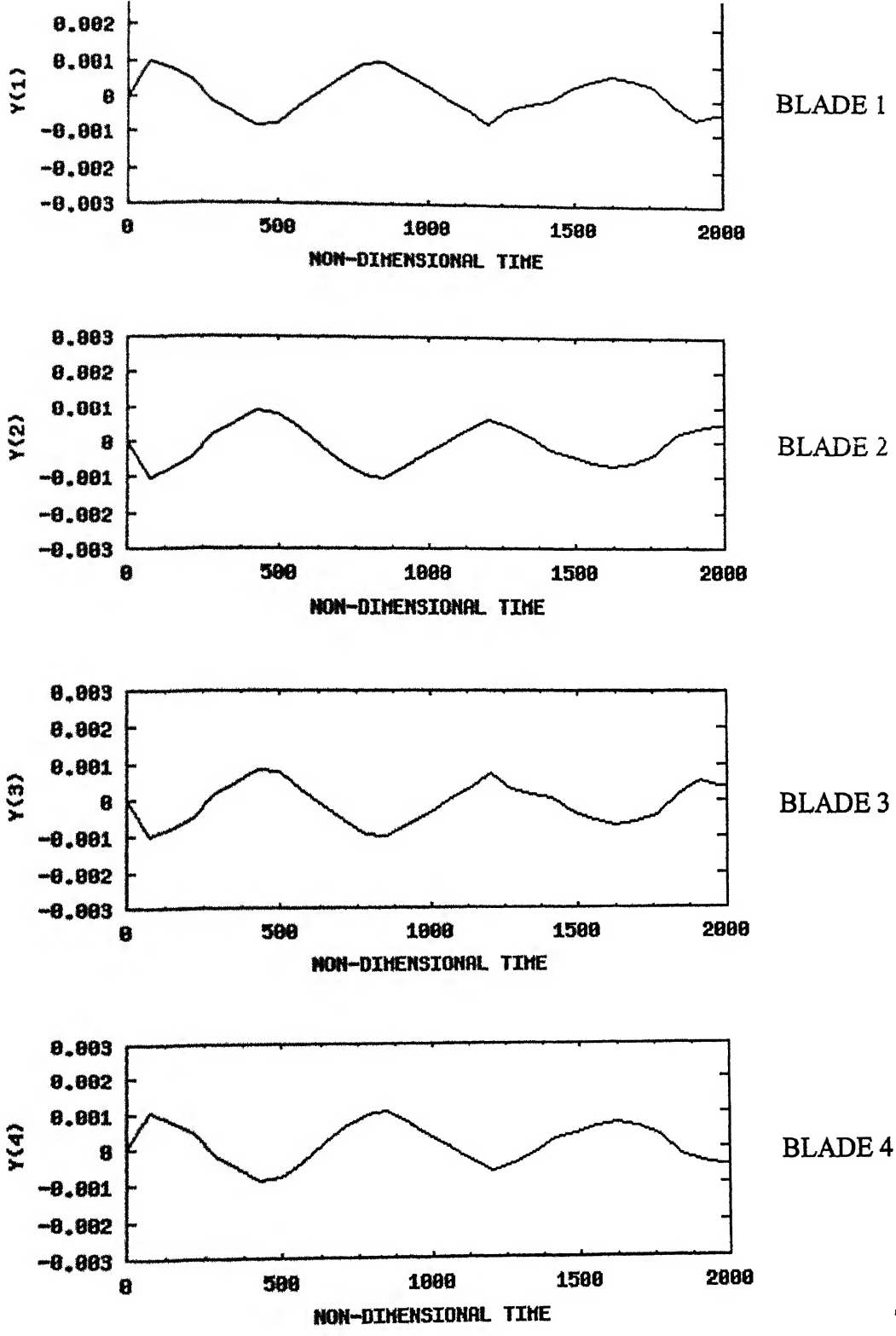

Fig. 4.12(a) Blade response in non-dimensional time domain

700 rpm , $\theta_X(0) = 4$ degree, ($\zeta_{\theta X} = 0.082$, $\zeta_{\theta Y} = 0.0529$)

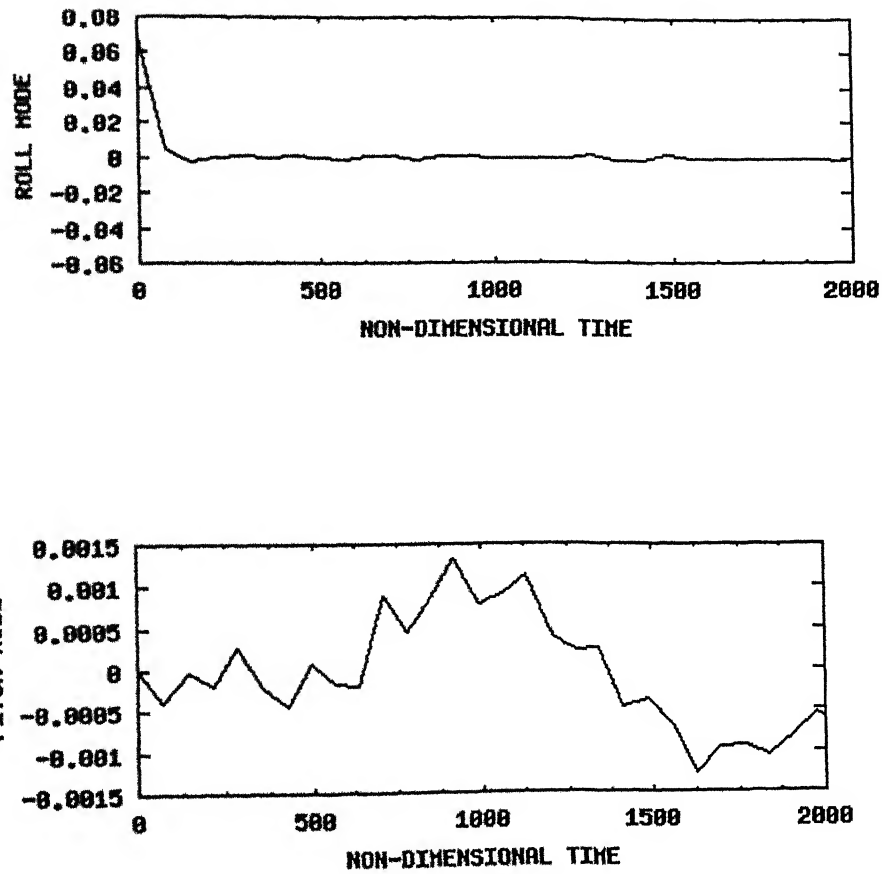

Fig. 4.12 (b) Fuselage motion in non-dimensional time domain

700 rpm , $\theta_X(0) = 4$ degree, ($\zeta_{\theta X} = 0.082$, $\zeta_{\theta Y} = 0.0529$)

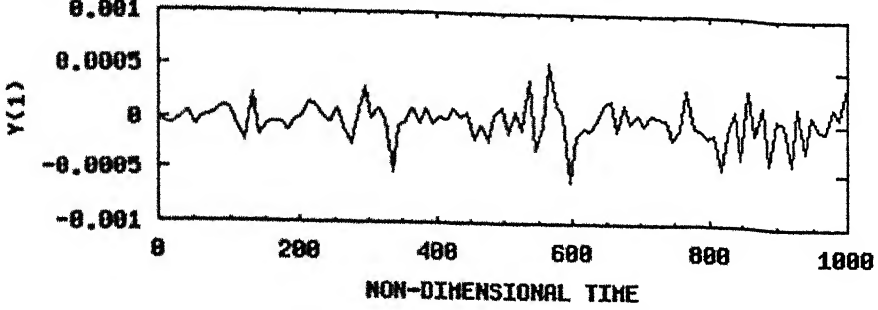

BLADE 1

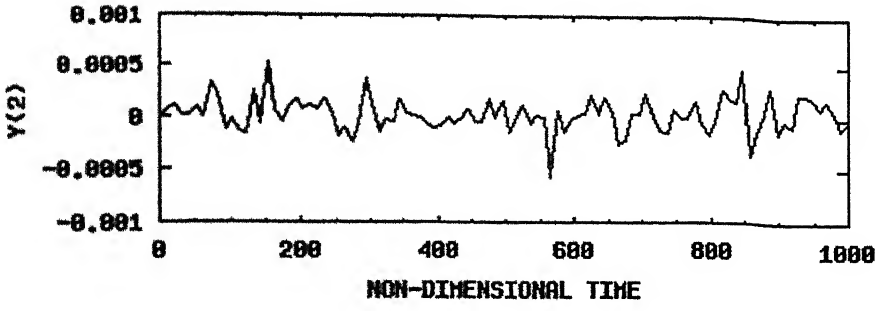

BLADE 2

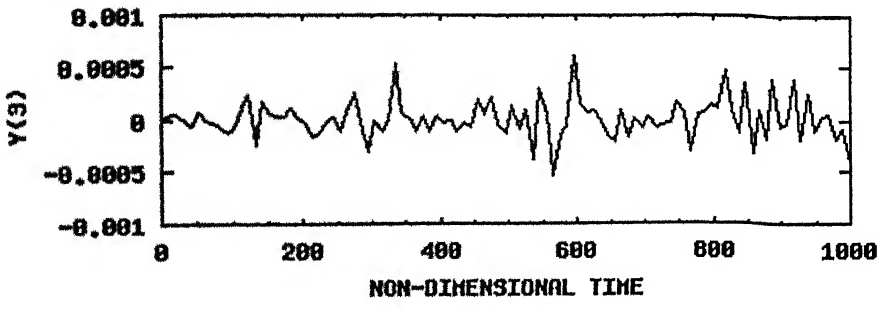

BLADE 3

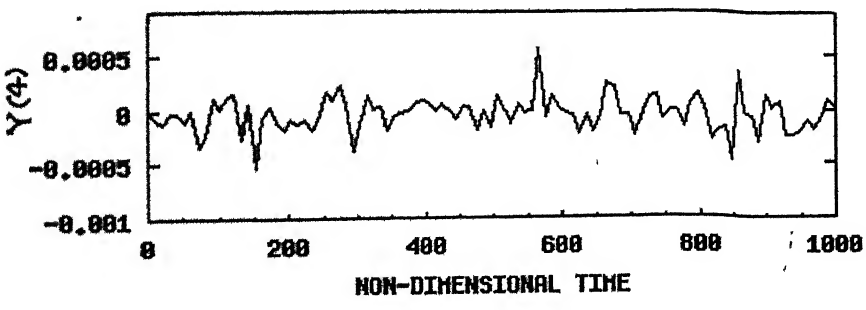

BLADE 4

Fig. 4.13(a) Blade motion in non-dimensional time domain
250 rpm, $\theta_X(0) = 4$ degree, ($\zeta_{\theta X} = 0.0$, $\zeta_{\theta Y} = 0.0$)

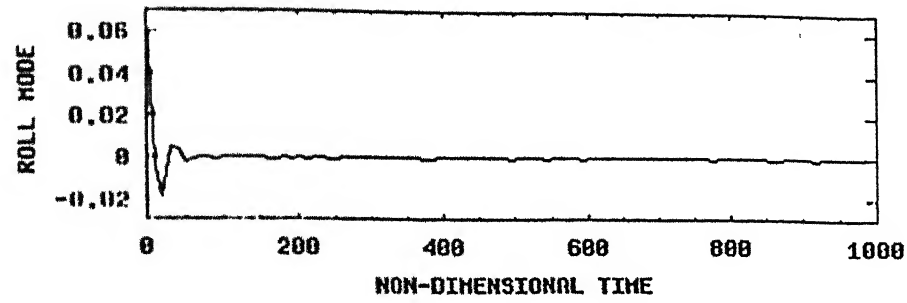

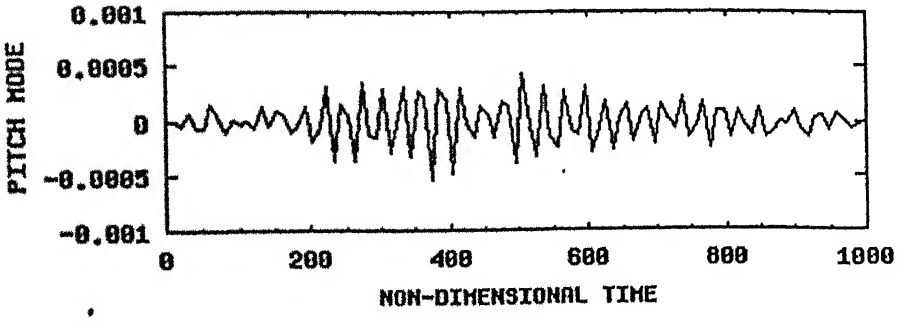

Fig. 4.13(b) Fuselage motion in non-dimensional time domain 250 rpm, $\theta_X(0) = 4$ degree, ($\zeta_{0X} = 0.0$, $\zeta_{0Y} = 0.0$)

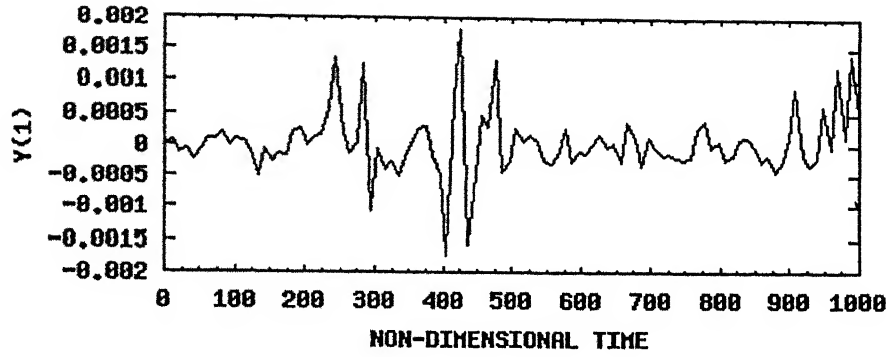

BLADE 1

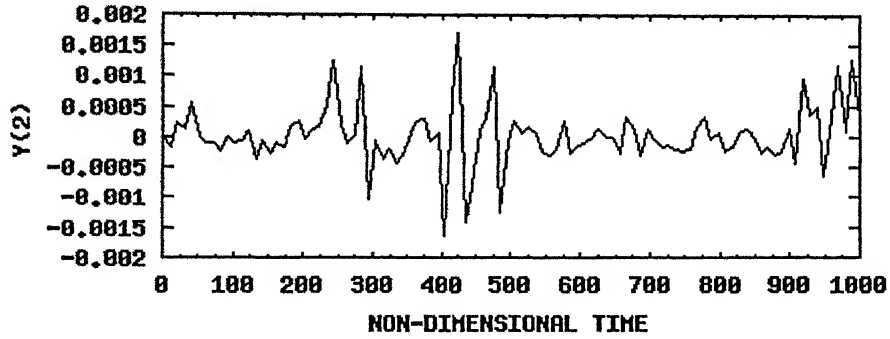

BLADE 2

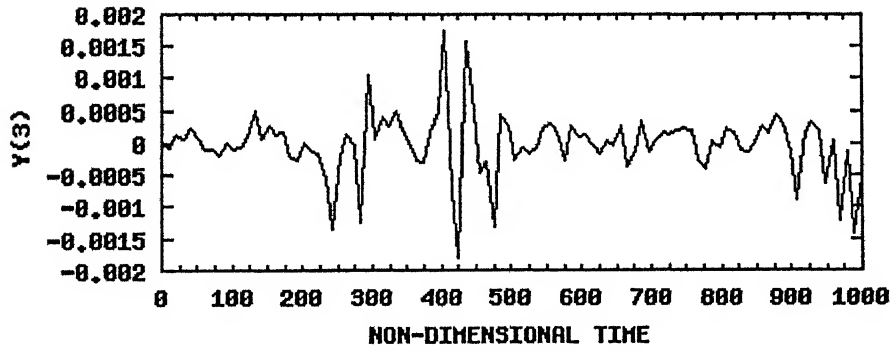

BLADE 3

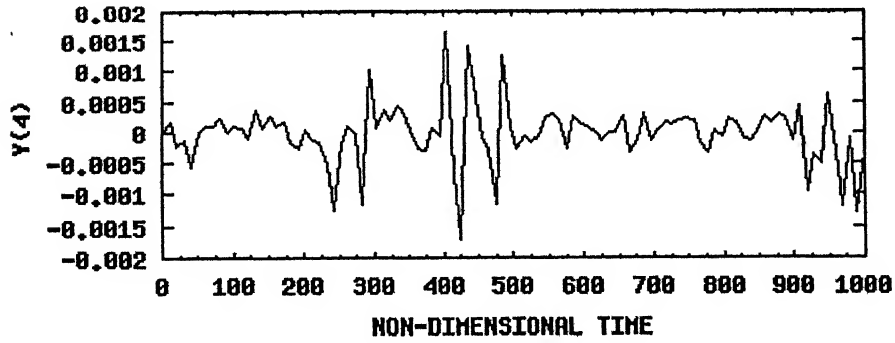

BLADE 4

Fig. 4.14(a) Blade response in non-dimensional time domain
Operating condition: 350 rpm, Initial condition: 4 degree ($\zeta_{\theta x}$=0.0, $\zeta_{\theta y}$=0.0)

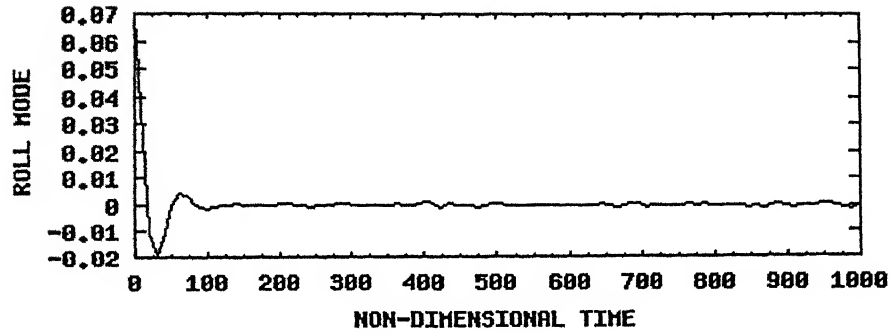

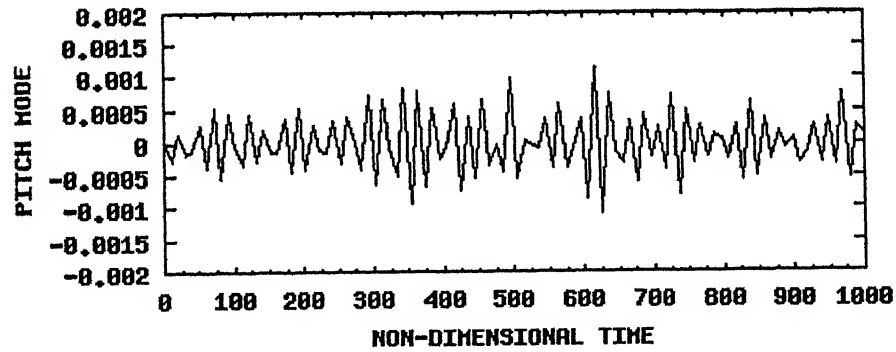

Fig. 4.14(b) Fuselage motion in non-dimensional time domain

Operating condition: 350 rpm, Initial condition: 4 degree ($\zeta_{\theta X} = 0.0$, $\zeta_{\theta Y} = 0.0$)

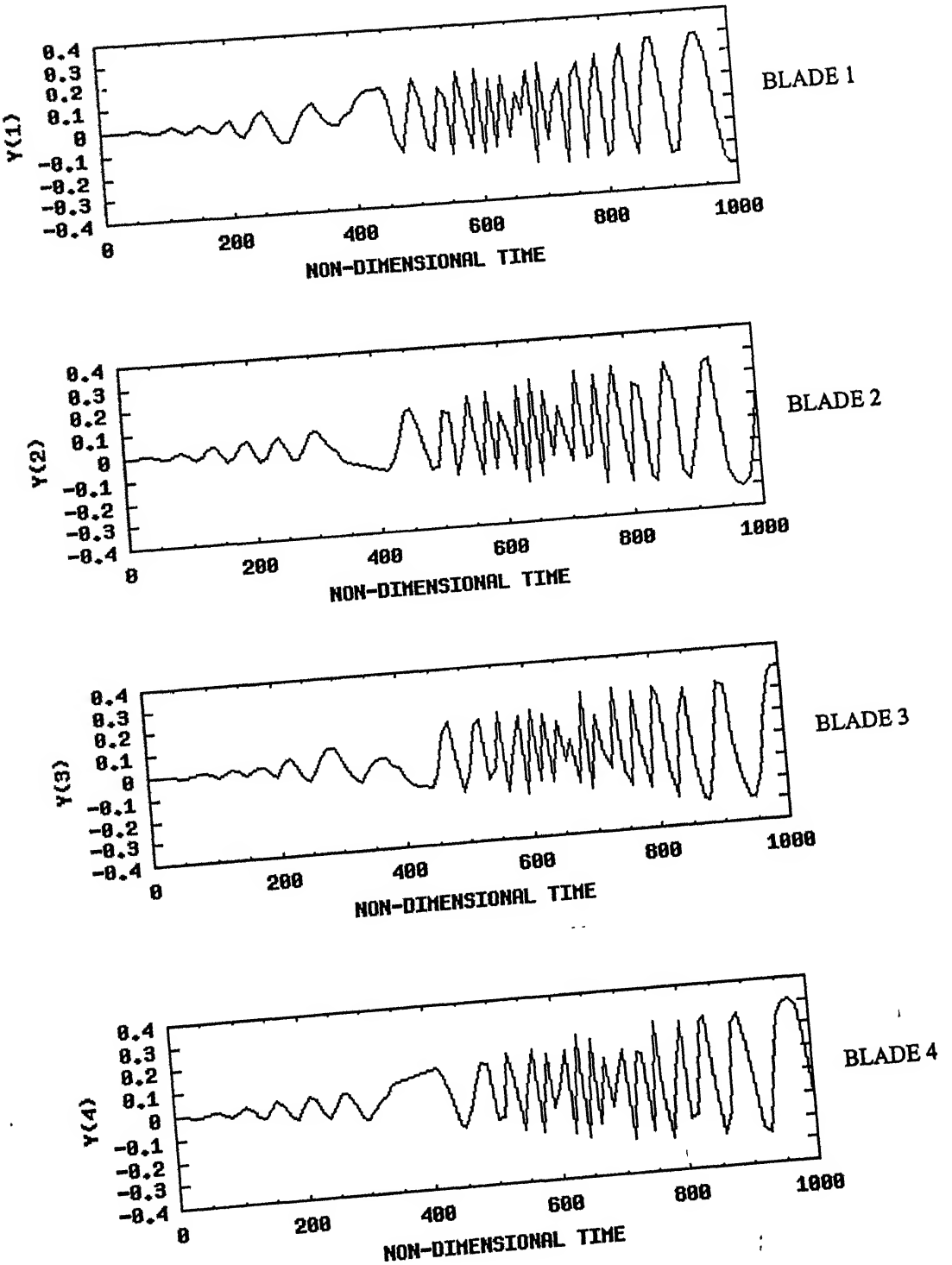

Fig. 4.15 (a) Blade motion in non-dimensional time domain
350 rpm, $\theta_X(0) = 6$ degree, ($\zeta_{\theta X} = 0.0$, $\zeta_{\theta Y} = 0.0$)

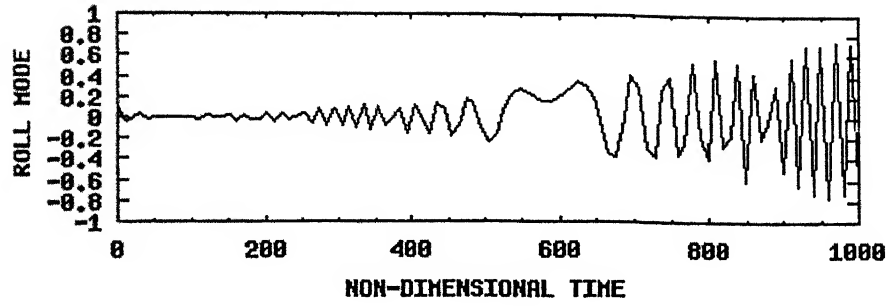

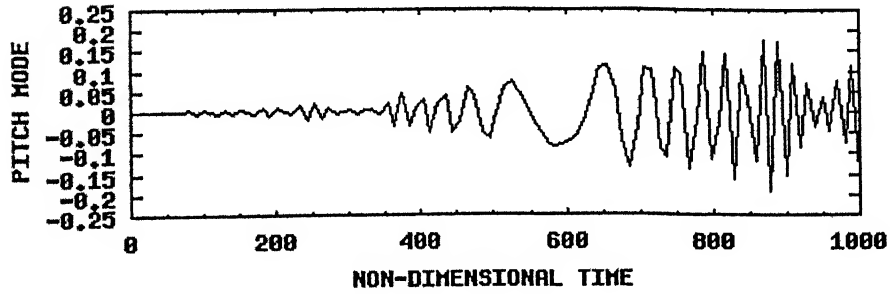

Fig. 4.15 (b) Fuselage motion in non-dimensional time domain 350 rpm, $\theta_X(0) = 6$ degree, ($\zeta_{\theta X} = 0.0$, $\zeta_{\theta Y} = 0.0$)

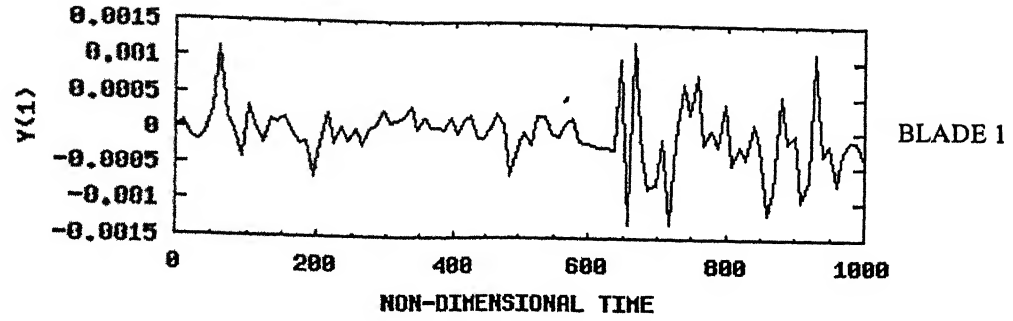

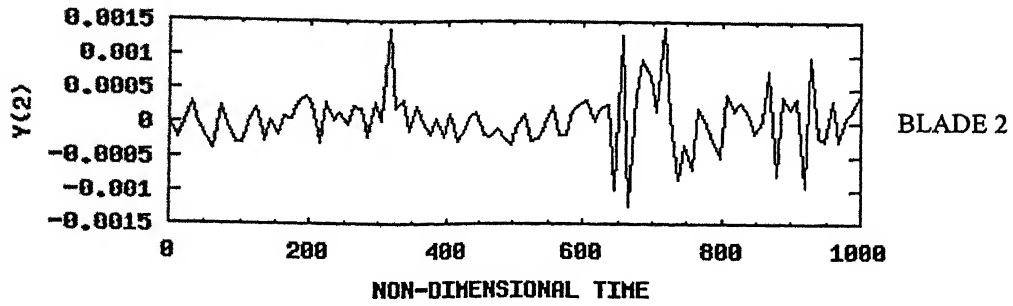

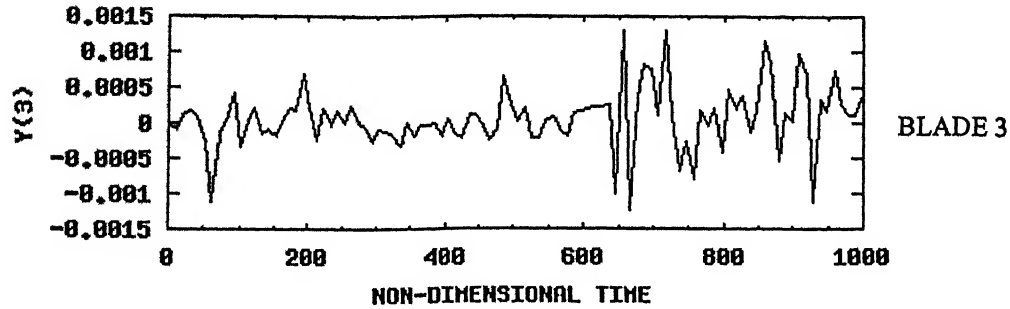

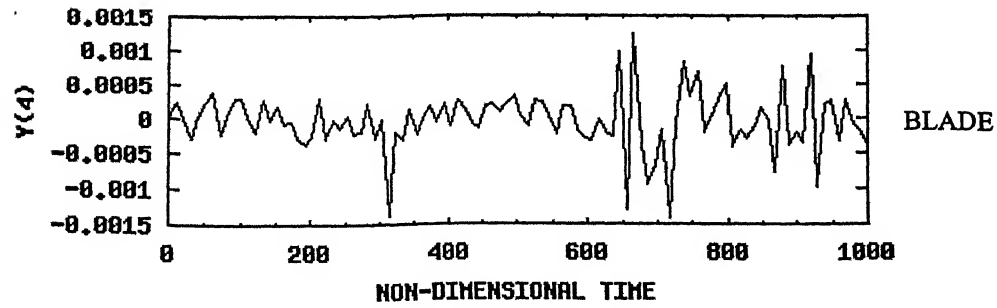

Fig. 4.16 (a) Blade motion in non-dimensional time domain
450 rpm, $\theta_X(0) = 4$ degree, ($\zeta_{\theta X} = 0.0$, $\zeta_{\theta Y} = 0.0$)

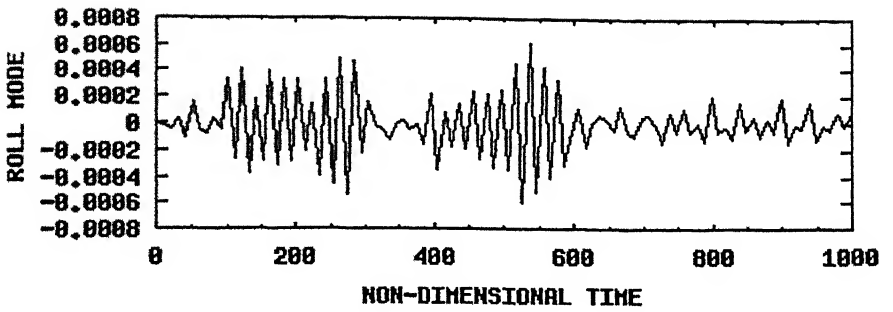

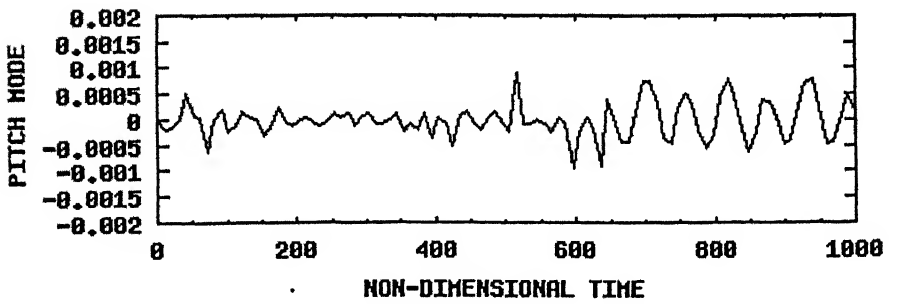

Fig. 4.16 (b) Fuselage motion in non-dimensional time domain 450 rpm, $\theta_X(0) = 4$ degree, ($\zeta_{\theta X} = 0.0$, $\zeta_{\theta Y} = 0.0$)

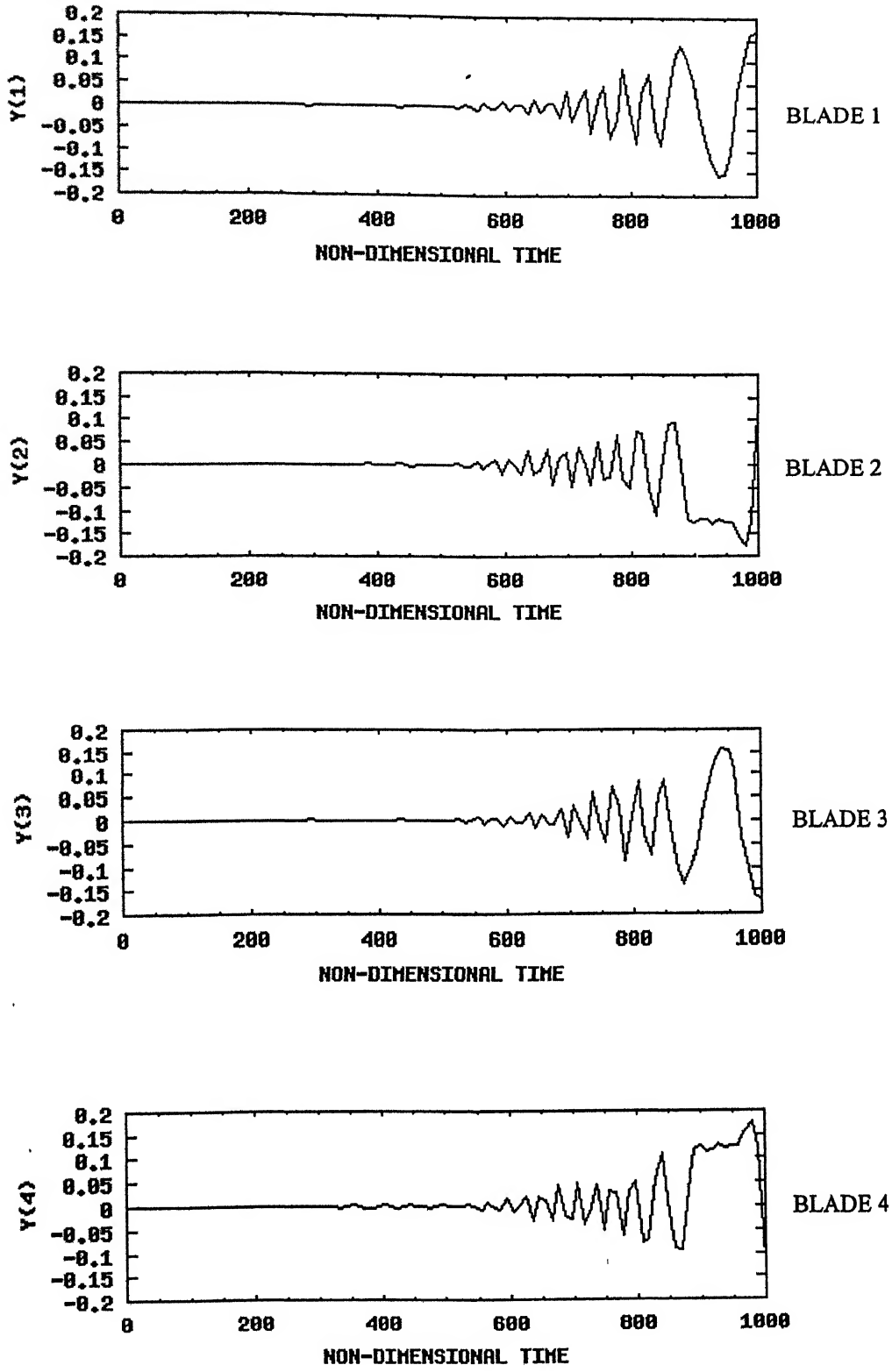

Fig. 4.17 (a) Blade motion in non-dimensional time domain
450 rpm, $\theta_X(0) = 6$ degree, ($\zeta_{\theta X} = 0.0$, $\zeta_{\theta Y} = 0.0$)

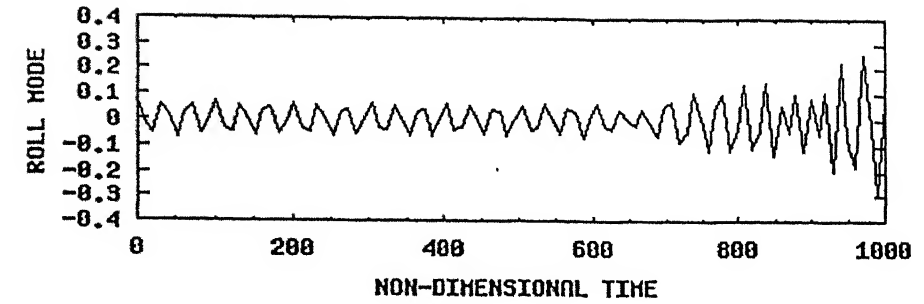

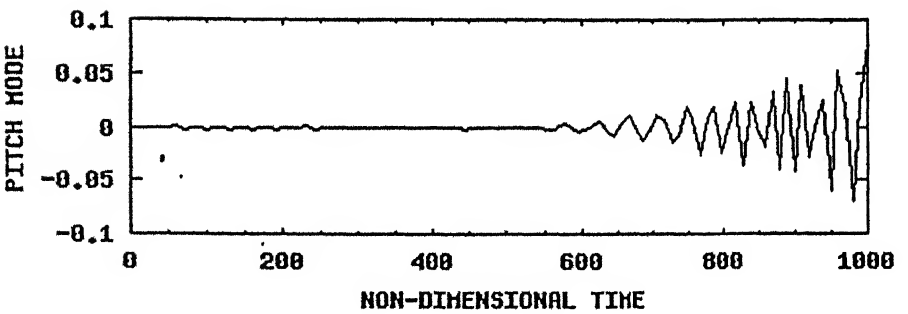

Fig. 4.17 (b) Fuselage motion in non-dimensional time domain 450 rpm, $\theta_X(0) = 6$ degree, ($\zeta_{0X} = 0.0$, $\zeta_{0Y} = 0.0$)

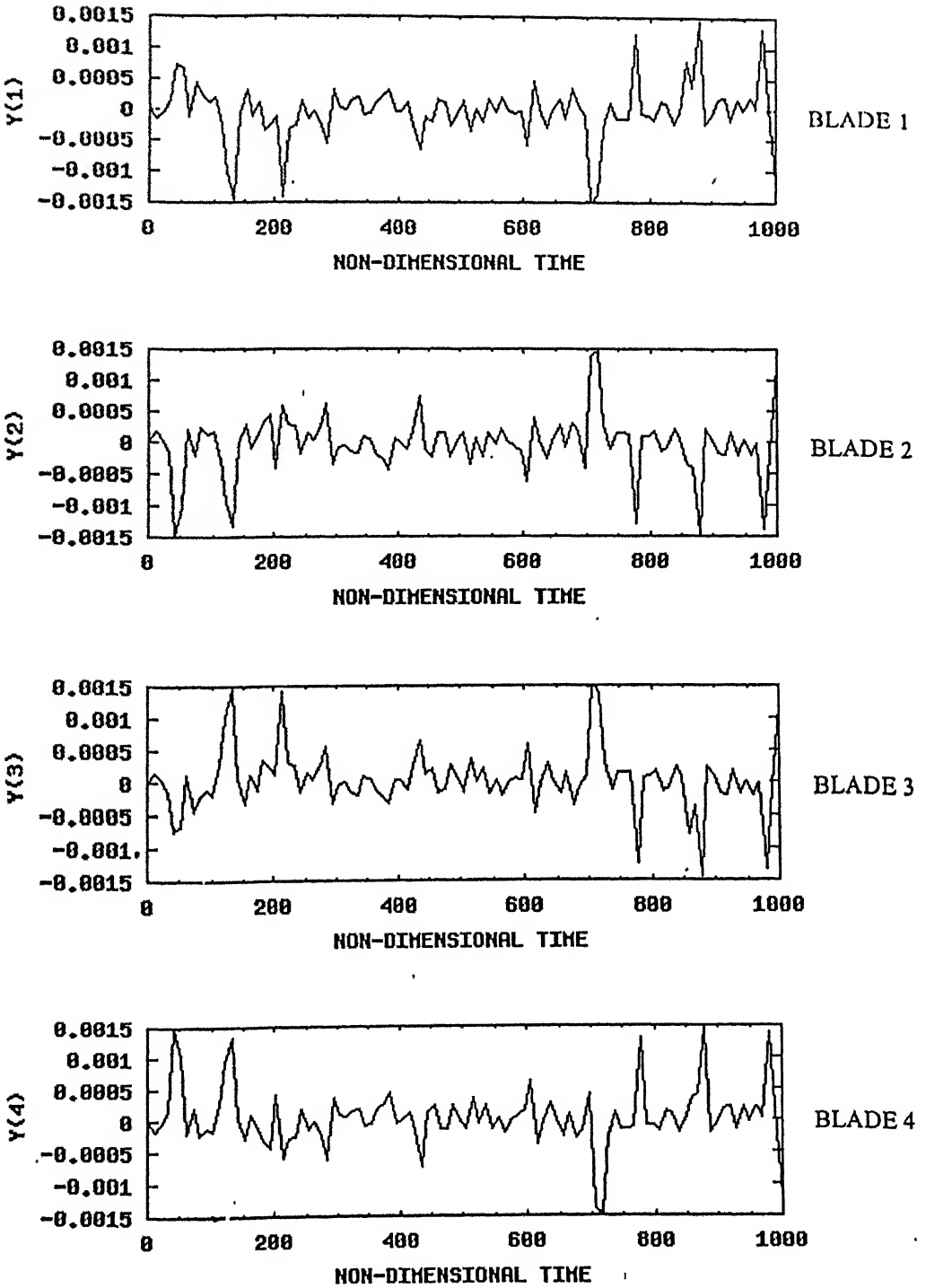

Fig. 4.18 (a) Blade motion in non-dimensional time domain
460 rpm, $\theta_X(0) = 0.8$ degree, ($\zeta_{0X} = 0.0$, $\zeta_{0Y} = 0.0$)

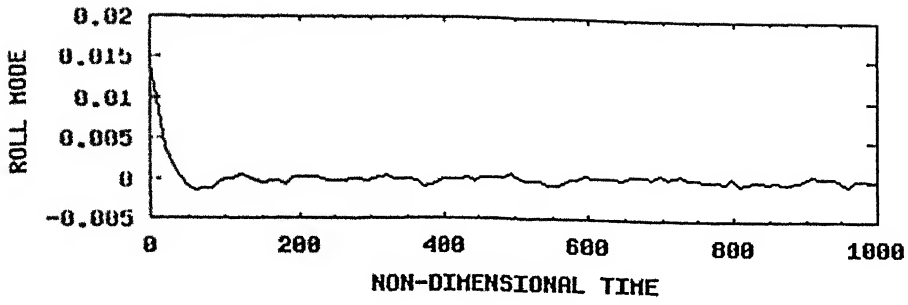

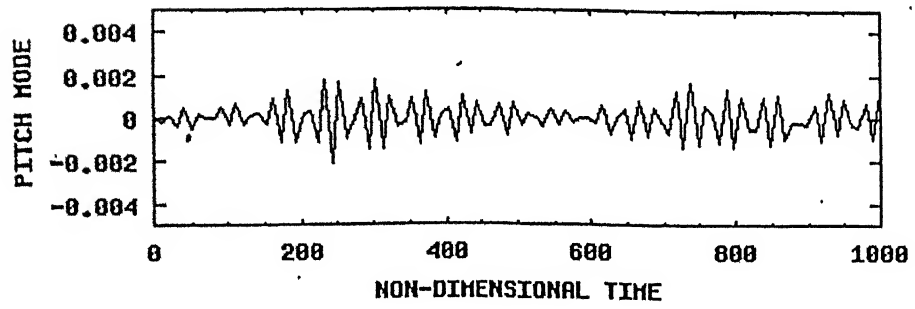

Fig. 4.18 (b) Fuselage motion in non-dimensional time domain 460 rpm, $0_X(0) = 0.8$ degree, ($\zeta_{0X} = 0.0$, $\zeta_{0Y} = 0.0$)

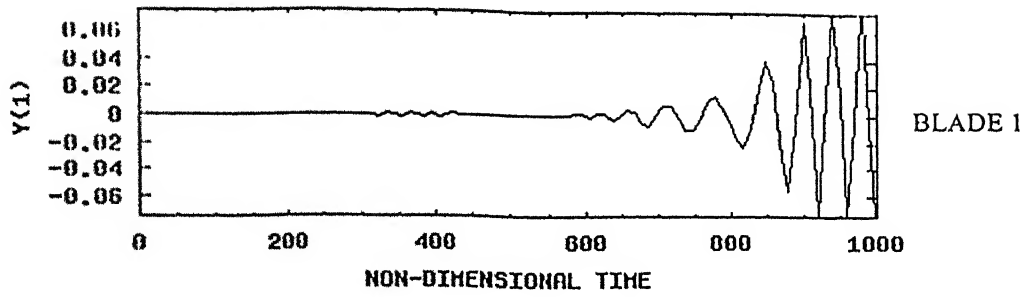

BLADE 1

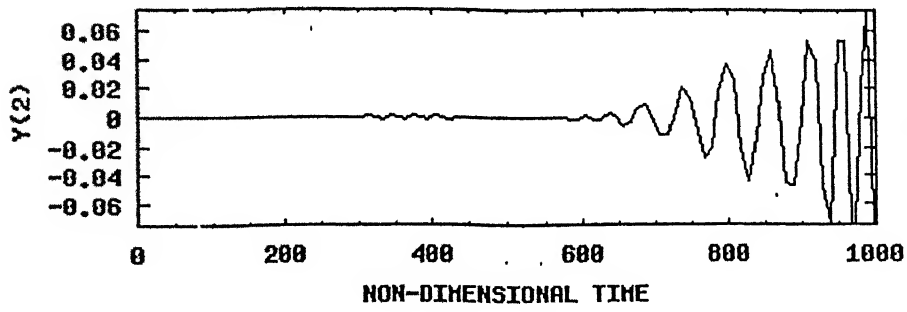

BLADE 2

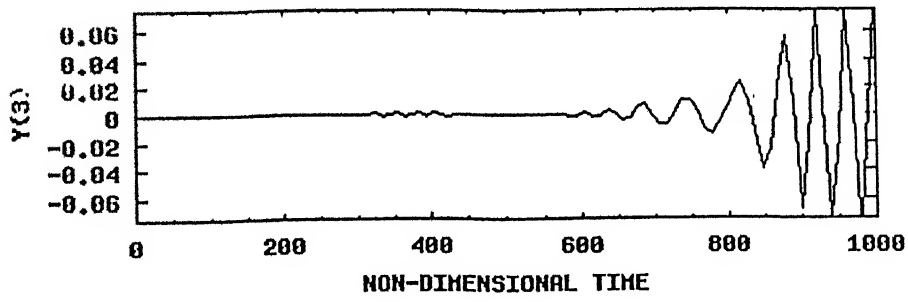

BLADE 3

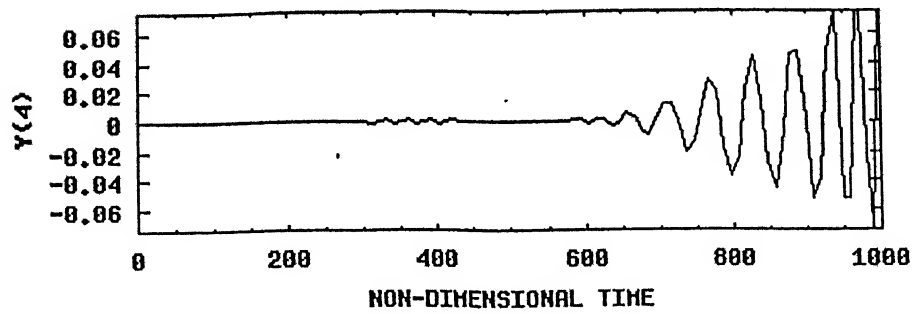

BLADE 4

Fig. 4.19 (a) Blade motion in non-dimensional time domain 460 rpm, $\theta_X(0) = 1$ degree, ($\zeta_{\theta X} = 0.0$, $\zeta_{\theta Y} = 0.0$)

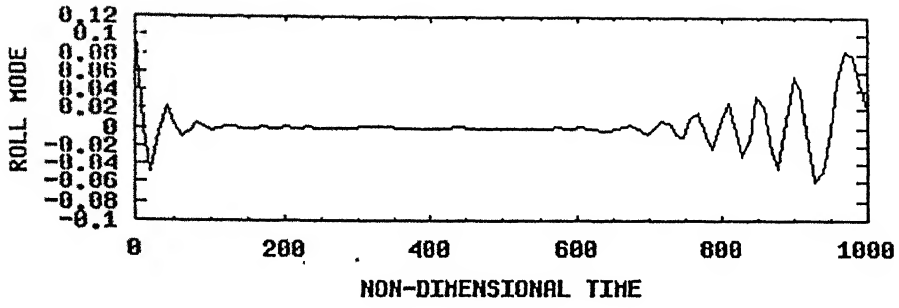

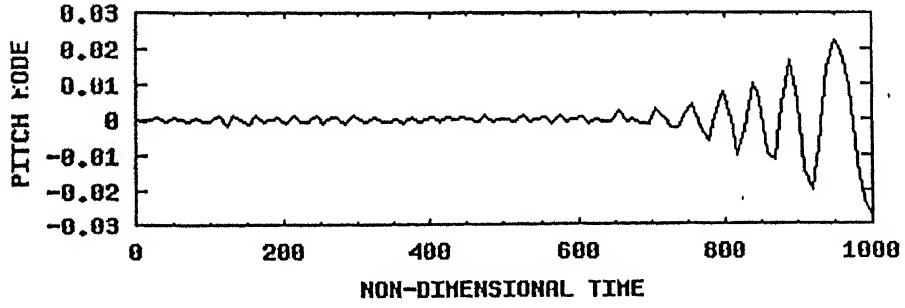

Fig. 4.19 (b) Fuselage motion in non-dimensional time domain 460 rpm, $\theta_X(0) = 1$ degree, ($\zeta_{\theta X} = 0.0$, $\zeta_{\theta Y} = 0.0$)

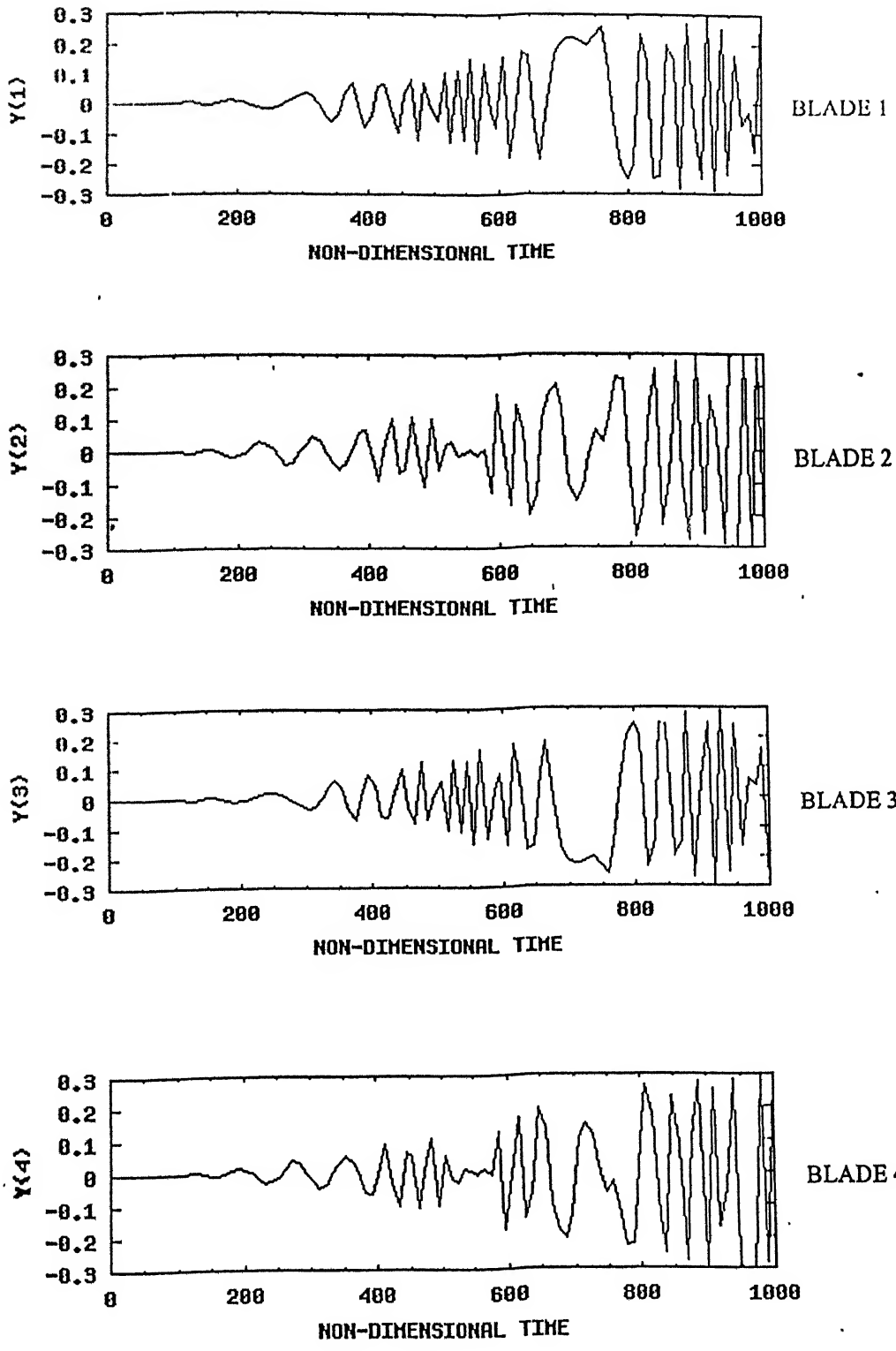

Fig. 4.20 (a) Blade motion in non-dimensional time domain
550 rpm, $0_X(0) = 4$ degree, ($\zeta_{0X} = 0.082$, $\zeta_{0Y} = 0.0529$)

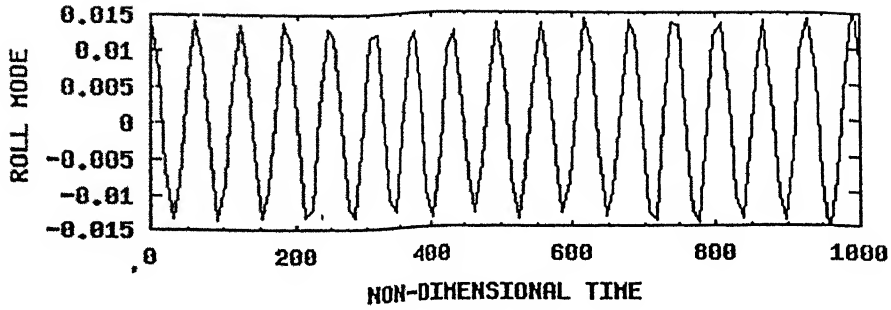

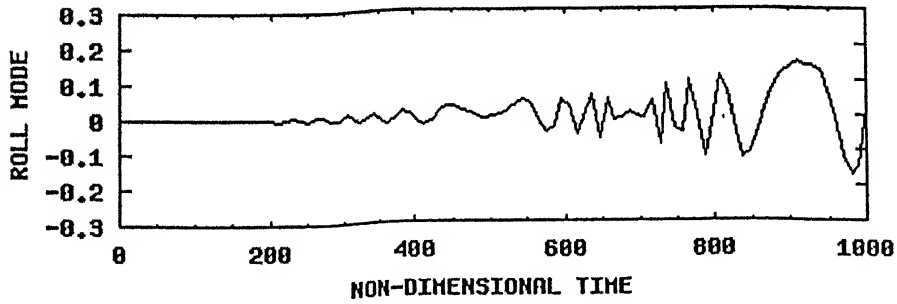

Fig. 4.20(b) Fuselage motion in non-dimensional time domain 550 rpm, $\theta_X(0) = 4$ degree, ($\zeta_{0X} = 0.0$, $\zeta_{0Y} = 0.0$)

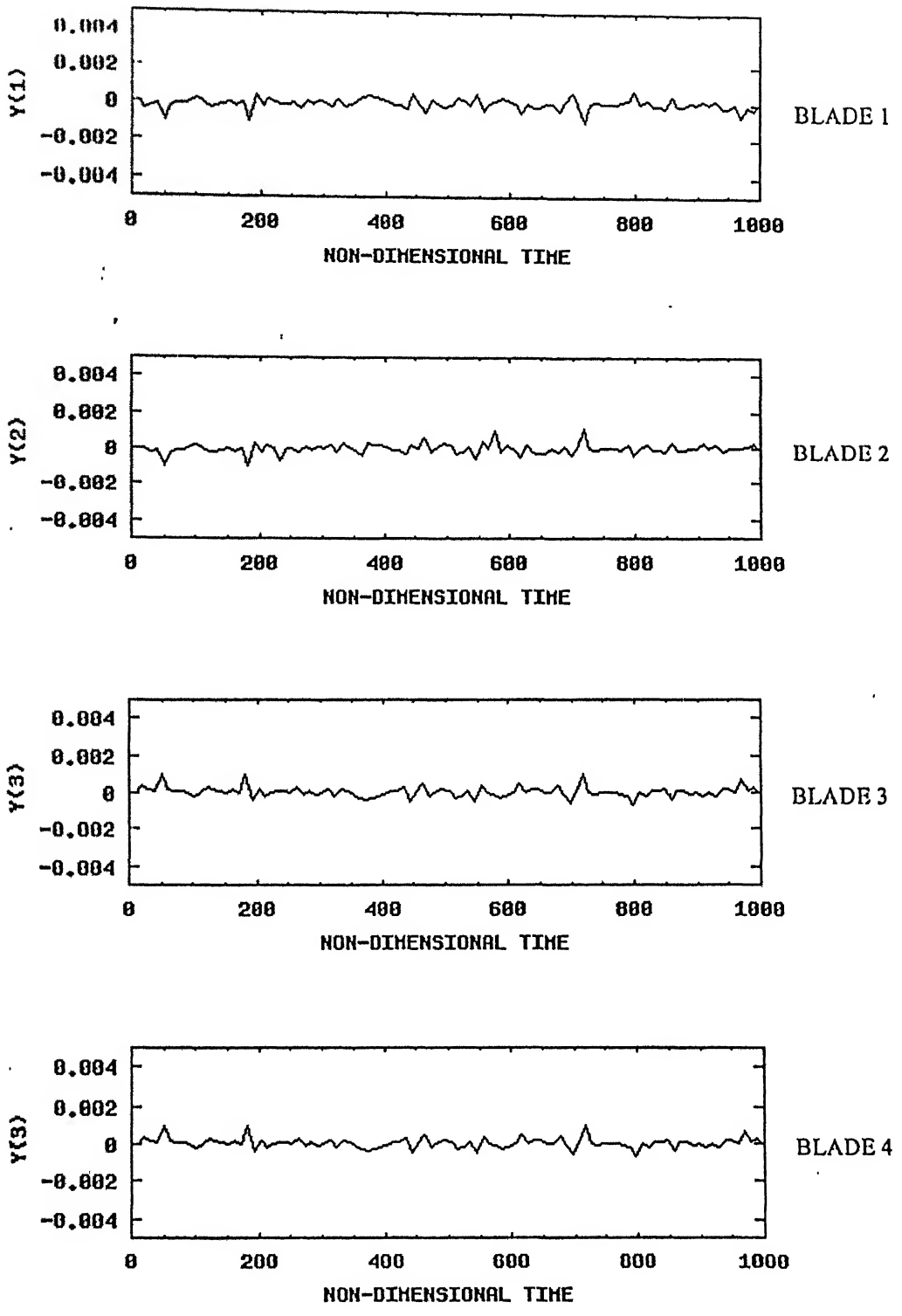

Fig. 4.21 (a) Blade motion in non-dimensional time domain 640 rpm, $\theta_X(0) = 0.8$ degree, ($\zeta_{\theta X} = 0.0$, $\zeta_{\theta Y} = 0.0$)

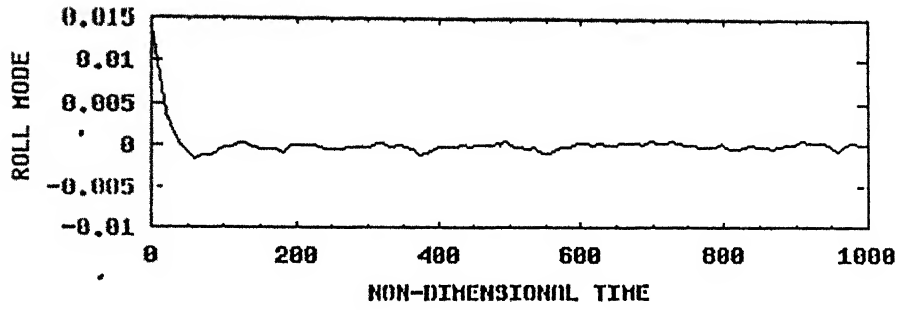

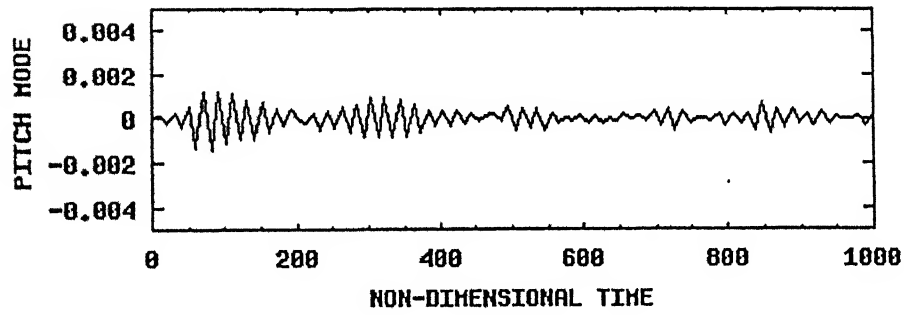

Fig. 4.21 (b) Fuselage motion in non-dimensional time domain 640 rpm, $\theta_X(0) = 0.8$ degree, ($\zeta_{0X} = 0.0$, $\zeta_{0Y} = 0.0$)

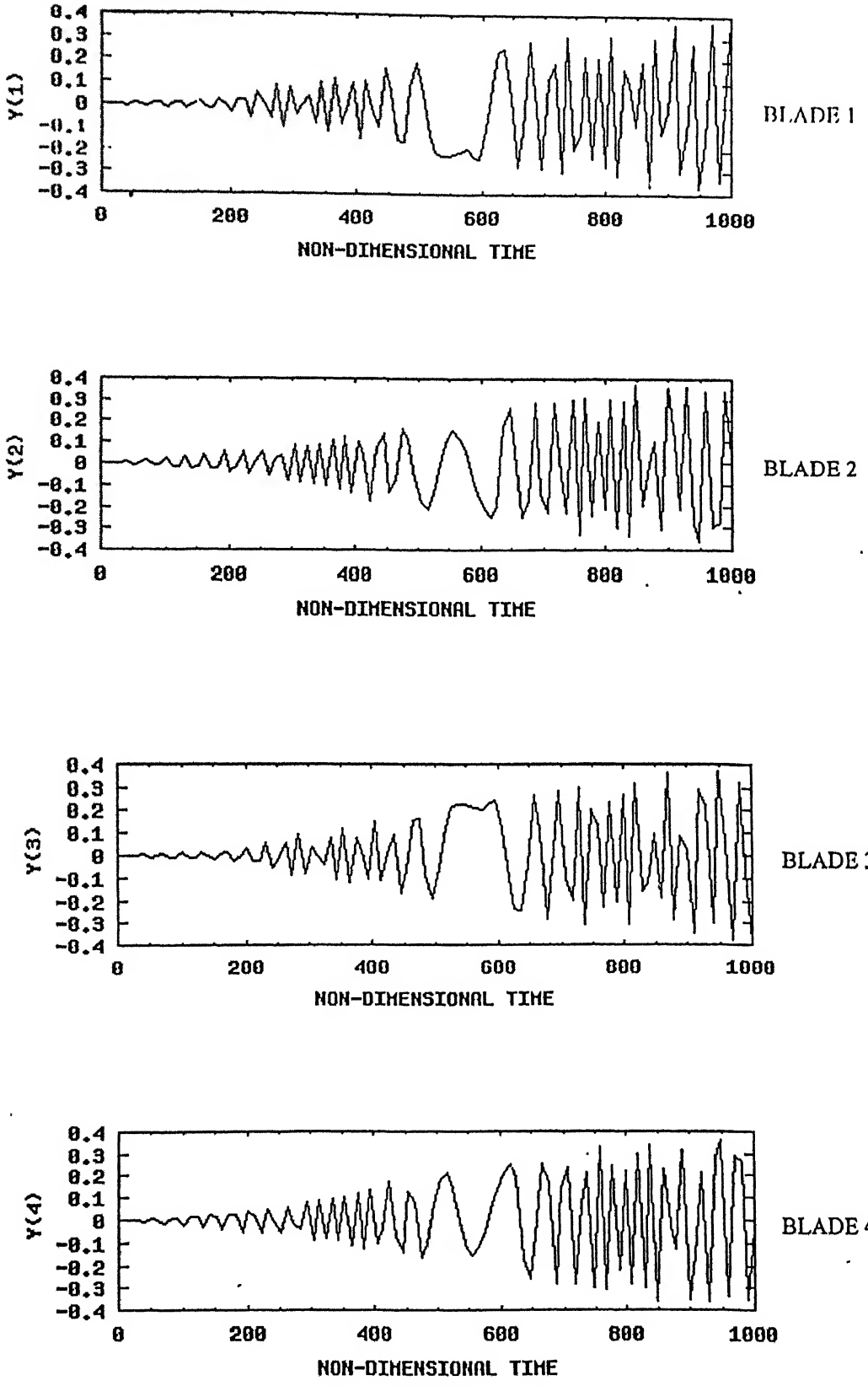

Fig. 4.22 (a) Blade motion in non-dimensional time domain 640 rpm, $\theta_X(0) = 1$ degree, ($\zeta_{\theta X} = 0.0$, $\zeta_{\theta Y} = 0.0$)

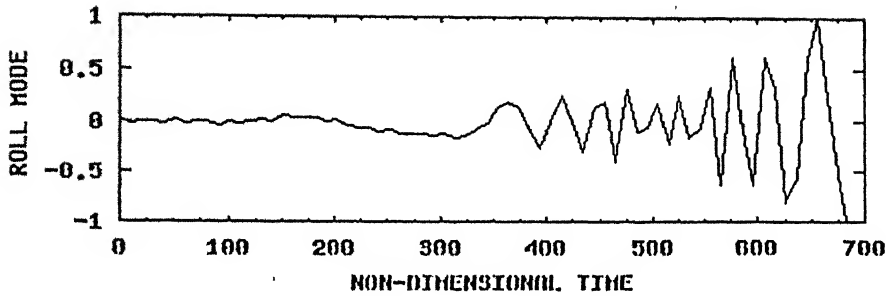

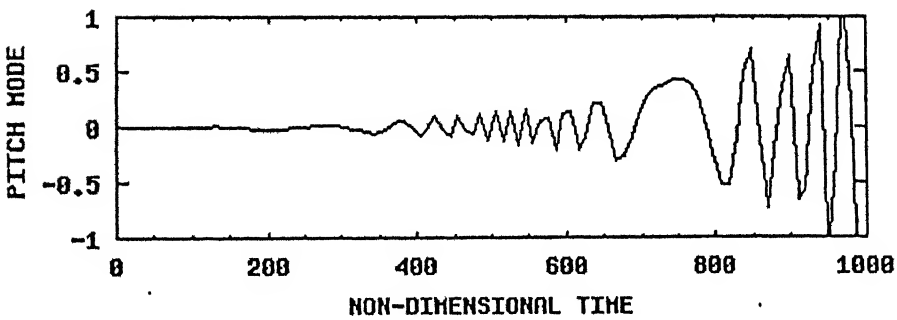

Fig. 4.22 (b) Fuselage motion in non-dimensional time domain 640 rpm, $\theta_X(0) = 1$ degree, ($\zeta_{\theta X} = 0.0$, $\zeta_{\theta Y} = 0.0$)

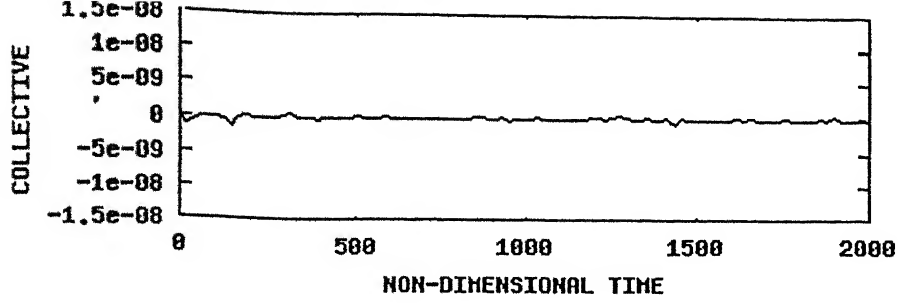

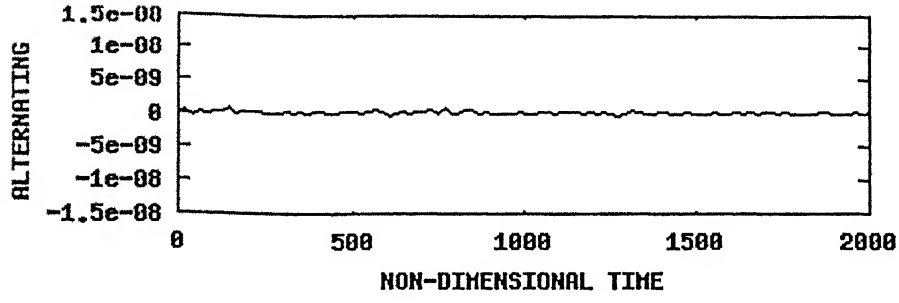

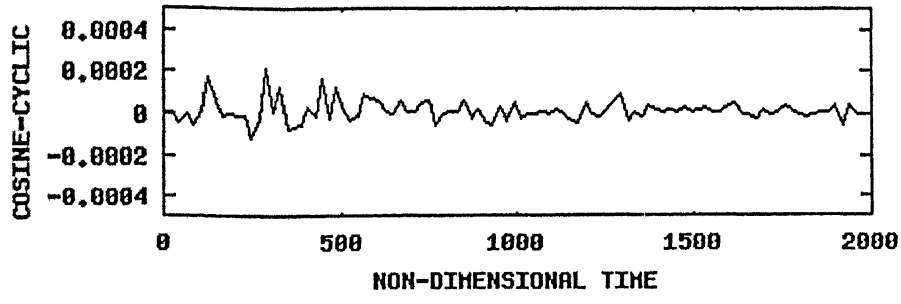

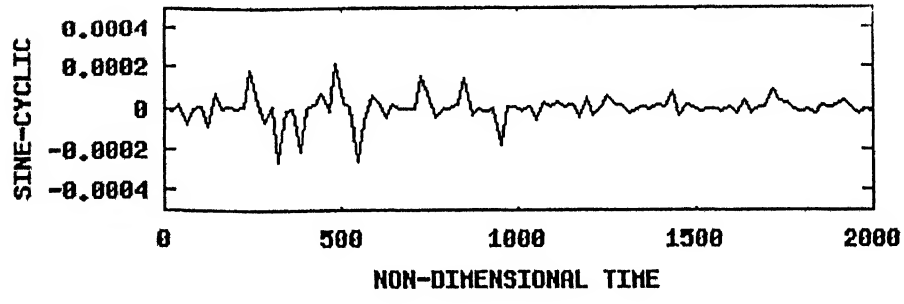

Fig. 4.23 Multiblade Coordinate Transformation
250 rpm, $\theta_X(0) = 4$ degree, ($\zeta_{0X} = 0.082$, $\zeta_{0Y} = 0.0529$)

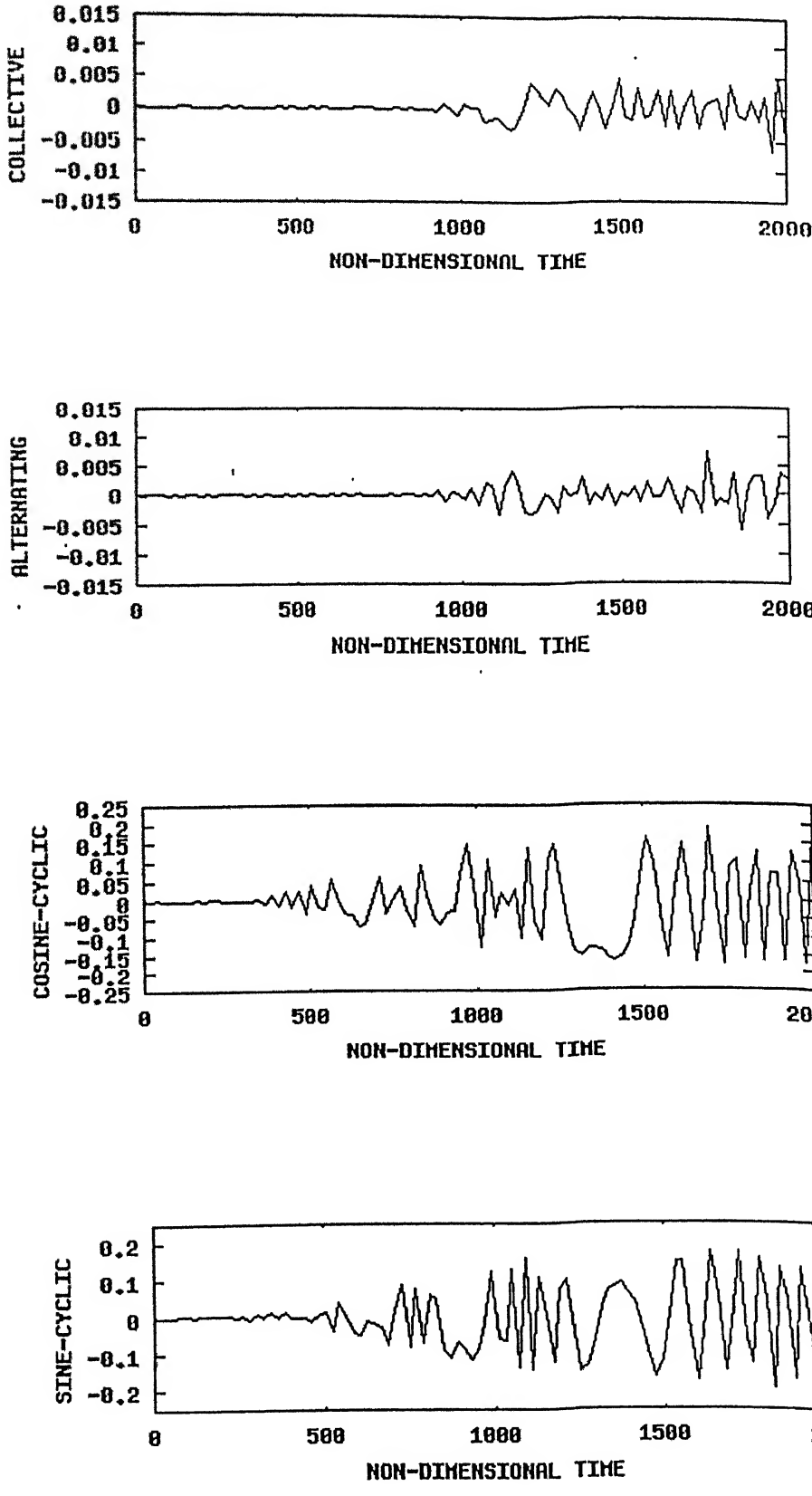

Fig. 4.24 Multiblade Coordinate Transformation
550 rpm, $\theta_X(0) = 4$ degree, ($\zeta_{0X} = 0.082$, $\zeta_{0Y} = 0.0529$)

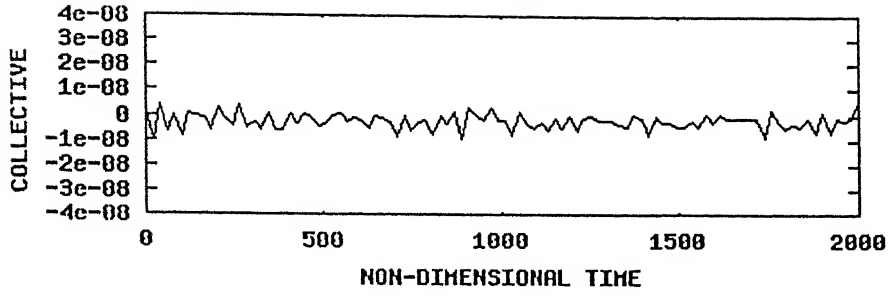

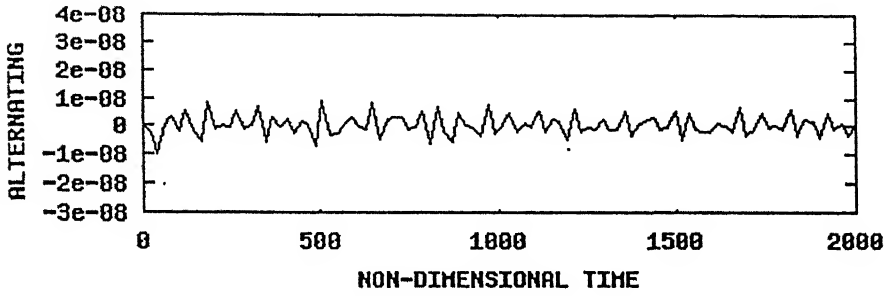

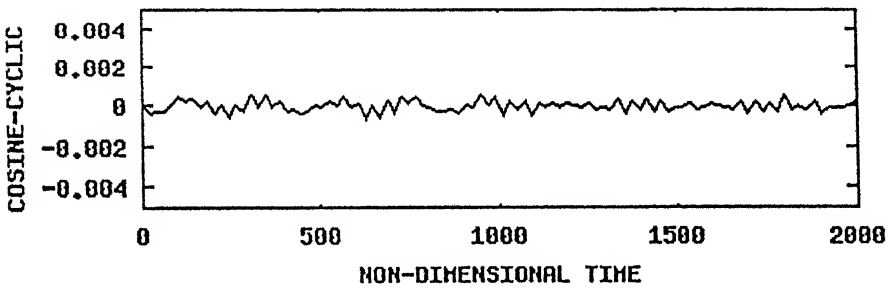

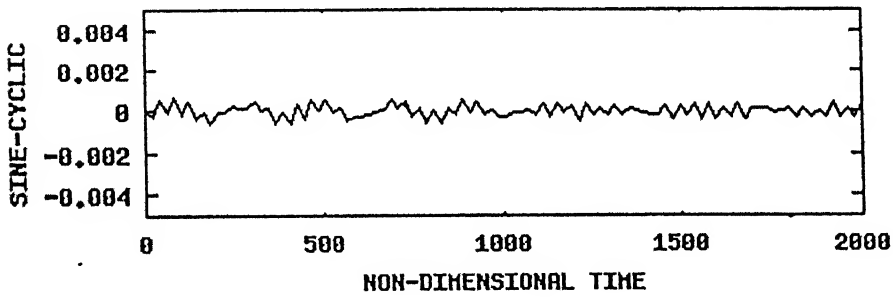

Fig. 4.25 Multiblade Coordinate Transformation
700 rpm, $0_X(0) = 4$ degree, ($\zeta_{0X} = 0.082$, $\zeta_{0Y} = 0.0529$)

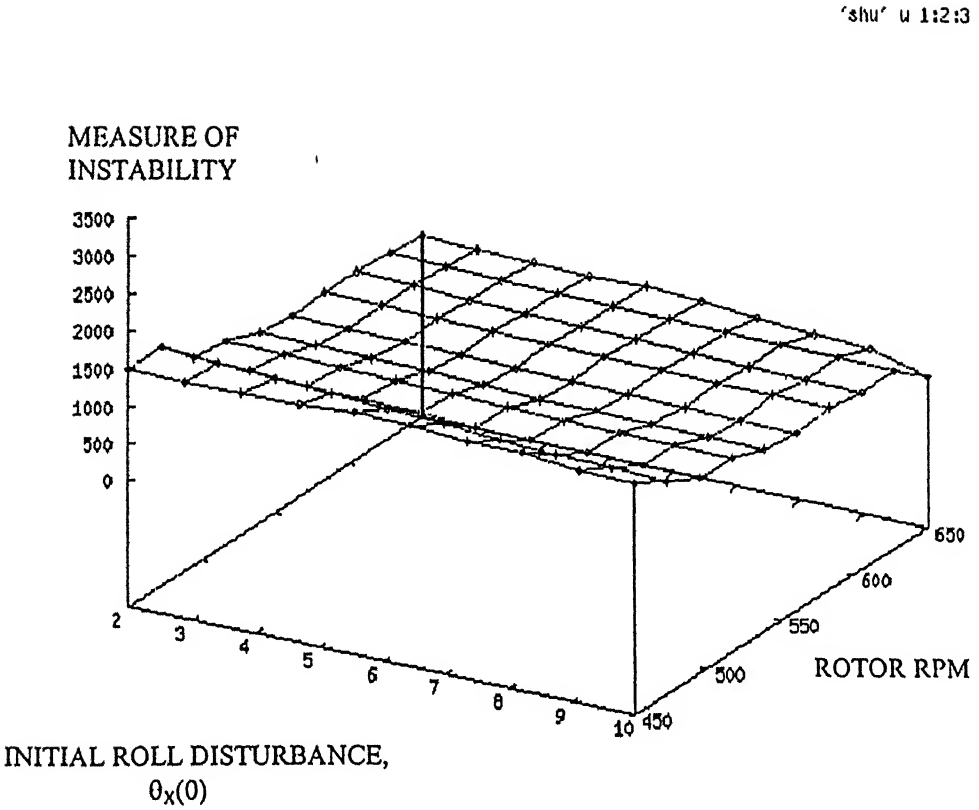

Fig. 4.26 Three dimensional plot to show the variation of index of instability with the operating and initial condition

STABILITY

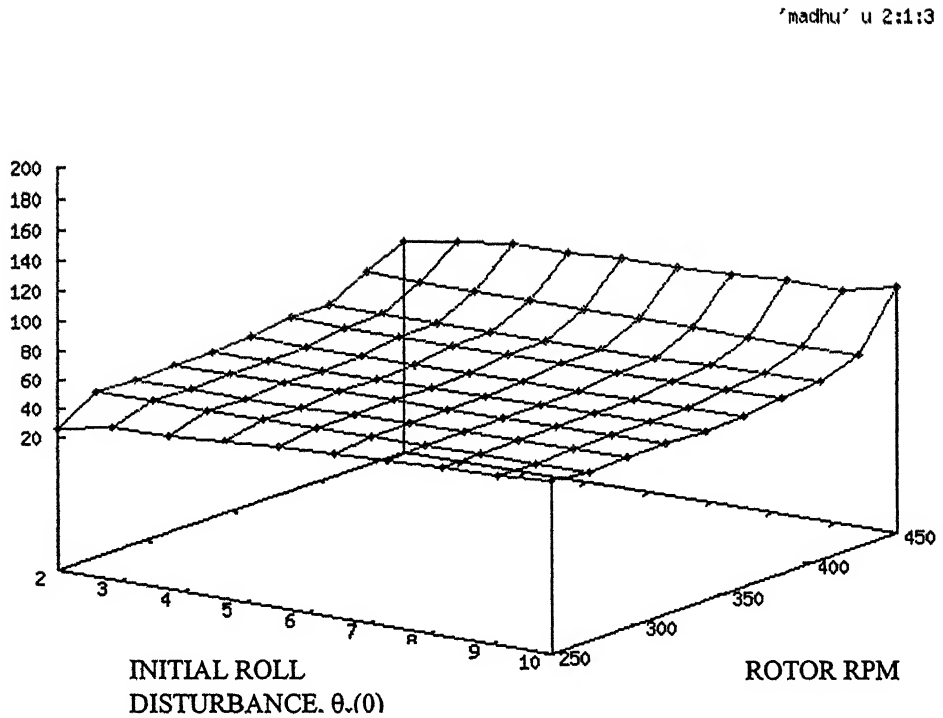

Fig. 4.27 (a)

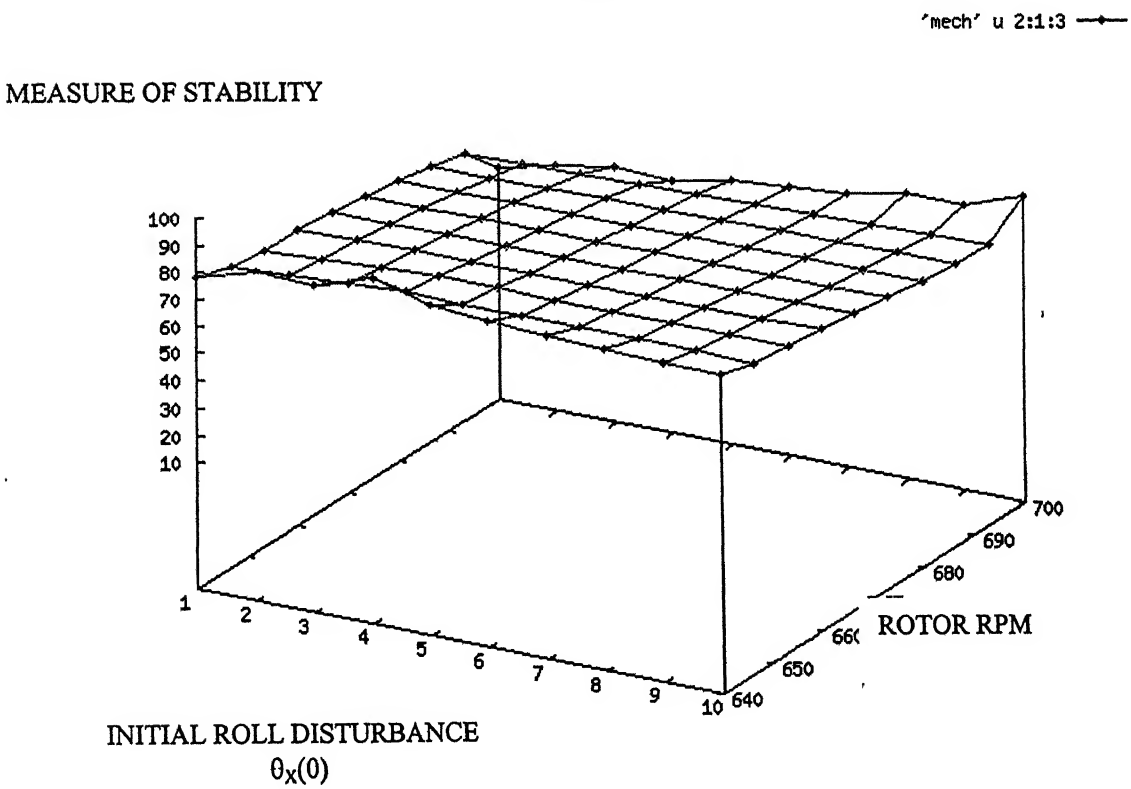

Fig. 4.27 (b)

Fig.4.27 Three dimensional plot for measure of stability

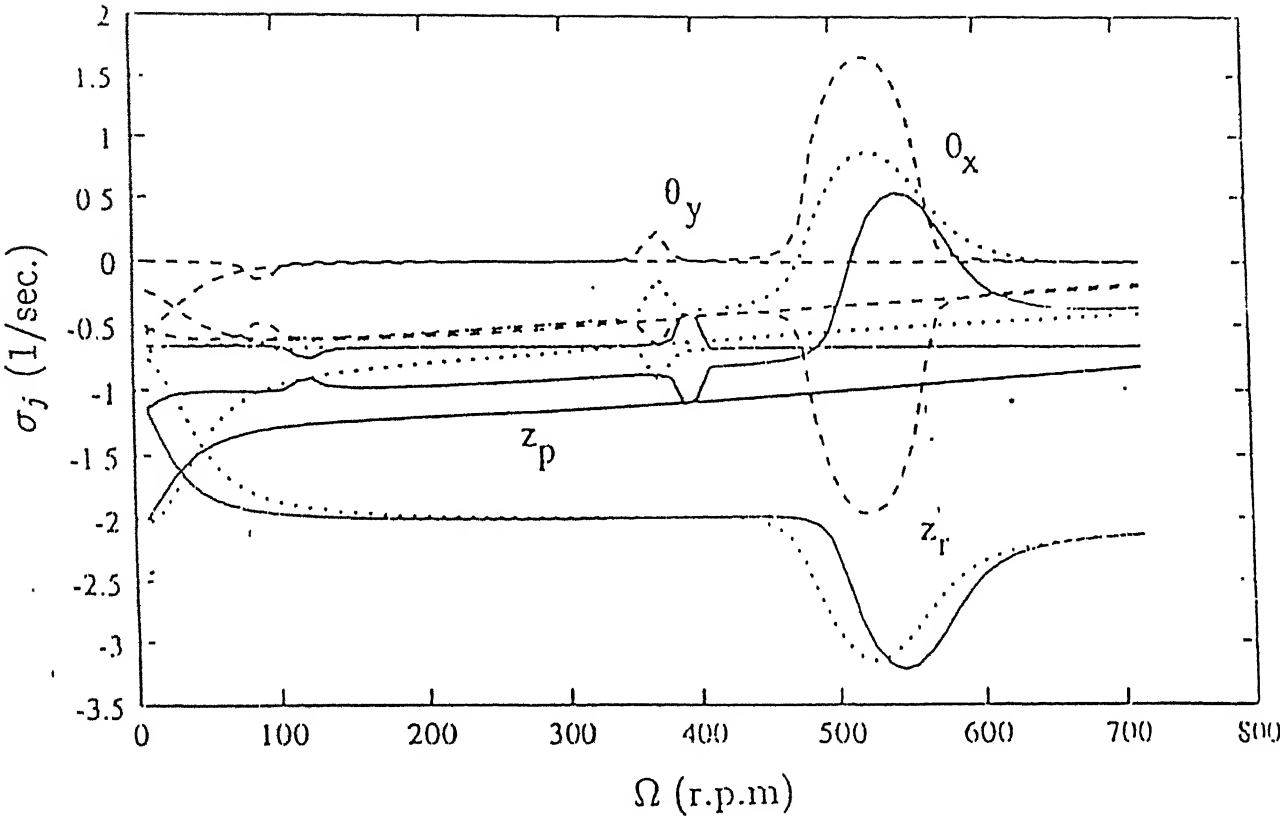

Fig 4.28 Effect of support damping on stability ($\zeta_{0x} = 0.082$, $\zeta_{0y} = 0.0529$)

- ---- no support damping ($\xi_1 = 0.1$, $\xi_2 = 0.25$)

- ..... with support damping ($\xi_1 = 0.1$, $\xi_2 = 0.25$)

$\theta_x(0)$ RPM	0.1 (in deg)	0.2 (in deg)	0.4 (in deg)	0.6 (in deg)	0.8 (in deg)	1.0 (in deg)	2.0 (in deg)	4.0 (in deg)	6.0 (in deg)	8.0 (in deg)	10.0 (in deg)
250	Converge	Converge	Converge	Converge	Converge	Converge	Converge	Converge	Converge	Converge	Converge
350	Converge	Converge	Converge	Converge	Converge	Converge	Converge	Converge	Converge	Converge	Converge
360	Converge	Converge	Converge	Converge	Converge	Converge	Converge	Converge	Converge	Converge	Converge
400	Converge	Converge	Converge	Converge	Converge	Converge	Converge	Converge	Converge	Converge	Converge
450	Converge	Converge	Converge	Converge	Converge	Converge	Converge	Converge	Diverge	Diverge	Diverge
460	Converge	Converge	Converge	Converge	Converge	Converge	Diverge	Diverge	Diverge	Diverge	Diverge
470	Diverge	Diverge	Diverge	Diverge	Diverge	Diverge	Diverge	Diverge	Diverge	Diverge	Diverge
480	Diverge	Diverge	Diverge	Diverge	Diverge	Diverge	Diverge	Diverge	Diverge	Diverge	Diverge
490	Diverge	Diverge	Diverge	Diverge	Diverge	Diverge	Diverge	Diverge	Diverge	Diverge	Diverge
500	Diverge	Diverge	Diverge	Diverge	Diverge	Diverge	Diverge	Diverge	Diverge	Diverge	Diverge
550	Diverge	Diverge	Diverge	Diverge	Diverge	Diverge	Diverge	Diverge	Diverge	Diverge	Diverge
600	Diverge	Diverge	Diverge	Diverge	Diverge	Diverge	Diverge	Diverge	Diverge	Diverge	Diverge
620	Converge	Converge	Converge	Converge	Converge	Converge	Converge	Diverge	Diverge	Diverge	Diverge
640	Converge	Converge	Converge	Converge	Converge	Converge	Converge	Converge	Diverge	Diverge	Diverge
650	Converge	Converge	Converge	Converge	Converge	Converge	Converge	Converge	Diverge	Diverge	Diverge
700	Converge	Converge	Converge	Converge	Converge	Converge	Converge	Converge	Converge	Converge	Converge

Table 4.1 Qualitative response of the coupled rotor/fuselage system in non-dimensional time domain with support damping ($\zeta_{\theta X} = 0.082$, $\zeta_{\theta Y} = 0.0529$)

$\theta_x(0)$ RPM	0.1 (in deg)	0.2 (in deg)	0.4 (in deg)	0.6 (in deg)	0.8 (in deg)	1.0 (in deg)	2.0 (in deg)	4.0 (in deg)	6.0 (in deg)	8.0 (in deg)	10.0 (in deg)
250	Converge	Converge	Converge	Converge	Converge	Converge	Converge	Converge	Converge	Converge	Converge
350	Converge	Converge	Converge	Converge	Converge	Converge	Converge	Converge	Diverge	Diverge	Diverge
360	Converge	Converge	Converge	Converge	Converge	Converge	Converge	Converge	Converge	Converge	Converge
400	Converge	Converge	Converge	Converge	Converge	Converge	Converge	Converge	Converge	Converge	Converge
450	Converge	Converge	Converge	Converge	Converge	Converge	Converge	Converge	Diverge	Diverge	Diverge
460	Converge	Converge	Converge	Converge	Converge	Diverge	Diverge	Diverge	Diverge	Diverge	Diverge
470	Diverge	Diverge	Diverge	Diverge	Diverge	Diverge	Diverge	Diverge	Diverge	Diverge	Diverge
480	Diverge	Diverge	Diverge	Diverge	Diverge	Diverge	Diverge	Diverge	Diverge	Diverge	Diverge
490	Diverge	Diverge	Diverge	Diverge	Diverge	Diverge	Diverge	Diverge	Diverge	Diverge	Diverge
500	Diverge	Diverge	Diverge	Diverge	Diverge	Diverge	Diverge	Diverge	Diverge	Diverge	Diverge
550	Diverge	Diverge	Diverge	Diverge	Diverge	Diverge	Diverge	Diverge	Diverge	Diverge	Diverge
600	Diverge	Diverge	Diverge	Diverge	Diverge	Diverge	Diverge	Diverge	Diverge	Diverge	Diverge
620	Converge	Converge	Converge	Converge	Diverge	Diverge	Diverge	Diverge	Diverge	Diverge	Diverge
640	Converge	Converge	Converge	Converge	Converge	Diverge	Diverge	Diverge	Diverge	Diverge	Diverge
650	Converge	Converge	Converge	Converge	Converge	Converge	Converge	Converge	Converge	Converge	Converge
700	Converge	Converge	Converge	Converge	Converge	Converge	Converge	Converge	Converge	Converge	Converge

Table 4.2 Qualitative response of the system in non-dimensional time domain for set of rotor rpm and initial roll disturbance

Without support damping ($\zeta_{\theta x} = 0.0$, $\zeta_{\theta y} = 0.0$)

Chapter 5

CONCLUSION

The time domain behavior of the coupled rotor/fuselage system has been studied. The properties of the elastomer are taken from the experimental results published in the open literature. The major conclusions of the present study are summarised below.

1. It has been observed that the magnitude of initial disturbance affects the aeromechanical stability of the coupled system under ground resonance condition.
2. The effect of support damping on the response behavior obtained in the present work agrees well with that reported in Ref. [6] where linearized stability analysis was carried out also the range of rotor rpm, in which the system is unstable, matches well with range predicted by the linearized stability analysis.

References

1. Huber, H., "Will Rotor Hubs hose Their Bearings? A Survey of Bearingless Main Rotor Development," *Eighteenth European Rotorcraft Forum*, Avignon, France, Sept, 1992, pp. 506.1-506.19.
2. Panda, B., and Mychalowycx, E., "Aeroelastic Stability Wind Tunnel Testing with Analytical Correlation of the Comanche Bearingless Main Rotor," *Journal of the American Helicopter Society*, Vol 42, No. 3, 1997, pp. 207-217.
3. Weller, W. H., "Variation in Hover Aeromechanical Stability Trends with Bearingless Main Rotor Design," *Journal of the American Helicopter Society*, Vol 42, No. 3, 1997, pp. 207-217.
4. Kampa,K., Enenkl, B., Roth, G. and Polz , G., " Aeromechanics aspects in the design of the EC135" , *23rd European Rotorcraft Forum*, Germany, pp. 38.1-38.14, 1997
5. Pohit, G. Venkatesan, C. and Mallik, A. K., "Influence of Non-linear Elastomer on isolated lag Dynamics and rotor/fuselage Aeromechanical Stability," *AIAA 2000-1691, 41st AIAA/ASME/ASCE/AHS/ASC structures, structural Dynamics and materials conference*, Atlanta, Georgia
6. Pohit, G. "Dynamics of a Bearingless Helicopter Rotor Blade with a Non-linear Elastomeric Constraint, Ph.D Thesis, *Dept. of Mechanical Engg., Indian Institute of Technology, Kanpur*, India, 1999.
7. Gandhi, F., and Chopra, I., "Analysis of Bearingless Main Rotor Dynamics with the Inclusion of and Improved Time Domain Nonlinear Elastomeric Damper Model," *Journal of the American Helicopter Society*, Vol. 41, No. 3, 1996, pp. 267-277.
8. Friedmann, P. P., and Venkatesan, C., "Voupled Helicopter Rotor/Body Aeromechanical Stability, comparison of Experimental and Theoretical results," *Journal of Aircraft*, Vol. 22, No. 2, 1985, pp. 148-155.

9. Friedmann, P. P., and Venkatesan, C.," Influence of Unsteady Aerodynamic Models on Aeromechanical Stability in Ground Resonance," *Journal of the American Helicopter Society*, Vol. 31, No. 1, 1986, pp. 65-74.

10. Bousman, W. G., "An Experimental Investigation of the Effects of Aeroelastic Coupling on Aeromechanical Stability of Hingeless Rotor Helicopter," *Journal of the American Helicopter Society*, Vol. 26, No. 1, 1981, pp. 46-54.

11. Venkatesan, C., "Influence of Aeroelastic Coupliing on Coupled Rotor/Body Dynamics," 6th International Workshop on Dynamics, *Aeroelastic Stability Modelling, of Rotorcraft*, University of California, Los Angeles, Nov. 8-10, 1995.